

STELLAR ROTATION IN M35: MASS-PERIOD RELATIONS, SPIN-DOWN RATES, AND GYROCHRONOLOGY

1

Søren Meibom^{2,3,4} and Robert D. Mathieu⁴*Department of Astronomy, University of Wisconsin - Madison, Madison, WI, 53706, USA*Keivan G. Stassun⁴*Physics and Astronomy Department, Vanderbilt University, Nashville, TN - 32735, USA*

ABSTRACT

We present the results of a 5 month photometric time-series survey for stellar rotation over a $40' \times 40'$ field centered on the 150 Myr open cluster M35. We report rotation periods for 441 stars within this field and determine their cluster membership and binarity based on a decade-long radial-velocity survey, proper-motion measurements, and multi-band photometric observations. We find that 310 of the stars with measured rotation periods are late-type members of M35. The distribution of rotation periods for cluster members spans more than two orders of magnitude from $\sim 0.1 - 15$ days, with the shortest and longest periods not constrained by the sampling frequency and the time-span of the survey. With an age bridging the gap between the zero-age main-sequence (ZAMS) and the Hyades, and with ~ 6 times more rotation periods than measured in the Pleiades, these new data permit detailed studies of early main-sequence rotational evolution of late-type stars. Nearly 80% of the 310 rotators lie on two distinct sequences in the color-period plane, and define clear relations between stellar rotation period and stellar color (mass). The M35 color-period diagram

¹WIYN Open Cluster Study. XXXIII.

²*smeibom@cfa.harvard.edu*

³Now at Harvard-Smithsonian Center for Astrophysics, Cambridge, MA, 02138, USA

⁴Visiting Astronomer, Kitt Peak National Observatory, National Optical Astronomy Observatory, which is operated by the Association of Universities for Research in Astronomy, Inc. (AURA) under cooperative agreement with the National Science Foundation.

enables us to determine the timescale for the transition between the two rotational states as a function of stellar mass, ~ 60 Myr and ~ 140 Myr for G and K dwarfs, respectively. These timescales are inversely related to the mass of the convective envelope, and may offer valuable constraints on the rates of internal and external angular momentum transport and on the evolution rates of stellar dynamos. From a comparison to the Hyades, our data for stars in one rotational state confirm the Skumanich (1972) spindown time-dependence for G dwarfs, but suggest that K dwarfs spin down more slowly. The locations of the rotational sequences in the M35 color-period diagram support the use of rotational isochrones to determine ages for coeval stellar populations. We use such gyrochronology to determine a “gyro-age” of M35 of 134 Myr with a formal uncertainty of 3 Myr. The M35 rotation data are also used to evaluate new color dependencies for the rotational isochrones.

Subject headings: open clusters and associations:general - stars:late-type - stars:rotation - stars:ages - stars:spots - binary stars:rotation

1. INTRODUCTION

Observations of coeval populations of late-type stars younger than the Hyades have revealed that they rotate with periods ranging over two orders of magnitude - from near breakup to periods similar to the Sun. Understanding why some stars deplete their angular momentum faster than others, which physical processes are at work, when, and to what extent, is a primary mandate for stellar evolution research.

The discovery from photometric and spectroscopic measurements in the Pleiades of sub 1-day rotation periods for K dwarfs (Alphenaar & van Leeuwen 1981; van Leeuwen & Alphenaar 1982; Meys et al. 1982; Soderblom et al. 1983) challenged prior understanding of the early angular momentum evolution for late-type stars, and sparked a renewed interest in the topic. Observations of mainly projected rotation velocities ($v \sin(i)$) of late-type stars in α Persei (50 Myr; Stauffer et al. (1985, 1989)), the Pleiades (100 Myr; Soderblom et al. (1983); Stauffer et al. (1984); Benz et al. (1984); Stauffer & Hartmann (1987); Soderblom et al. (1993a); Terndrup et al. (2000)), and the Hyades (625 Myr; Soderblom (1982); Benz et al. (1984); Radick et al. (1987)), and photometric studies of the Hyades (Lockwood et al. 1984; Radick et al. 1987), confirmed the coexistence of slowly and rapidly rotating stars in α Persei and the Pleiades, but found an absence of rapid rotators in the Hyades. Furthermore, the rapid rotators in the youngest clusters were found primarily among K and M dwarfs and not among G dwarfs.

The emerging evidence for an age- and mass-dependence of rapid rotation prompted new ideas about the rotational evolution of late-type stars. For example the suggestion of epochs of decoupling and recoupling of the stellar core and envelope (e.g. Stauffer et al. 1984; Soderblom et al. 1993b; Jianke & Collier Cameron 1993). The idea of decoupling - allowing the more shallow convective envelope of G dwarfs to spin down faster than the envelopes in K and M dwarfs - had developed in parallel in models of stellar rotation (e.g. Endal & Sofia 1981; Pinsonneault et al. 1990; MacGregor & Brenner 1991; Barnes & Sofia 1996). However, the concept of decoupling, if permanent, is in conflict with helioseismic observations of the sun as a solid-body rotator (Gough 1982; Duvall et al. 1984; Goode et al. 1991; Eff-Darwich et al. 2002). Furthermore, recoupling - giving access to the angular momentum reservoir of the faster spinning core - was suggested by Soderblom et al. (1993b) as being necessary to explain the evolution beyond the age of the Pleiades of slowly rotating stars (Soderblom et al. 1993b).

Understanding the formation of the rapid rotators is a separate problem. The fastest spinning stars in the youngest clusters cannot be explained from Skumanich-style spin-down (Skumanich 1972) of the fastest spinning T Tauri stars. The rapid rotators can be explained only by introducing “magnetic saturation” of the angular momentum loss via stellar winds (Stauffer & Hartmann 1987; MacGregor & Brenner 1991; Barnes & Sofia 1996; Bouvier et al. 1997; Krishnamurthi et al. 1997; Sills et al. 2000), and by allowing the saturation threshold to depend on the stellar mass. The physical meaning of “saturation” is still unclear.

During the pre main-sequence (PMS) phase, large dispersions and substructure (bimodalities) in the rotation-period distributions has also been observed for coeval stellar populations. Here, a popular explanation for coeval rapid and slow rotators originates from the work of Koenigl (1991) and Edwards et al. (1993) on interactions between T Tauri stars and their circumstellar disks. “Magnetic disk-locking” was introduced to provide a means to brake the spin-up of the central star by transferring angular momentum from the star to the disk (e.g. Shu et al. 1994; Najita 1995, and references therein). Accordingly, rotation-period dispersions (bimodalities) should result if some stars lose their disks faster than others (e.g. weak vs. classic T Tauri stars). Whether magnetic disk-braking is a dominant process regulating stellar rotation during the early PMS remains under debate on both observational and theoretical grounds.

Recently, taking advantage of results from an increasing number of photometric monitoring programs of late-type stars in young main-sequence clusters, Barnes (2003) presented an interpretation of his own and other published rotation period data. Free of the ambiguities of $v \sin(i)$, Barnes identified, in each coeval stellar population, separate groups of fast and intermediate/slowly rotating stars with different dependencies on color (mass). He specifically

proposed that coeval stars fall along two “rotational sequences” in the color vs. rotation period plane. From an analysis of these sequences and their dependencies on stellar age, Barnes (2003) proposed a framework for connecting internal and external magneto-hydrodynamic processes to explain the evolution in the observed period distributions, including bimodalities. This approach combines the ideas of (e.g. Stauffer et al. 1984; Soderblom et al. 1993b) of an initial decoupling of the stellar core and envelope with re-connection of the two zones through a global dynamo-field at a later and mass-dependent time. It does not (yet) interface with PMS angular momentum evolution. Importantly, Barnes (2003) also proposed that the age-dependence of the location of the rotational sequences in the color-period plane, could be used to measure the age of a stellar population, much like the sequences in the color-magnitude diagram. Barnes (2007) further developed this idea of “gyrochronology”.

Interpretation aside, it has become desirable and increasingly possible to eliminate the ambiguity of projected rotation velocities ($v \sin i$) by measuring photometric rotation periods from light modulation by spots on the surfaces of young late-type stars. While more labor and time intensive, photometric measurements of rotation periods in coeval populations, promise to reveal important details about dependencies of rotation on other stellar properties - most obviously mass and age, but likely also stellar activity, internal/external magnetic configurations, and binarity.

We present in this paper the results of an extensive time-series photometric survey for rotation periods and a decade-long spectroscopic surveys for membership and binarity for late-type stars in the field of the open cluster M35 (NGC 2168). The combination of time-series and multi-band photometry with time-series radial-velocity data enable us to explore the distribution of rotation periods vs. stellar color (mass) for *bona fide* single and binary members of M35.

M35 is a rich ($\gtrsim 2500$ stars; Barrado y Navascués et al. (2001)), ~ 150 Myr (Barrado y Navascués et al. 2001; von Hippel et al. 2002; Kalirai et al. 2003; Deliyannis 2008) northern hemisphere cluster located ~ 800 -900 pc (Barrado y Navascués et al. 2001; Kalirai et al. 2003) toward the galactic anti-center ($\alpha_{2000} = 6^h 9^m$, $\delta_{2000} = 24^\circ 20'$; $l = 186^\circ 59$, $b = 2^\circ 19$). At the distance of M35 the majority of cluster members are confined to within a $\sim 0.5^\circ$ diameter field, facilitating photometric and spectroscopic observations of a large number of stars through wide-field CCD imaging and multi-object spectroscopy. Older and much more populous than the Pleiades, and younger than the Hyades, M35 nicely bridges a gap in the age sequence of star clusters with comprehensive information about rotation and membership, permitting a more detailed study of the rotational evolution of late-type stars beyond the zero-age main-sequence (ZAMS).

We begin in Section 2 by describing our time-series photometric observations, our meth-

ods for data-reduction and for photometric period detection, and the information about cluster membership available from our spectroscopic survey and the M35 color-magnitude diagram. In Section 3 we present the distribution of rotation periods in M35, discuss the short- and long-period tails in the context of our period detection limits, and assess the stability/lifetime of spots or groups of spots by comparison of our short- and long-term photometric data. Section 4 introduces the M35 color-period diagram and the observed dependencies of stellar rotation on mass. In Section 5 we discuss and interpret the M35 color-period diagram in the context of present ideas for stellar angular momentum evolution. In particular we use the diagram to estimate spin-down rates for G and K dwarfs, to test the time-dependence on rotational evolution from a comparison with measured rotation periods in the Hyades, determine M35’s gyrochronology age, and to evaluate the best functional representation of the color-period dependence in the M35 data. Section 6 summarizes and presents our conclusions.

2. OBSERVATIONS, DATA REDUCTION, AND METHODS

2.1. Time-Series Photometric Observations

We photometrically surveyed stars in a region approximately $40' \times 40'$ centered on the open cluster M35 over a timespan of 143 days. The photometric data were obtained in the Johnson V-band with the WIYN ¹ 0.9m telescope ² on Kitt Peak equipped with a $2k \times 2k$ CCD camera. The field of view of this instrument is $20.5' \times 20.5'$ and observations were obtained over a 2×2 mosaic.

The complete dataset presented is composed of images from high-frequency (approximately once per hour for 5-6 hours per night) time-series photometric observations over 16 full nights from 2-17 December 2002, complemented with a queue-scheduled observing program over 143 nights from 22 October 2002 to 11 March 2003, obtaining one image per night interrupted only by bad weather and scheduled instrument changes. The result is a database of differential V-band light curves for more than 14,000 stars with $12 \lesssim V \lesssim 19.5$. The sampling frequency of the December 2002 observations allow us to detect photometric variability with periods ranging from less than a day to about 10 days. The long time-span

¹The WIYN Observatories are joint facilities of the University of Wisconsin-Madison, Indiana University, Yale University, and the National Optical Astronomy Observatories.

²The 0.9m telescope is operated by WIYN Inc. on behalf of a Consortium of ten partner Universities and Organizations (see <http://www.noao.edu/0.9m/general.html>)

of the queue-scheduled observations provide data suitable for detecting periodic variability of up to ~ 75 days, and for testing the long-term stability of short-period photometric variations. From this database we derive rotation periods for 441 stars.

Figure 1 shows the surveyed region (solid square) and the spatial distribution of the 441 rotators. The region is roughly coincident with that of Deliyannis (2008) in which they obtained UBVRI CCD photometry for $\sim 19,000$ stars (dashed square). Also shown is the circular target region of our spectroscopic survey described in Section 2.4 and in Meibom & Mathieu (2005). The photometric survey was carried out within the region of the spectroscopic survey to optimize information about spectroscopic membership and binarity³.

Figure 2 displays the time-series data from both programs for a photometrically non-variable star. Filled symbols represent the high-frequency observations and open symbols represent the queue-scheduled observations.

2.2. Basic Reductions, PSF Photometry, and Light Curves

Basic reductions of our CCD frames, identification of stellar sources, and computations of equatorial coordinates⁴ were done using standard IRAF packages. Instrumental magnitudes were determined from Point Spread Function (PSF) photometry using the IRAF DAOPHOT package. The analytical PSF and a residual lookup table were derived for each frame based on ~ 30 evenly distributed isolated stars. The number of measurements in the light curve of a given star vary because stars near the edges of individual frames may be missed due to telescope pointing errors, while bright stars near the CCD saturation limit and faint stars near the detection threshold may be excluded on some frames because of variations in seeing, sky brightness, and sky transparency. To ensure our ability to perform reliable time-series analysis on stars in our database, we have eliminated stars that appear on fewer than half of the total number of frames. The resulting database contains 14022 stars with a minimum of 75 measurements.

We applied the Honeycutt (1992) algorithm for differential CCD photometry to our raw light curves to remove non-stellar frame-to-frame photometric variations. We favor this technique for differential photometry because it does not require a particular set of

³All of these mutually supportive studies are parts of the WIYN Open Cluster Study (WOCS; Mathieu (2000)).

⁴We used data from the STScI Digitized Sky Survey; The Digitized Sky Surveys were produced at the Space Telescope Science Institute under U.S. Government grant NAG W-2166.

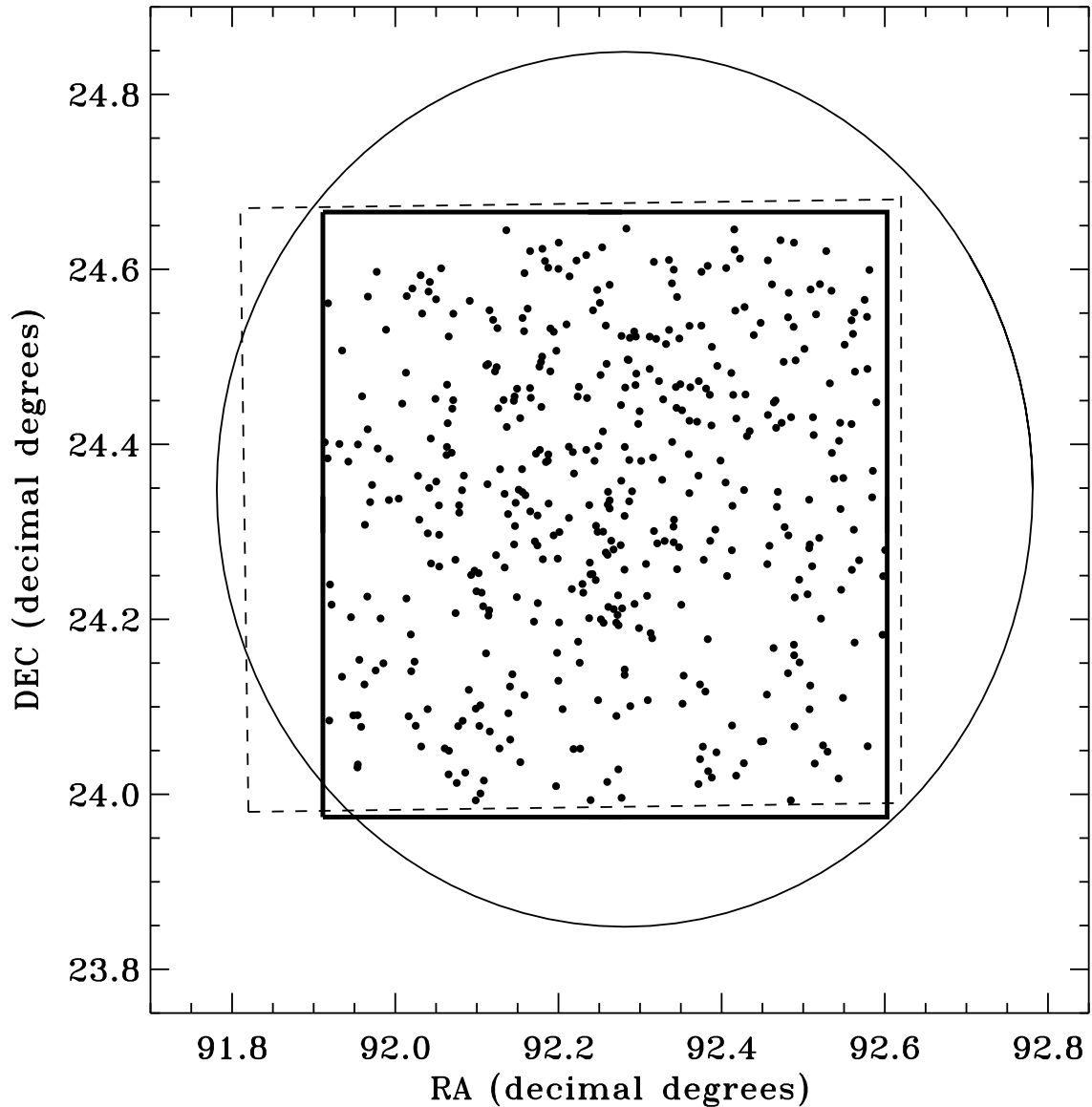


Fig. 1.— The locations and spatial extents of the photometric and spectroscopic surveys used in this study. The innermost solid square denotes the $40' \times 40'$ region of our time-series photometric survey. Within it we show the distribution of the 441 stars with measured rotation periods (black dots). The dashed rectangle displays the region of the multi-band photometric study by Deliyannis (2008) and the circle represents the 1-degree diameter field of our spectroscopic survey of M35 (Meibom & Mathieu 2005).

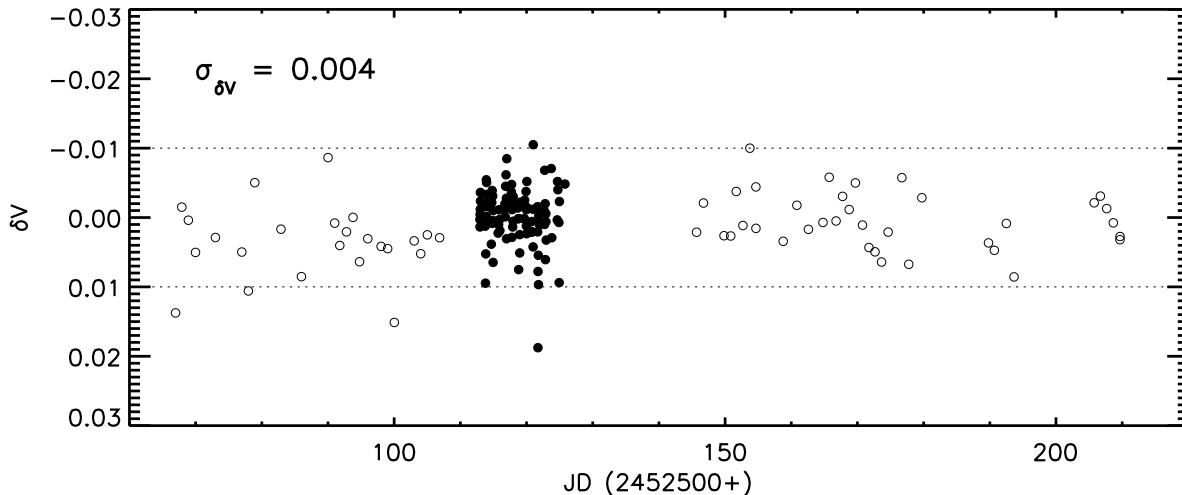


Fig. 2.— Sample time-series data from from our photometric database for a non-variable $V \simeq 14$ th magnitude star. Filled symbols represent measurements from the high-frequency December 2002 observing run and open symbols represent the low-frequency queue-scheduled observations. The data span a total of 143 days. The star was observed in all 157 images of the north-east quadrant of the 2×2 mosaic. The standard deviation ($\sigma_{\delta V}$) of the 157 measurements is $0^{\text{m}}004$, representative of our best photometric precision. The horizontal dotted lines denote $\delta V = \pm 0^{\text{m}}01$.

comparison stars to be chosen *a priori*, nor does it require a star to appear in every frame. Figure 2 shows the light curve for a $V \sim 14$ th magnitude star. The standard deviation from 157 photometric measurements is $0^{\text{m}}004$, representative of our photometric precision at that brightness. Figure 3 shows the standard deviation of the photometric measurements as a function of the V magnitude for each star in the field of M35. The relative photometric precision is $\sim 0.5\%$ for stars with $12 \lesssim V \lesssim 14.5$.

2.3. Photometric Period Detection

We employed the Scargle (1982) periodogram analysis to detect periodic variability in the light curves because of its ability to handle unevenly sampled data. We searched a grid of 5000 frequencies corresponding to periods between 0.1 day and 90 days. The lower search limit was set at a period ensuring critical sampling based on the Nyquist critical frequency for our high-frequency data ($f_c = 1/(2\delta t)$, where δt is the sampling interval of ~ 1 hour). The upper limit was set at 90 days because a star with a 90-day period would complete about

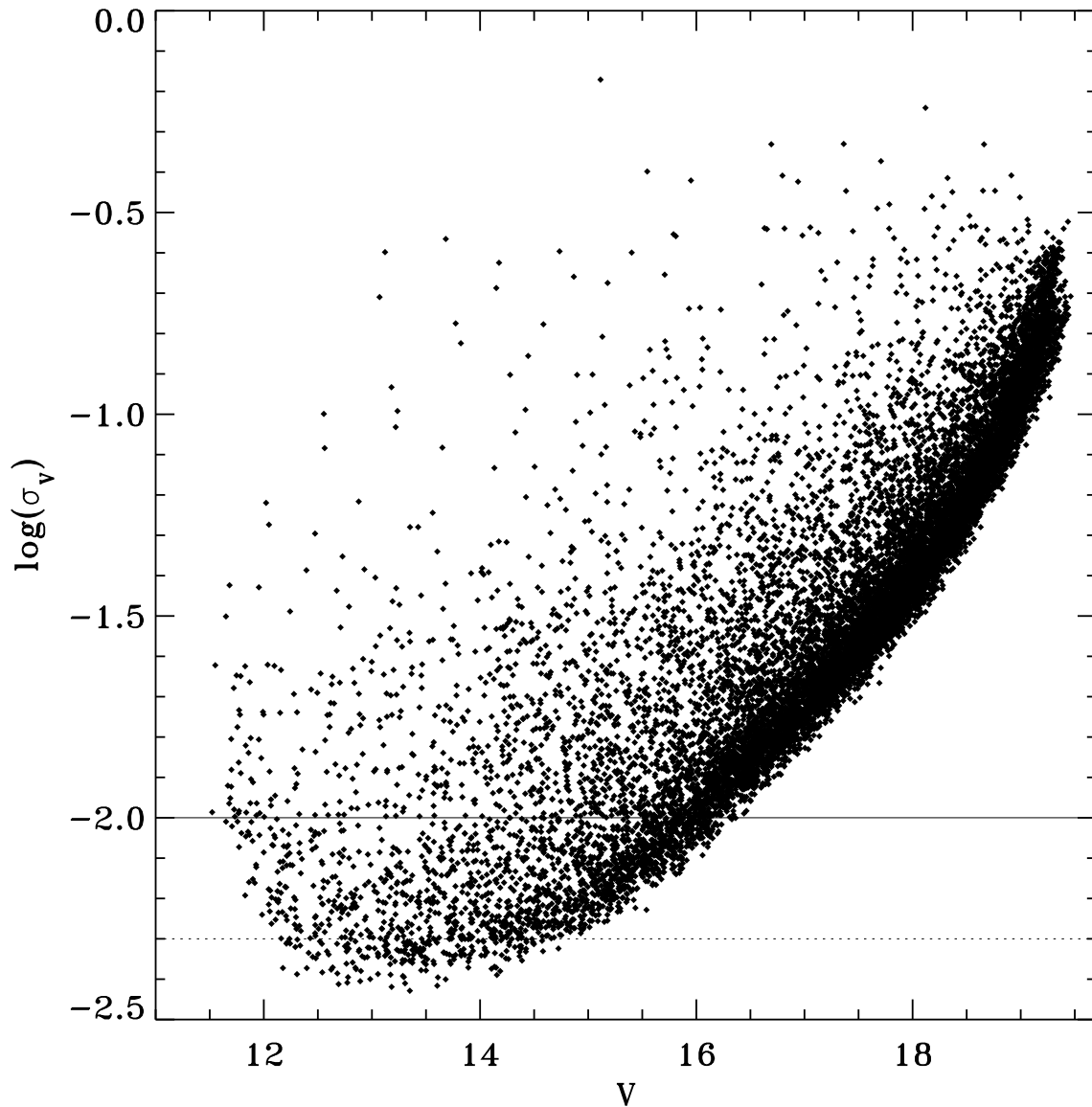


Fig. 3.— The logarithm of the standard deviation of all instrumental magnitudes as a function of V magnitude for 14022 stars in the field of M35. The number of measurements for each star range from 75 to 216. The solid and dashed horizontal lines represent σ_V of 0.01 (1%) and 0.005 (0.5%), respectively. A relative photometric precision of $\sim 0.5\%$ is obtained for stars with $12^m0 \lesssim V \lesssim 14.5^m0$.

1.5 cycle over the 143 nights of the survey.

A false alarm probability (FAP), the probability that a signal detected at a certain power level can be produced by statistical fluctuation, was calculated as the measure of confidence in a detected period. An analytical expression for estimating a FAP is given by Scargle (1982) and Horne & Baliunas (1986). However, these methods are not entirely suitable when applied to time-series photometric studies of young stars because they only test against random fluctuations of a purely statistical nature (i.e., measurement errors) and do not account for correlated fluctuations intrinsic to the source such as variability on timescales long compared to the sampling frequency. For young stars our repeated measurements during a single night are not necessarily independent and uncorrelated. Consequently, the analytical expressions estimating a FAP will likely overestimate the significance of any measured periodic variability. Hence, we performed a two-dispersion Monte Carlo calculation to estimate the FAP of our detected periods, as per Herbst & Wittenmyer (1996) and Stassun et al. (1999). For each star, we generated a set of 100 synthetic light curves, each consisting of normally distributed noise with two dispersions: one representing the variability of the star during a night and one representing the night-to-night variability of the star. The former was estimated by taking the mean of each night’s standard deviation, and the latter by taking the standard deviation of nightly means. With this approach, the test light curves can vary on timescales that are long compared to our sampling interval, allowing them to mimic the random slow variability of stellar origin that could produce spurious periodic behavior over our limited observing window. The maximum power of the 100 periodograms of the test light curves was adopted as the level of 1% FAP, and used as the initial threshold for detecting significant photometric variability. For all stars that met the FAP criterion we examined (by eye) the periodogram and raw and phased light curves. We report stellar rotation periods for 441 stars in our database (see Table 1 in Appendix B).

We do not have multiple seasons of observations or observations in multiple pass-bands at our disposal by which to confirm rotation periods of individual stars. However, the reliability of the derived periods is supported by an observed correlation between photometric period and rotational line broadening within a subset of 16 single cluster members. Figure 4 shows the projected rotation velocities measured by Barrado y Navascués et al. (2001) for 16 stars for which we have determined rotation periods. The shortest period stars ($P_r \lesssim 2.5$ days) show increasing $v \sin(i)$ with decreasing rotation period. For rotation periods of ~ 4 days or longer the upper limits on the projected rotation velocities are consistent with slower rotation. For comparison, the solid, dashed, and dotted curves in Figure 4 indicate the relation between rotation period and the projected rotational velocity for a solar-like star with a 90° , 70° , and 50° inclination of the rotational axis, respectively. Thus, for all 16 stars, the projected rotation velocities are consistent with the measured rotation periods.

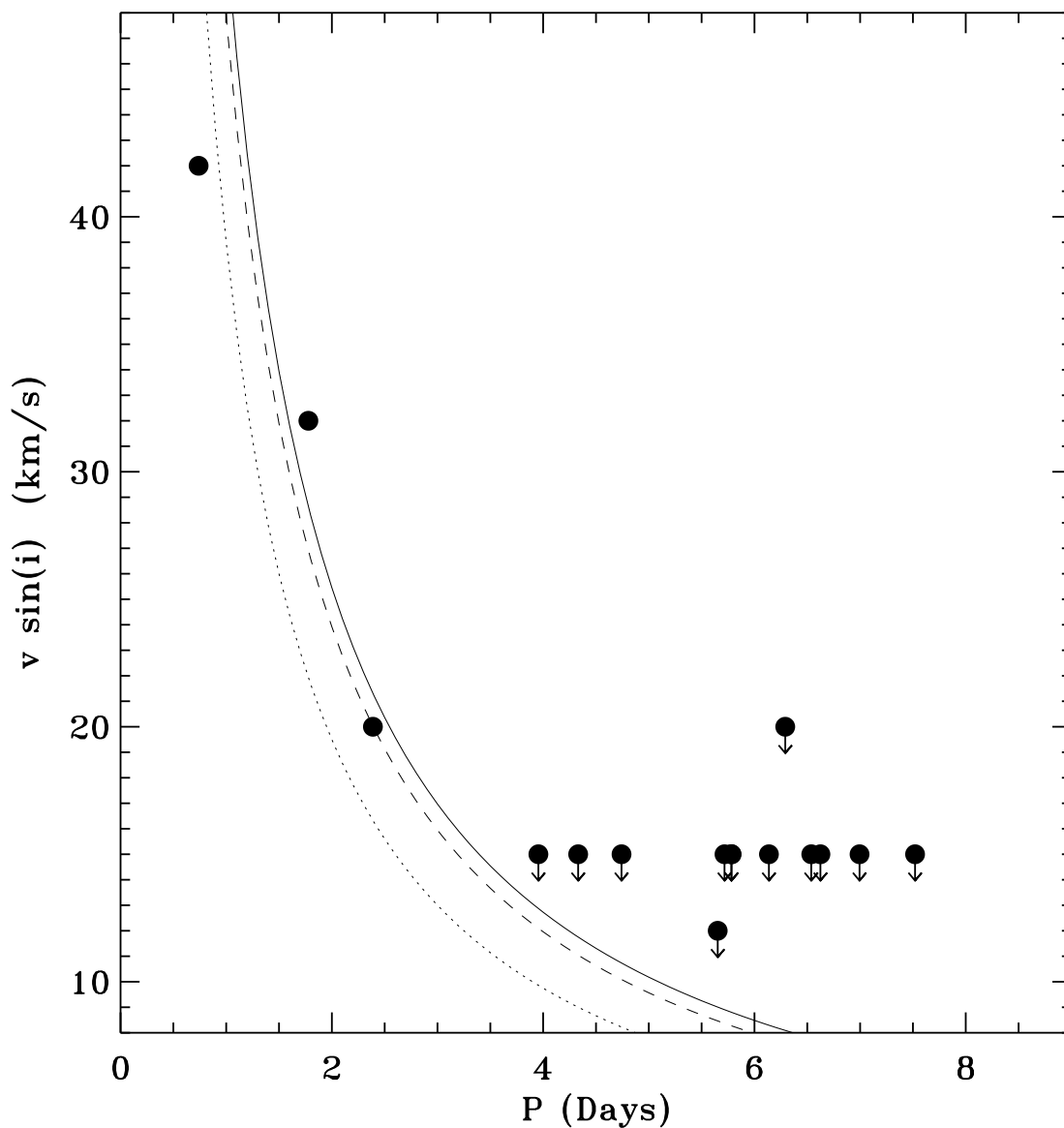


Fig. 4.— Projected rotation velocities (Barrado y Navascués et al. 2001) plotted against the measured rotation period for 16 stars in M35. All stars have $P_{RV} \geq 60\%$ and none of the 16 stars are spectroscopic binaries. For comparison, the solid, dashed, and dotted curves indicate the relation between rotation period and the projected rotational velocity for a solar-like star with a 90° , 70° , and 50° inclination of the rotational axis, respectively. The rotation periods and the projected rotation velocities are consistent for all 16 stars.

2.4. The Spectroscopic Survey

M35 has been included in the WIYN Open Cluster Study (WOCS; Mathieu (2000)) since 1997. As part of WOCS more than 6000 spectra has been obtained of approximately 1500 solar-type stars within a 1-degree field centered on M35. The selection of survey target stars was based on photometric (Deliyannis (2008), see Section 2.5) and proper-motion (McNamara & Sekiguchi 1986; Cudworth 1971) membership data. Stars on or less than $\sim 1^m0$ above the cluster main sequence were selected, with brightness and color ranges corresponding to a range in mass from $\sim 0.7 M_{\odot}$ to $\sim 1.4 M_{\odot}$. All spectroscopic data were obtained using the WIYN 3.5m telescope equipped with a multi-object fiber optic positioner (Hydra) feeding a bench mounted spectrograph. Observations were done at central wavelengths of 5130Å or 6385Å with a wavelength range of $\sim 200\text{Å}$ providing many narrow absorption lines. Radial velocities with a precision of $\lesssim 0.5 \text{ km s}^{-1}$ (Geller et al. 2008; Meibom et al. 2001) were derived from the spectra via cross-correlation with a high S/N sky spectrum. From this extensive radial-velocity survey we have 1) calculated the cluster membership probability; 2) detected the cluster binary stars; and 3) determined the orbital parameters for the closest binaries.

Of the 441 stars with rotation periods presented in this study, 259 have one or more radial-velocity measurements (the remainder being below the faint limit of the spectroscopic survey or photometric non-members). The radial-velocity cluster membership probability of each star is calculated using the formalism by Vasilevskis et al. (1958). The mean or center-of-mass radial velocity of a single or binary star was used when calculating the membership probability. We have adopted 50% as the threshold for assigning radial-velocity and proper-motion cluster membership. Of the 259 rotators with one or more radial-velocity measurement, 203 are radial-velocity members of M35 and 20 of those 203 stars are also proper-motion members. More detailed descriptions of the radial-velocity survey and membership determination can be found in Meibom & Mathieu (2005), Meibom et al. (2006), and Braden et al. (2008).

2.5. The M35 Color-Magnitude Diagram and Photometric Membership

Figure 5 shows the (V-I) vs. V color-magnitude diagram (CMD) for M35. The photometry was kindly provided by Deliyannis (2008) who obtained UBVRI data in a $23' \times 23'$ central field and BVRI data in a 2×2 mosaic for a total of $\sim 40' \times 40'$ using the WIYN 0.9m telescope. In the CMD the 441 stars for which we have measured rotation periods are highlighted in black. The solid lines enclosing stars within or above the cluster sequence (allowing for inclusion of equal-mass binaries) show our criteria for photometric member-

ship. The insert in Figure 5 shows the location in the M35 CMD of only radial-velocity members (open symbols), and radial-velocity and proper-motion members (filled symbols), the location of which was used to define the criteria for photometric membership. There are 23 photometric members have 3 or more radial-velocity measurements and a radial-velocity membership probability of less than 50%. Those 23 stars were also removed from the list of cluster members. The final number of stars with measured rotation periods selected as radial-velocity and/or photometric members of M35 is 310.

3. THE ROTATION-PERIOD DISTRIBUTION

The 310 members of M35 with determined rotation periods correspond to $\sim 12\%$ of the photometric cluster population within the brightness and areal limits of our photometric survey. Figure 6a shows the distribution of rotation periods, which spans more than 2 orders of magnitude from ~ 0.1 days to ~ 15 days. The distribution peaks shortward of 1 day and has a broader and shallower peak centered at about 6 days.

Figure 6b displays with an increased resolution of 0.1 day the distribution of rotation periods shortward of 1 day. The dashed and grey histograms, respectively, represent all stars and all cluster members with detected rotation periods. The distribution shows that we are capable of detecting rotation periods down to the pseudo-Nyquist period-limit of about 2 hours (~ 0.08 day) resulting from our typical sampling cadence of about 1 hr^{-1} in December 2002. The distribution of rotation periods for cluster members falls off shortward of 0.3-0.4 days. Two member stars have rotation periods between 0.1 days and 0.2 days, corresponding to surface rotational velocities of 50% or more of their breakup velocities ($v_{br} = \sqrt{GM_{\star}/R_{\star}}$). We argue based on this inspection of the short-period tail of the distribution that the lower limit of 0.1 days for our period search was set appropriately for the stars in M35.

The long-period ends of the period distributions for members and non-members (Figure 14, Appendix C) show that the long time-span of the queue-scheduled data enable us to detect rotation periods beyond the ~ 10 days typically found to be the upper limit in photometric surveys with durations similar to our short-term December 2002 observing run. We report the detection of 18 stars with rotation periods longer than 10 days, 7 of which are members of M35. The longest rotation period among members is 15.3 days, and among the field stars rotation periods of up to ~ 17 and 23 days have been measured. In the M35 period distribution we see a drop-off at ~ 10 days. If the $\sim 12\%$ of the cluster’s late-type population with measured rotation periods is a representative sample of the late-type stellar population in M35, then the ~ 10 day cutoff may represent a physical upper limit on the

rotation-period distribution at 150 Myr. However, it is also possible that we are not capable of detecting the slowest rotators despite our long-baseline photometric survey. Indeed, the modest number of rotation periods longer than 10 days found in the much larger sample of field stars may reflect that the frequency and size of spots on stars rotating slower than ~ 10 days is insufficient for detection with the photometric precision of our data. Indeed, X-ray observations in Orion (Stassun et al. 2004) indicate that rotation-period studies of young stars may in general be biased against very slow rotators because such stars likely do not generate strong activity, and thus are not sufficiently spotted to allow detection of photometric periods.” Measuring the rotation for such slowly rotating stars will likely require either higher photometric precision or high resolution ($R \gtrsim 50,000$) spectroscopic observations to measure projected rotation velocities. The small sample of M35 member stars with periods above 10 days will be discussed in Section 5.5.

3.1. Long-term stability of the number, sizes, and configurations of stellar spots and spot-groups

We find that for almost all cluster and field stars with measured rotation periods, the long-term queue-scheduled data, spanning ~ 5 months in time, phase up with and coincide with the short-term data (16 nights in December 2002) in the light curves. We tested further the agreement between the short-term and long-term photometric variability, by measuring the rotation period separately from the short- and long-term data for 20 randomly chosen stars. For all but one star we found a difference between the two rotation periods that was less than 1% of the period measured from the short-term data alone (in most cases the difference was less than 0.1%). We examined the 20 light curves with all data phased to the period derived from only the short-term data. For all but one star, the long-term data produced light curves of the same shape and phase as the light curves based only on the short-term data. Even for two light curves with clear signs of multiple spots (spot-groups), the short- and long-term data coincided very well. Because it is unlikely that the disappearance and recurrences of spots will result in a light curve with the same shape, amplitude, and phase, the agreement suggests stability of individual spots and/or spot-groups over the ~ 5 month time-span of our photometric observations.

We find that the stability of the sizes and configurations of spots on young stars have recently been studied for e.g. the solar analog PMS star V410 Tau (Stelzer et al. 2003) and for stars in the PMS cluster IC348 (Nordhagen et al. 2006). For V410 Tau data has been collected for over two decades, showing changes in the shape of the light curve over the last decade. The authors suggest that the observed changes reflect variations of the structure of

the active regions over timescales of years. However, stability in the rotation period and the recurrence of the light curve minimum, suggest stability of the largest spots over years, and either a lack of latitudinal differential rotation in V410 Tau, or confinement of its spots to a narrow range of latitudes. Similarly, Nordhagen et al. (2006) finds a remarkable stability over 7 years in the rotations periods for stars in IC348, suggesting again that these PMS stars do not have significant differential rotation, or that their spots are constrained to a narrow range of stellar latitudes. However, contrary to what is observed over 5 months in M35, all periodic stars in IC348, as well as V410 Tau, do show changes in the light curve shape and amplitude from year to year.

4. THE M35 COLOR-PERIOD DIAGRAM - THE DEPENDENCE OF STELLAR ROTATION ON MASS

In Figure 7 we display the rotation periods for the 310 members plotted against their $B - V$ color indices, or equivalently their masses. The color indices derive from the deep multi-band photometry by Deliyannis (2008, Section 2.5) and the corresponding stellar mass estimates (upper x-axis) from a fit of a 150 Myr Yale stellar evolutionary model (Yi et al. 2003) to the M35 color-magnitude diagram. The largest plotting symbols are used for radial-velocity members of M35 with more than one velocity measurement. Smaller symbols are used for members with only one radial-velocity measurement, and the smallest symbols represent photometric members. Proper-motion members are marked with additional squares.

The M35 color-period diagram shows striking structure. The coeval stars fall along two well-defined sequences apparently representing two different rotational states. One sequence displays clear dependence between period and color, starting at the blue end at $(B - V)_0 \simeq 0.5$ ($M_\star \simeq 1.2 M_\odot$) and $P_{rot} \simeq 2$ days and forming a rich diagonal band of stars whose periods are increasing with increasing color index (decreasing mass). This sequence terminates at about $(B - V)_0 \simeq 1.2$ ($M_\star \simeq 0.65 M_\odot$) and $P_{rot} \simeq 10$ days. The second sequence consists of rapidly rotating ($P_{rot} \lesssim 1$ day) stars and extends from $(B - V)_0 \simeq 0.7 - 0.8$ ($M_\star \simeq 0.9 - 1.0 M_\odot$) to $(B - V)_0 \simeq 1.5$ ($M_\star \lesssim 0.5 M_\odot$). This well defined sequence of rapidly rotating stars shows a small but steady decrease in rotation period with increasing color (decreasing mass). Finally, a subset of stars are distributed in between the two sequences, and 10 stars have rotation periods that are unusually long, placing them above the diagonal sequence in Figure 7.

The M35 color-period diagram gives a clear picture of preferred stellar rotation periods as a function of color for 150 Myr late-type dwarfs. With the added dimension of color, the diagram take us beyond the one-dimensional period distribution and shows which stars are responsible for the structure observed in Figure 6. The short-period peak at $\lesssim 1$ day is due

primarily to the rapidly rotating late G- and K-dwarfs ($M \lesssim 0.9 M_{\odot}$), and the sharpness of this peak is the result of little dependence of rotation on color within this group. The more slowly rotating mid to late G- and K-dwarfs give rise to the broader peak at ~ 6 days, while the early to mid G-dwarfs and some cooler stars fill in the distribution between the peaks.

The two sequences of stars in the color-period diagram represent the most likely/stable rotation period(s) for a given stellar mass at the age of M35. Under the assumption that rotation periods increase with time for all stars, the more sparsely populated area between the two sequences must then represent a phase of rotational evolution of shorter duration. We will discuss the different loci in the color-period diagram in more detail in Section 5.

5. ANGULAR MOMENTUM EVOLUTION AND THE COLOR-PERIOD DIAGRAM

Sequences similar to those observed in the M35 color-period diagram were noted by Barnes (2003, hereinafter B03) from careful examination of compilations of rotation-period data from photometric monitoring campaigns on open clusters and field stars. B03 named the diagonal sequence of stars on which rotation periods increase with color the *interface* sequence (or I sequence), and the sequence of rapidly rotating stars the *convective* sequence (or C sequence). In what follows we will adopt these names for the two sequences in the M35 color-period diagram.

B03 argues that the rapidly rotating stars on the C sequence have radiative cores and convective envelopes that are decoupled. For these stars he suggests that the evolution of their surface rotation rates is governed primarily by the moments of inertia of the convective envelope and by inefficient wind-driven loss of angular momentum linked to small-scale convective magnetic fields. For stars on the I sequence, large-scale (sun-like) magnetic fields provided by an interface dynamo couple the core and envelope, and the rotational evolution of the I sequence stars is thus primarily governed by the moments of inertia of the entire star and more efficient angular momentum loss (i.e., a Skumanich (1972) style spin-down). Accordingly, B03 suggests that a late-type star, in which the core and envelope are decoupled as it settles on the ZAMS, will begin its main-sequence life on the C sequence and evolve onto the I sequence when rotational shear between the stellar core and envelope establish a large-scale dynamo field that couples the two zones and provide efficient magnetic wind loss. Higher mass stars have thinner convective envelopes with smaller moments of inertia than low mass stars and thus leave the C sequence sooner. Stars that are either fully radiative or fully convective will remain as rapid rotators.

Color-period diagrams for coeval populations of different ages allow us to examine the rotational properties of late-type coeval stars as a function of their mass and age, and may bring us closer to understanding the physical mechanisms (internal and/or external) regulating their rotational evolution. The M35 color-period diagram, rich in stars and cleaned for spectroscopic and photometric non-members, reveals the morphology described by B03 more clearly than any published stellar populations. We therefore begin with a discussion of the M35 result in the context of the framework developed by B03.

5.1. Timescales for migration from the C to the I sequence

In Figure 8 we add M35 to Fig. 3 in B03 which shows the relative fractions of stars with $0.5 \leq (B - V)_0 \leq 1.5$ on the I and C sequences for stellar populations of distinct ages. With rotation periods measured over more than two orders of magnitude for confirmed spectroscopic and photometric cluster members, M35 adds the statistically most secure datapoints to this figure. M35 fit well with the evolutionary trends of increasing relative fractions of C sequence (and gap) stars and decreasing fractions of I sequence stars for younger cluster populations. The almost linear trends in Figure 8 suggest that the decrease and increase in the number of stars on the C and I sequences, respectively, are approximately exponential with time. Under the presumption of an exponential time dependence and that all stars start on the C sequence at the ZAMS, we can estimate the characteristic timescale for the rotational evolution of stars off the C sequence and onto the I sequence, by counting stars on both sequences and in the gap in the M35 color-period diagram. Such timescales may offer valuable constraints on the rates of internal and external angular momentum transport and on the evolution rates of stellar dynamos in late-type stars of different masses.

When counting the number of stars on the I and C sequences and in the gap, we use the following criteria. Stars located in the color-period diagram between the lines represented by $P_{rot} = 10(B - V)_0 - 2.5 \pm 2.0$ and with periods above 1.5 days were counted as I sequence stars (see dotted lines in Figure 11). Stars redder than $(B - V)_0 = 0.6$ and with periods between 0 and 1.5 days were counted as C sequence stars. Stars located below $P_{rot} = 10(B - V)_0 - 4.5$ and with periods above 1.5 days were counted as gap-stars. These selection criteria are subjective and although the sequences are well defined, the I sequence becomes broader redward of $(B - V)_0 \simeq 1.0$ making the distinction between I sequence and gap stars more difficult. However, due to the large number of rotation periods in M35, the small number of stars that might be moved from the gap to the I sequence or vice versa by using slightly different criteria will not influence the relative fractions and thus the timescales in any significant way.

The number of C sequence stars (N_c) at a time t can then be expressed by:

$$N_c = N_{c_0} e^{-t/\tau_c} \quad (1)$$

where N_{c_0} and τ_c are, respectively, the total number of stars on the I and C sequences and in the gap, and the characteristic exponential timescale. We use the B-V color index to divide the stars into G-dwarfs ($0.6 < B - V < 0.8$) and K-dwarfs ($0.8 < B - V < 1.3$), and adopt 150 Myr as the age of M35. We derive from equation [1] $\tau_c^G = 60$ Myr and $\tau_c^K = 140$ Myr as the characteristic exponential timescales for transition between the C and the I sequence for G and K dwarfs, respectively.

We can qualitatively verify these time scales by a comparison between the M35 color-period diagram and those of the younger Pleiades cluster and the older cluster NGC3532 presented in B03. In M35 only 7 G dwarfs ($0.6 \lesssim (B - V)_0 \lesssim 0.8$) are found on the C sequence and in the gap, while the G dwarf I sequence is well defined and rich. In contrast, In contrast, the M35 C sequence and gap are rich in K dwarfs ($0.8 \lesssim (B - V)_0 \lesssim 1.3$), whereas the K dwarf I sequence is less densely populated and less well defined. The lack of G dwarfs on the C sequence seen in M35 is already apparent at 100 Myr in the Pleiades color-period diagram, indicating that the characteristic timescale for G dwarfs to evolve off the C sequence and onto the I sequence is less than ~ 100 -150 Myr. The rich population of early and mid K dwarfs on the M35 C sequence have evolved off the C sequence and onto a well defined I sequence by the age of NGC 3532 (300 Myr). The NGC 3532 C sequence and gap, however, are populated by late K dwarfs, suggesting that early to mid K dwarfs evolve onto the I sequence on a timescale between 150 and 300 Myr, or approximately twice the time required for G dwarfs. Finally, by the age of the Hyades only 3 late K or early M dwarfs have been found off the I sequence, or in the gap (see Fig. 1 in B03 or Figure 9 below), suggesting that such stars evolve off the C sequence and possibly onto the I sequence on a timescale of ~ 600 Myr, or approximately twice the time required for the early to mid K dwarfs.

There is thus good agreement between the exponential timescales derived from the M35 color-period diagram alone and the estimated timescales based on a comparison of color-period diagrams of different ages. We note that although the relative fractions displayed in Figure 8 represent all rotators with $0.5 \leq (B - V)_0 \leq 1.5$, a least-squares fit of an exponential function to the C sequence fractions in Figure 8, gives a timescale of 106 Myr for a decrease in the number of C sequence stars by a factor of e .

5.2. Testing the Skumanich \sqrt{t} spin-down rate between M35 and Hyades

The color-period diagram for the Hyades contains 25 stars (Radick et al. 1987; Prosser et al. 1995), 22 of which form an I sequence of G and K dwarfs. Despite the smaller number of stars, the blue part of the Hyades I sequence, populated by G dwarfs, is well defined. By comparing the rotation periods for the I sequence G dwarfs in M35 to those of the I sequence G dwarfs in the ~ 4 times older Hyades, we can directly test the Skumanich (1972) \sqrt{t} time-dependence on the rotation-period evolution for stars in this mass-range. We follow B03 in assuming separate mass and time dependencies for stellar rotation, and that the same mass dependence can be applied to different stellar populations. Adopting an age of 625 Myr for the Hyades (Perryman et al. 1998) and of 150 Myr for M35, we decrease the Hyades rotation periods by $\sqrt{625/150} \simeq 2$. We show in Fig. 9 the color-period diagram with the 310 M35 members (all grey symbols) and with the locations of the 25 Hyades stars overplotted (black symbols). The spun-up Hyades I sequence G dwarfs coincide nicely with the M35 I sequence G dwarfs, in support of the Skumanich \sqrt{t} time-dependence for such stars. Curiously, the Hyades K-dwarfs, also spun-up according to the Skumanich law, have rotation periods systematically shorter than the M35 K dwarfs. At face value, this suggests that the time-dependence for spin-down of K dwarfs is different and slower than for G dwarfs between 150 Myr and 625 Myr.

5.3. The gyro-age of M35 - fitting rotational isochrones to the M35 color-period diagram

Arguing that the rotation of stars on the C and I sequences follow separate mass (M) and age (t) dependencies ($P(t, M) = g(t) \times f(M)$), B03 introduced heuristic functional forms to represent these separate dependencies of the I and C sequences. Barnes (2007, hereinafter B07) presents a modified functional form for the I sequence. These functions define one-parameter families, with that parameter being the age of the stellar population, and the resulting curves in the color-period plane represent a set of rotational isochrones.

The well-defined sequences in the M35 color-period diagram make possible a test of the rotational isochrones proposed in B03 and B07. We show in Figure 10 the M35 color-period diagram with the B03 and B07 rotational isochrones for the independently determined stellar-evolution age for M35 of 150 Myr (von Hippel et al. 2002; Deliyannis 2008). The rotational isochrones match the M35 I and C sequences well, suggesting that they can indeed provide a consistent age estimate (gyro-age) for a cluster based on a well populated color-period diagram cleaned for non-members. To illustrate the sensitivity to age, rotational isochrones for 130 Myr and 170 Myr are also displayed in Figure 10.

Assuming no prior knowledge about the age of M35 (thus letting age be a free parameter), we perform a non-linear least squares fit to the I sequence stars (enclosed by the dotted lines in Figure 11) of the functional form of the rotational I sequence isochrones from B03:

$$P(t, (B - V)) = \sqrt{t} \times (\sqrt{((B - V) - a)} - b((B - V) - a)) \quad (2)$$

with $a = 0.50$, and $b = 0.15$, and from B07:

$$P(t, (B - V)) = t^{0.52} \times (c((B - V) - d)^f) \quad (3)$$

with $c = 0.77$, $d = 0.40$, and $f = 0.60$.

When fitting, the I sequence stars were weighted according to their cluster membership with most weight given to confirmed radial-velocity and proper motion members and least weight given to stars with only photometric membership. The weights given to individual stars are listed in Table ?? in Appendix B. We show in Figure 11 the best fits of both eq. [2] and eq. [3] to the M35 I sequence. The derived age is 134 Myr for both functional forms, each with a $1 - \sigma$ uncertainty of ~ 3 Myr. The close agreement of the two ages likely reflects the similar shape of the two isochrones over the color interval from $\sim 0.5 - 1.0$ where the M35 I sequence is most densely populated. The small formal uncertainties reflect a well-defined I sequence rich in stars. However, the gyro-ages may still be affected by systematic errors in the stellar evolutionary ages for the young open clusters.

5.4. Improving the I sequence mass-rotation relation using M35

The method of gyro-chronology relies on fitting the I sequence rotational isochrone, with age as a free parameter, to populations of cluster stars or to individual field stars in the color-period plane B07. The functional dependence between stellar color and rotation period of the isochrone will thus directly affect the derived gyro-age, and will, if not accurately determined, introduce a systematic error. It is therefore important to constrain and test the mass-rotation relation for stars on the I sequence as new data of sufficiently high quality becomes available.

Our data for M35 are well suited for such a test because of the rich and well-defined I sequence, the extensive knowledge about cluster membership, and the independent stellar evolution age for the cluster. To constrain the color-period relation, we fit equations [2] and [3] to the M35 I sequence, using the same selection of stars and the same fitting weights as

described in Section 5.3. We determine all coefficients in equations [2] and [3] for the fixed cluster age (t) of 150 Myr. The coefficients with 1σ uncertainties are listed in Table 1 and the corresponding rotational isochrones are shown in Figure 12. To illustrate how closely the isochrones trace the selected I sequence stars, Figure 12 also displays a dashed curve representing the moving average of the rotation periods along the I sequence.

We can compare the coefficients derived using the M35 data to those chosen and/or derived by B03 and B07. Our best fit of the B03 isochrone confirms the value of 0.5 for the a coefficient chosen (not fitted) by B03 to best represent the color-period data included in his study. a is a translational term that determines the color for which the isochrone gives a period of zero days. For the b coefficient our best fit give a value of 0.20 compared to the choice of 0.15 by B03. Our larger value of the b coefficient results in an isochrone with slightly more curvature.

From our best fit of the B07 rotational isochrone to the M35 I sequence, we determined a c coefficient of 0.77, equal to the value used by B07, while our value 0.55 for the f coefficient is smaller than the value of 0.60 used by B07. In the case of the c and f coefficients, B07 also determined their values from least squares fitting to the I sequence stars of several young open clusters. However, for the translational term d , he chose a fixed value of 0.4 to allow for more blue stars to be fitted. We left the d coefficient as a free parameter when fitting to the M35 I sequence, and got a value of 0.47.

The new value of 0.47 for d is particularly interesting as it corresponds to the approximate $B - V$ color for F-type stars at the transition from a radiative to a convective envelope. This transition was noted from observations of stellar rotation (known as the break in the Kraft curve (Kraft 1967)), and is associated with the onset of effective magnetic wind breaking (e.g. Schatzman 1962). The value of 0.47 for the d coefficient therefore suggest that, for M35, the blue (high-mass) end of the I sequence begins at the break in the Kraft curve.

5.5. Prediction: Tidal Evolution is Responsible for the Unusually Slow Rotators

Ten stars fall above the M35 I sequence, and thus rotate unusually slowly in comparison to other members of M35 with similar masses. All 10 stars are photometric members of M35 and 2 are also spectroscopic members. We have no reason to believe that the rotation periods for these stars are due to aliases in the power spectra, and we note that a similar pattern is seen in NGC 3532 with 7 stars located above the I sequence B03 and in M34 with 6 stars above the I sequence (Meibom et al. 2008).

What causes the rotational evolution of these stars to deviate significantly from that of most similar-color stars in M35? We propose here that tidal interactions with a close stellar companion has acted to partially or fully synchronize the stellar spins of these stars to the orbital motions, and that such tidal synchronization is responsible for their slower-than-expected rotation. We thus predict that these 10 stars are the primary stars in binaries with periods of ~ 10 -15 days.

This proposition finds support from the star of M35 located in the color-period diagram at $(B - V)_0 = 0.68$ and $P_{rot} = 10.13$ days. This star is the primary in a circular binary with an orbital period of 10.33 days. The rotation of this star has been synchronized to the orbital motion of the companion (Meibom et al. 2006), forcing it to rotate more slowly than stars of similar mass. In addition to the spectroscopic binary, 3 of the remaining 9 slow rotators are photometric binaries. Spectroscopic observations has begun of those stars and of the remaining 5 stars as of fall 2007 to determine their status as binary or single stars, and in the case of binarity, the degree of tidal evolution.

5.6. Stellar angular momentum evolution near the ZAMS

The trend in Figure 8 of an increasing fraction of C sequence (and gap) stars for younger cluster populations leads naturally to the suggestion that most, if not all, late-type stars pass through a phase of rapid rotation (the C sequence) at the ZAMS. We note that even should this be the case, an *observed* C sequence fraction of 1 is not expected for even the youngest coeval populations, as stars of different masses will reach the ZAMS, and thus hypothetically the C sequence, at different times. For example, late-F stars will be the first to arrive at/on the ZAMS and C sequence, and leave it before the arrival of G and K type stars.

Table 1. New coefficients for the I sequence rotational isochrones

Isochrone	Coefficient	Value	1σ error
B03	a	0.507	0.005
B03	b	0.204	0.013
B07	c	0.770	0.014
B07	d	0.472	0.027
B07	f	0.553	0.052

The color-period diagrams for the youngest stellar populations presented in Figure 8 (see also Figure 1 in B03) show that most stars lay either on the C sequence or in the gap. B03 finds only 25% of the stars at 30 Myr to be on the I sequence. In fact the I sequence is not clearly identifiable at this age, and the stars identified as being on the I sequence are early-type rapid rotators near the intersection of the two sequences.

By 30 Myr very few of the cluster members have rotation periods longer than 5 days. This is in marked contrast to fractions of $\sim 60\%$ and $\sim 40\%$, respectively, for such slow rotators in the PMS populations of the Orion Nebula cluster (ONC) and NGC 2264 (see Herbst et al. 2007). The difference in the numbers of slowly rotating stars pre- and post-ZAMS, suggests that most, if not all, of the stars rotating slowly at $\sim 1\text{-}3$ Myr, spin up as they evolve onto the ZAMS. Such spin-up may have been observed. Comparison of the rotation period distributions for stars in the ~ 1 Myr ONC and the $\sim 2\text{-}3$ Myr NGC 2264 (Herbst et al. 2007, and references therein) shows a spin-up with time by a factor ~ 2 , presumably due to conservation of angular momentum as the stars contract on the PMS. On the other hand, the distribution of a smaller sample of rotation periods in the $\sim 2\text{-}3$ Myr IC 348 (Nordhagen et al. 2006) does not show similar evidence for spin-up when compared to the ONC.

From the point of view of modeling stellar angular momentum evolution, we emphasize the narrowness of the C sequence, with all rotation periods between 0.5 days and 1.5 days. We suggest that the broad distribution of rotation period among solar-like stars in the PMS populations must collapse into a narrow C sequence of similar rotation periods independent of mass. Indeed, we suggest that in the two 30 Myr clusters of B03 (Figure 1), the gap stars with $(B - V)_0 \gtrsim 0.9$ may in fact be evolving *toward* the C sequence, and point out that in the 50 Myr clusters in B03, mostly C sequence stars are observed redward of $(B - V)_0 \simeq 0.9$.

6. SUMMARY AND CONCLUSIONS

We present the results of an extensive time-series photometric survey over ~ 5 months of late-type members in the 150 Myr open cluster M35 (NGC 2168). We have obtained photometric light curves for 14022 stars with $12 \lesssim V \lesssim 19.5$ over a $40' \times 40'$ field centered on M35. We have determined the rotation periods for 441 stars. Cluster membership and binarity for stars with rotation periods are determined from the results of a decade long spectroscopic survey in M35. Of the 441 rotators 310 stars are radial-velocity and/or photometric members of M35.

With an age slightly older than the Pleiades but with a much larger population of late-type stars, M35 is particularly interesting for studying stellar rotational evolution during this

active phase of angular momentum evolution between the ZAMS and the age of the Hyades. The rotation periods of the 310 late-type members span over two orders of magnitude from 0.1 day (\gtrsim 50% of their breakup velocities), up to \sim 15 days. A drop-off in the period distribution is found at \sim 10 days, well below the upper limit of our period search. The \sim 10-day cutoff may represent a physical upper limit on the rotation-period distribution at 150 Myr. However, it is also possible that detecting more slowly rotating stars in M35 will require higher photometric precision or higher resolution spectroscopic observations.

We find in the phased light curves for almost all stars with measured rotation periods that the long-baseline (\sim 5 months), low-frequency (1/night) photometric measurements match the short-baseline (16 nights), high-frequency (\sim 1/hours) measurements in both phase, shape, and amplitude. Further tests on a subset of stars show that the same rotation periods are derived from the short- and long-term data to within 1%. This stability in the modulation of the stellar brightness suggest a similar stability in the configuration, size, and number of starspots.

In the color-period plane, the 310 M35 rotators reveal striking dependencies between surface rotation period and stellar color (mass). More than 75% of the stars lay along two distinct sequences in the color-period diagram, apparently representing two different states in their rotational evolution. Similar sequences were identified by Barnes (2003) for stars in other clusters. Comparison between M35 and these clusters of the locations of the sequences in color-period diagram, as well as the relative numbers of stars on each, support for the idea (proposed by Barnes (2003)) that stars evolve from one sequence (C) to the other sequence (I) at a rate that is inversely proportional to the stellar mass.

We determine from the M35 color-period diagram that the characteristic exponential timescale for rotational evolution off the C sequence and onto the I sequence is \sim 60 Myr and \sim 140 Myr for G and K dwarfs, respectively. These timescales may offer valuable constraints on the rates of internal and external angular momentum transport and on the evolution rates of stellar dynamos in late-type stars of different masses.

From the emerging trend (supported by M35) of an increasing relative fraction of rapidly rotating C sequence stars with decreasing population age, we propose the hypothesis that most, if not all, late-type stars pass through a phase of rapid rotation (C sequence) on the ZAMS. By conjecture, there may not be a need for a direct connection between slowly rotating stars observed in the early PMS and slowly rotating stars at \sim 100 Myr post the ZAMS. Such a connection has often been assumed and set as a constraint on models of stellar angular momentum evolution, motivating the introduction of mechanisms to prevent slowly rotating PMS stars from spinning up as they evolve onto the main-sequence.

By comparison with measured rotation periods in the Hyades, we put to the test the empirical Skumanich \sqrt{t} time-dependence on the stellar rotation period for G dwarfs. By reducing the Hyades rotation periods by a factor $\sqrt{Age_{Hyades}/Age_{M35}}$ we find that the \sqrt{t} law accounts very well for the rotational evolution of G dwarfs between M35 and the Hyades, whereas among the K dwarfs the \sqrt{t} time-dependence predicts a spin-down rate that is faster than observed between M35 and the Hyades.

We find that the heuristic rotational isochrones proposed by Barnes (2003) and Barnes (2007) match the location of M35 I and C sequences using the independently determined stellar evolution isochrone age for M35. A non-linear least-squares fit of the rotational isochrones to the M35 I sequence sets the cluster’s gyro-age to 134 Myr with a formal 1σ uncertainty of 3 Myr. These results suggest that a well-populated color-period diagram, cleaned for non-members, in combination with the rotational isochrones by Barnes, can provide a precise age estimate that is consistent with the age derived from isochrone fitting in the CMD. We also use the M35 I sequence to improve the coefficients for the color-dependence of the rotational isochrones.

Finally, to explain the ten M35 stars rotating with rates that are unusually slow compared to similar stars in the cluster, we propose that tidal synchronization in binary stars with orbital periods of order 10-15 days is responsible. Two of the 10 stars have already been found to be primary stars in tidally evolved spectroscopic binaries, while 3 other stars are photometric binaries. Accordingly, we predict that the remaining stars are also primary stars in spectroscopic binaries with orbital periods of \sim 10-15 days.

We wish to thank the University of Wisconsin - Madison Astronomy Department and NOAO for the time granted on the WIYN 0.9m and 3.5m telescopes. We express our appreciation to the site managers and support staff at both telescopes for their exceptional and friendly support. We are thankful to all observers in the WIYN 0.9m consortium who provided us with high-quality data through the queue-scheduled observing program. This work has been supported by NSF grant AST-0406615 to the UW-Madison, a Ph.D fellowship from the Danish Research Academy to S.M., partial support to S.M. from the Kepler mission via NASA Cooperative Agreement NCC2-1390, and by the Cottrell Scholarship from the Research Corporation to K.G.S.

A. PHASED LIGHT CURVES

This appendix presents in Figure 13 the light curves for the 441 stars in the field of M35 for which we measured rotation periods. The light curves have been divided into 3 groups according to the amplitude of the photometric variation. For each group the light curves are sorted by the rotation period and are presented with the same δV range on the ordinate. The group of stars with the largest photometric variability are shown first.

For each star we plot the data from the high-frequency survey (December 2002) as black symbols and data from the low-frequency survey (October 2002 through March 2003) as grey symbols. A running ID number corresponding to the ID number in Table 1 Appendix B is given in the upper left hand corner in each plot. The period to which the data are phased (the rotation period listed in Table 1 as P_{rot}) is given in the upper right corner. The 2-5 letter code in the lower right corner informs about the stars membership status. The codes have the following meaning: Photometric Member (PM; described in Section 2.5), Photometric Non-Member (PNM), Photometric and Spectroscopic Member (PSM), Photometric and Proper-motion Member (PPM), and Photometric Member but Spectroscopic Non-Member (PMSNM). For each star a horizontal grey line in each plot mark $\delta V = 0.0$ and a vertical grey line marks a phase of 1.0.

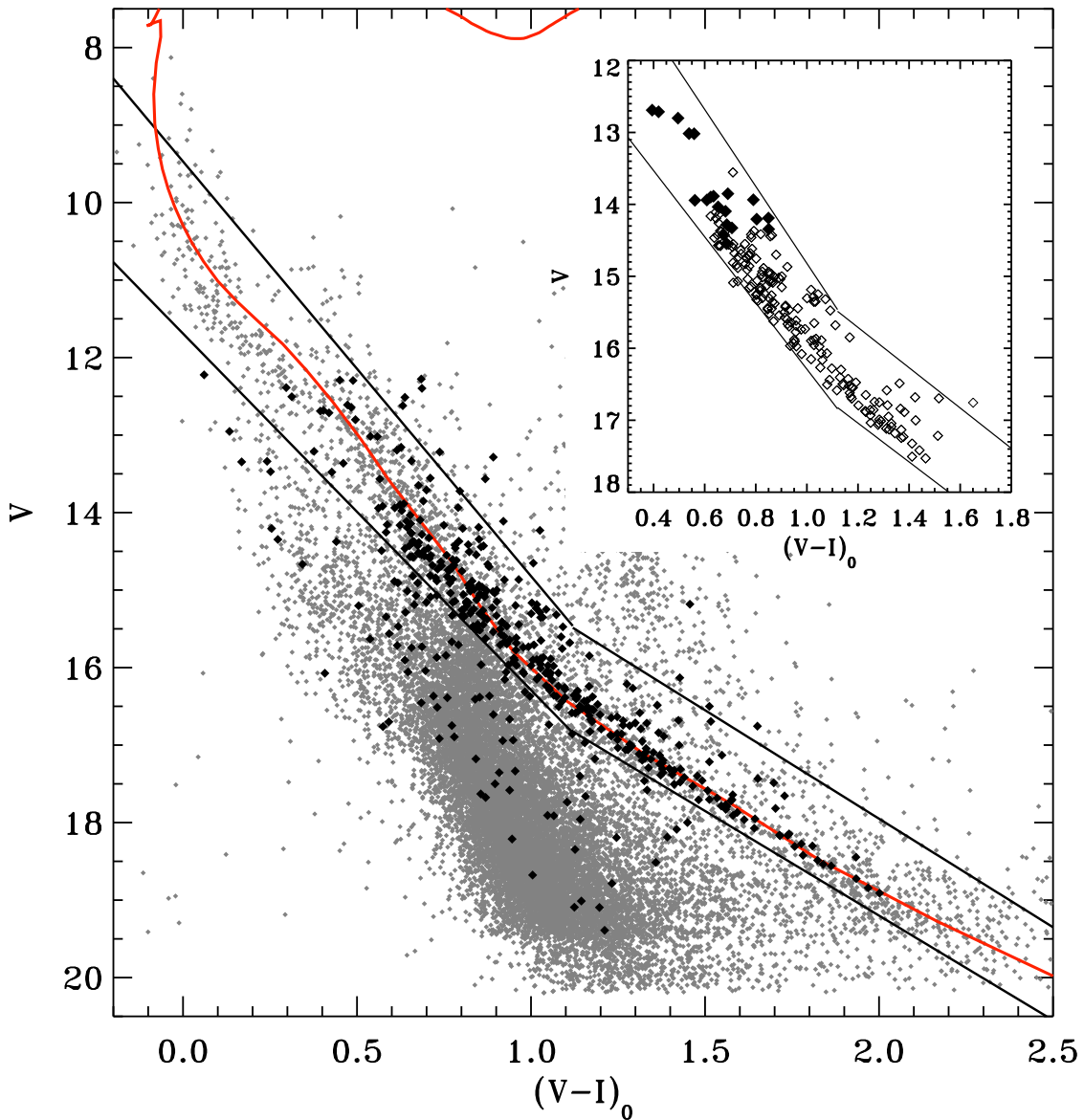


Fig. 5.— The M35 $(V - I)_0$ vs. V color-magnitude diagram. Photometry was provided by Deliyannis (2008). The 441 stars with rotation periods are highlighted in black. Stars located between the solid lines are considered photometric members of M35. Note that the faint limits for proper-motion and radial-velocity surveys are $V \simeq 14.5$ and $V \simeq 17.5$, respectively. The insert shows the location of stars that are radial-velocity members (open symbols), and radial-velocity and proper-motion members (filled symbols). These kinematic members of M35 were used to define the boundaries for photometric membership. The isochrone shown represents a 150 Myr Yale model (Yi et al. 2003).

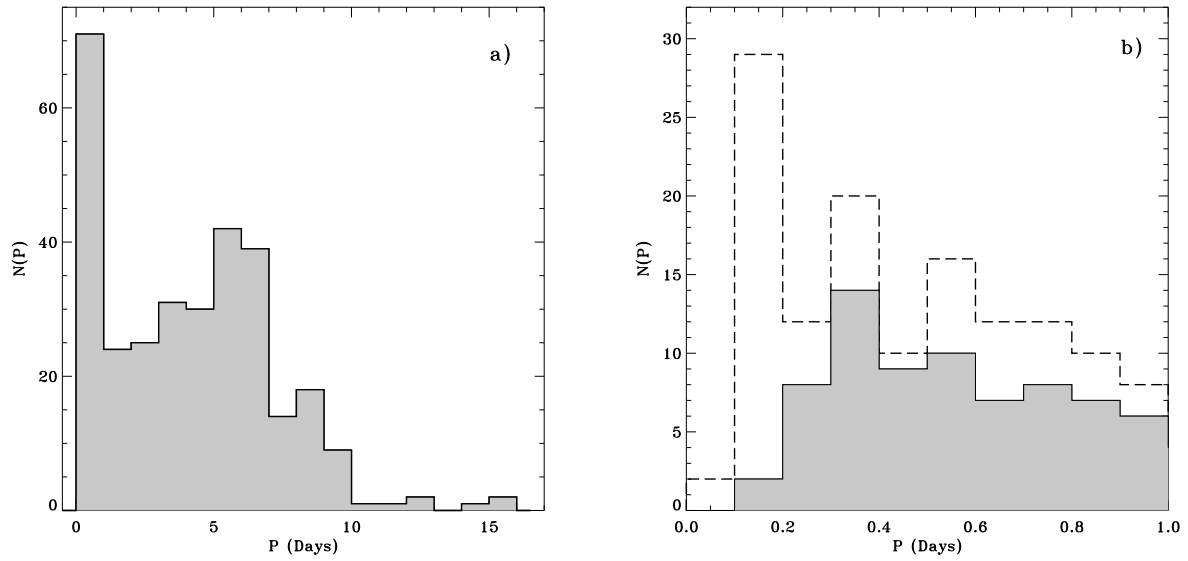


Fig. 6.— **a)** The distribution of rotation periods for the sample of 310 cluster members. The distribution show a large dispersion from ~ 0.1 days to ~ 15 days, and a distinct peak at ≤ 1 day and a shallower and broader peak centered at ~ 6 days. **b)** The distribution of rotation periods shortward of 1 day binned in 0.1 day bins. The dashed line histogram represents member as well as non-member stars with measured rotation periods in our sample. The grey histogram represents only members of M35.

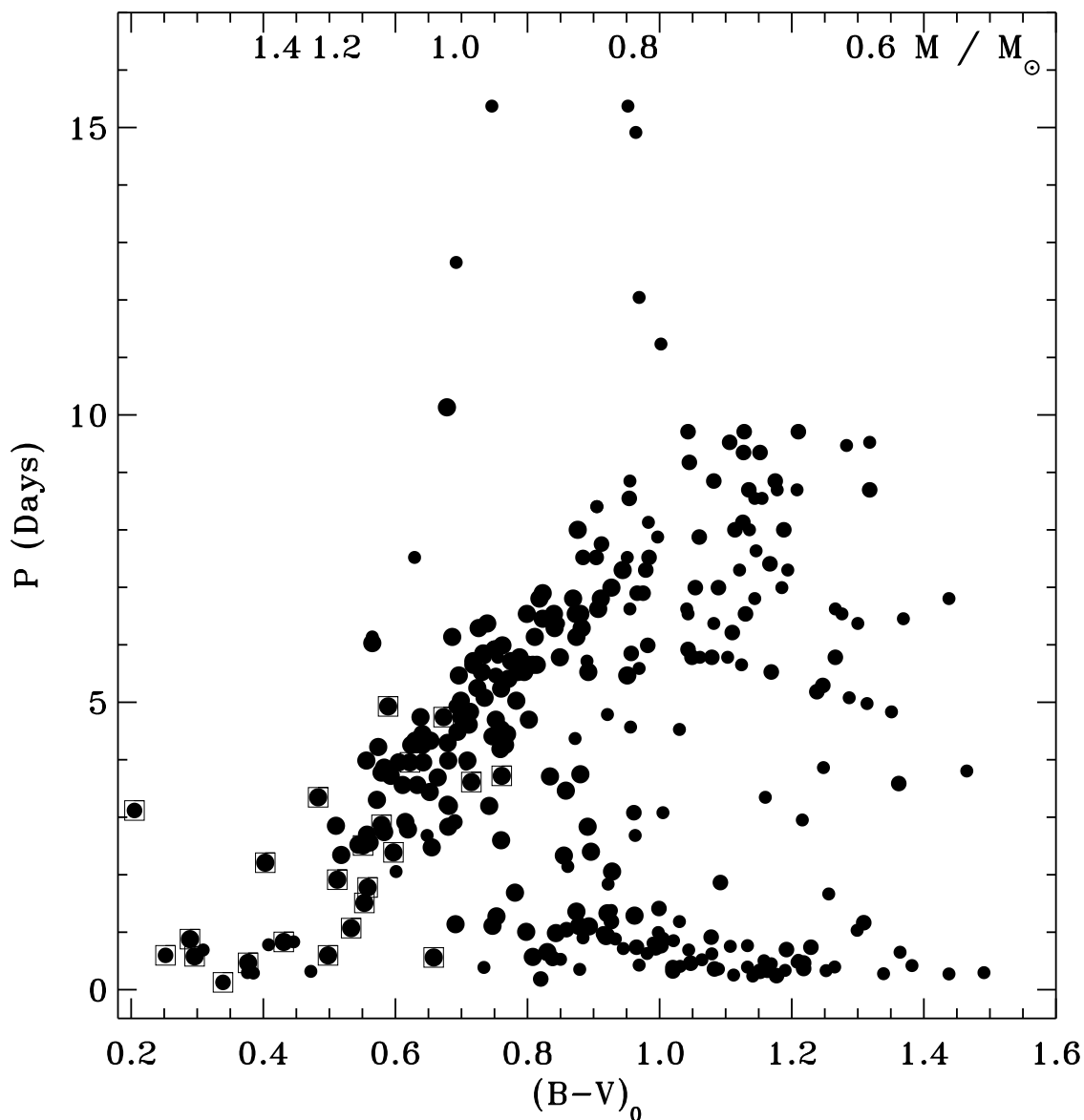


Fig. 7.— The distribution of stellar rotation periods with (B-V) color index for 310 members of M35. The largest plotting symbols are used for radial-velocity members of M35 with more than one velocity measurement. Slightly smaller symbols are used for stars with only one radial-velocity measurement, and smaller yet for stars that are photometric members only. Proper-motion members are marked with additional squares. The upper x-axis gives a stellar mass estimate corresponding to the color on the lower axis. Masses are derived using a 150 Myr Yale isochrone.

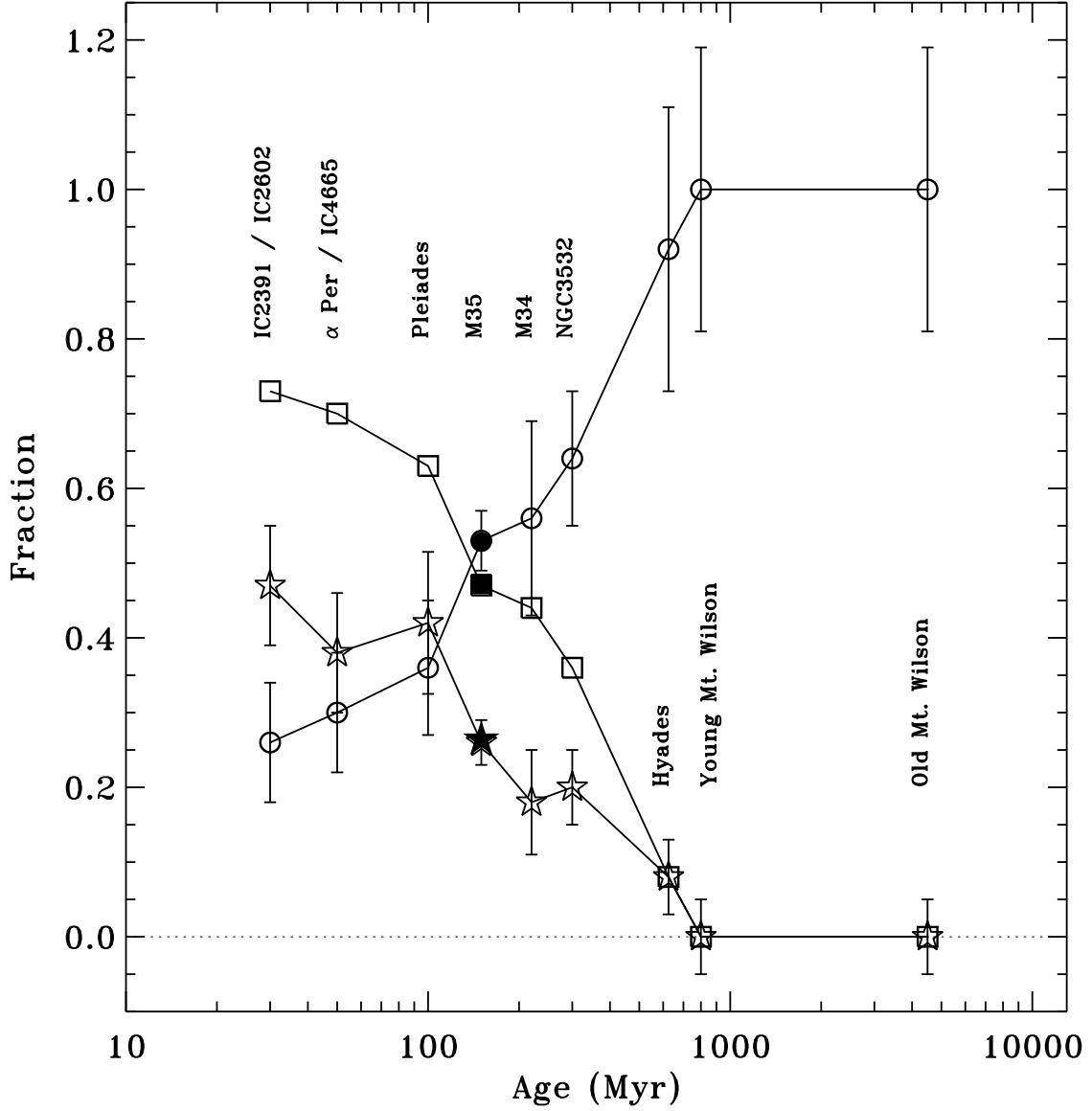


Fig. 8.— Figure 3 from B03 with M35 added. The figure shows the fractions of stars with $0.5 \leq (B - V)_0 \leq 1.5$ on the I sequence (circles) and the C sequence (stars) for clusters of different ages. The squares represent the relative fraction of the sum of C sequence and gap stars. The filled symbols show the relative fractions for M35. We follow B03 in estimating the uncertainties in the fractions by the square root of the number of stars.

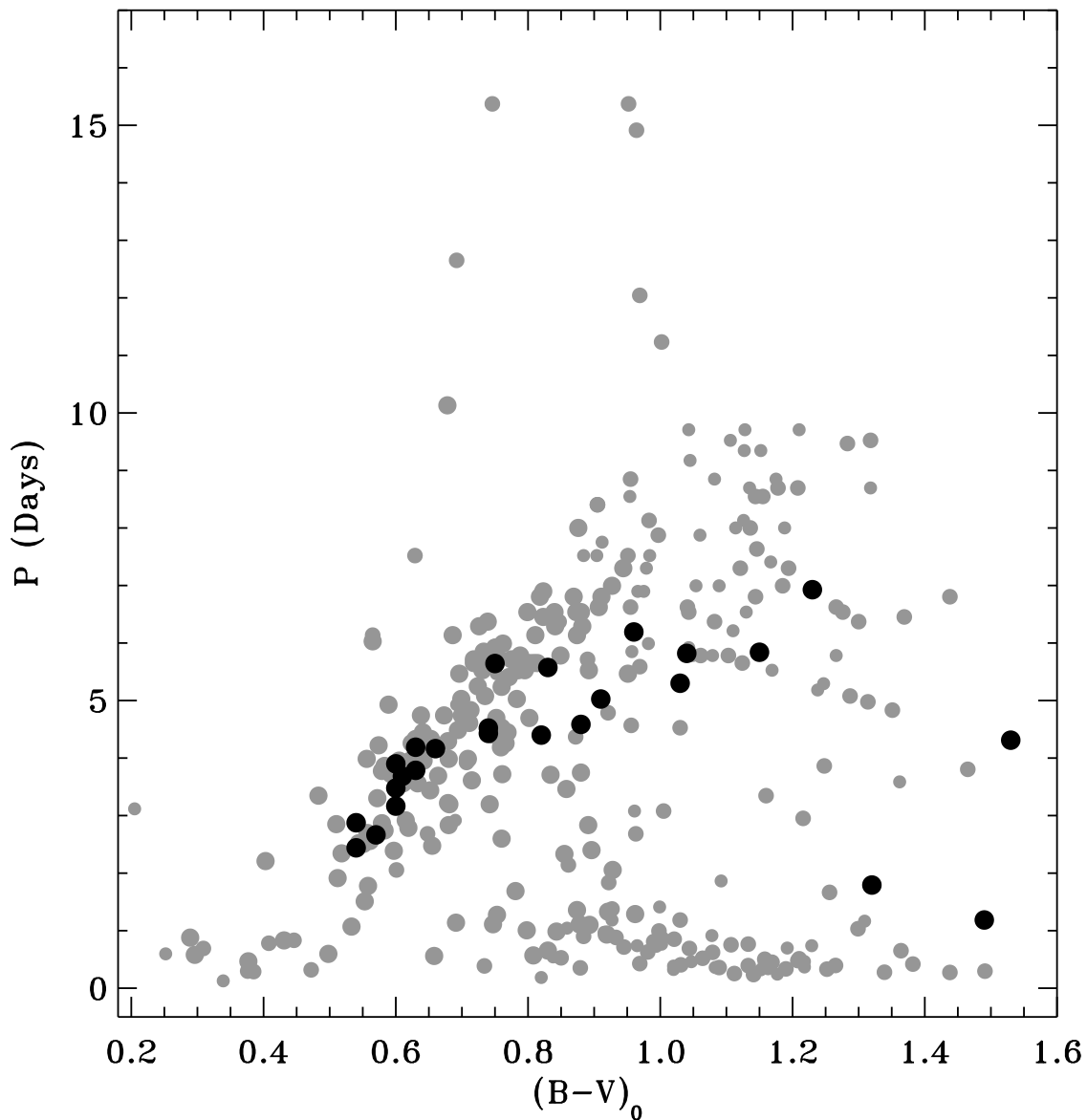


Fig. 9.— The M35 color-period diagram (grey symbols) with 25 Hyades stars overplotted (black; Radick et al. 1987; Prosser et al. 1995). All but the 3 reddest Hyades stars fall on a sequence similar to the M35 I sequence. All Hyades rotation periods were spun-up by a factor $\sqrt{625/150} \simeq 2$ in accordance with the Skumanich \sqrt{t} time-dependence on stellar rotation evolution, assuming ages of 625 Myr and 150 Myr for the Hyades and M35, respectively.

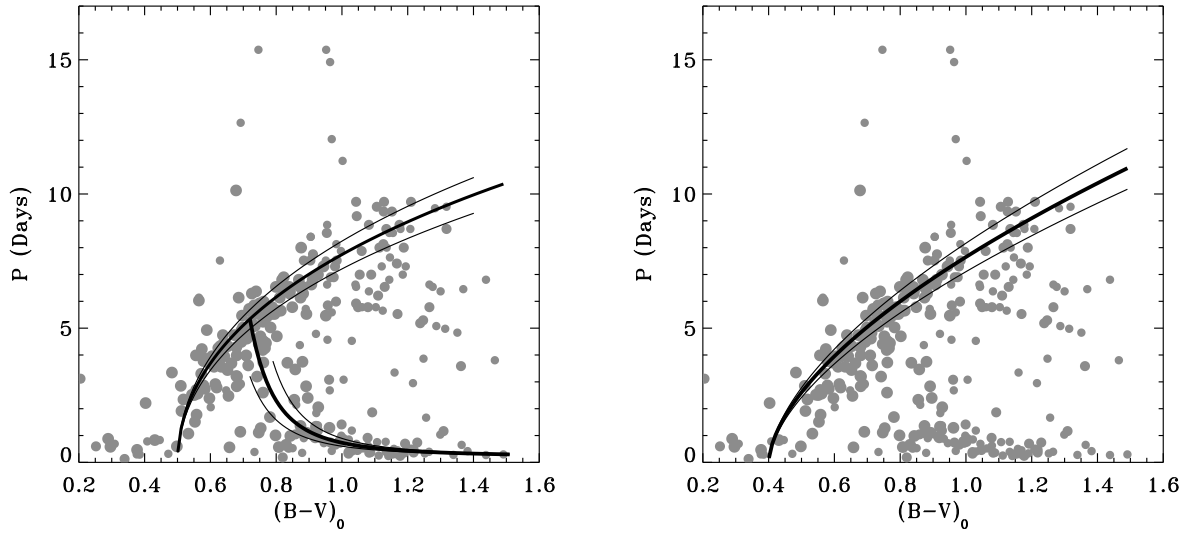


Fig. 10.— The M35 color-period diagram with the 150 Myr rotational isochrones from B03 (left) and B07 (right) overplotted as a thick black solid curves. To illustrate the sensitivity to age we show the 130 Myr and the 170 Myr isochrones as thinner curves flanking the 150 Myr isochrones.

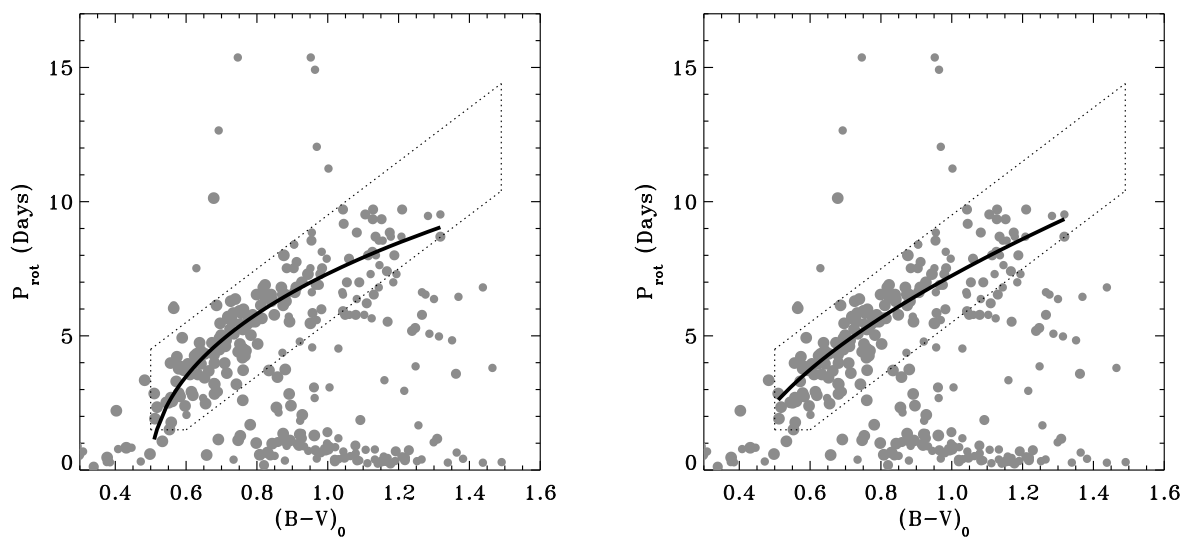


Fig. 11.— The least squares fit of the B03 I sequence isochrone (left; eq. [2]) and the B07 I sequence isochrone (right; eq. [3]) to the M35 I sequence with age (t) as a free parameter. The gyro-ages corresponding to the fits are $133.9 \pm 3\text{Myr}$ and $133.5 \pm 3\text{Myr}$, respectively. The I sequence stars to which the isochrones were fitted are enclosed by the dotted lines in both figures.

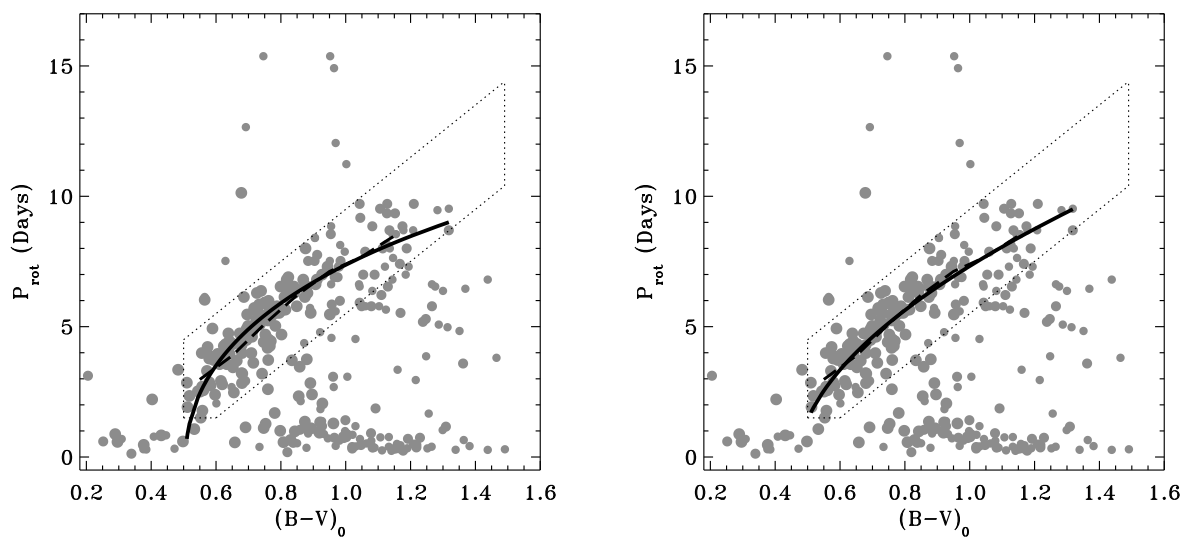


Fig. 12.— The least squares fits (solid curves) of 150 Myr B03 (left) and B07 (right) I sequence isochrones (eq. [2] and eq. [3]) to the M35 I sequence. The corresponding new values for the isochrone coefficients a , b , c , d , and f were determined from the fits and are listed in Table 1. The moving average of the rotation periods for the I sequence stars is also shown as a dashed curve for comparison.

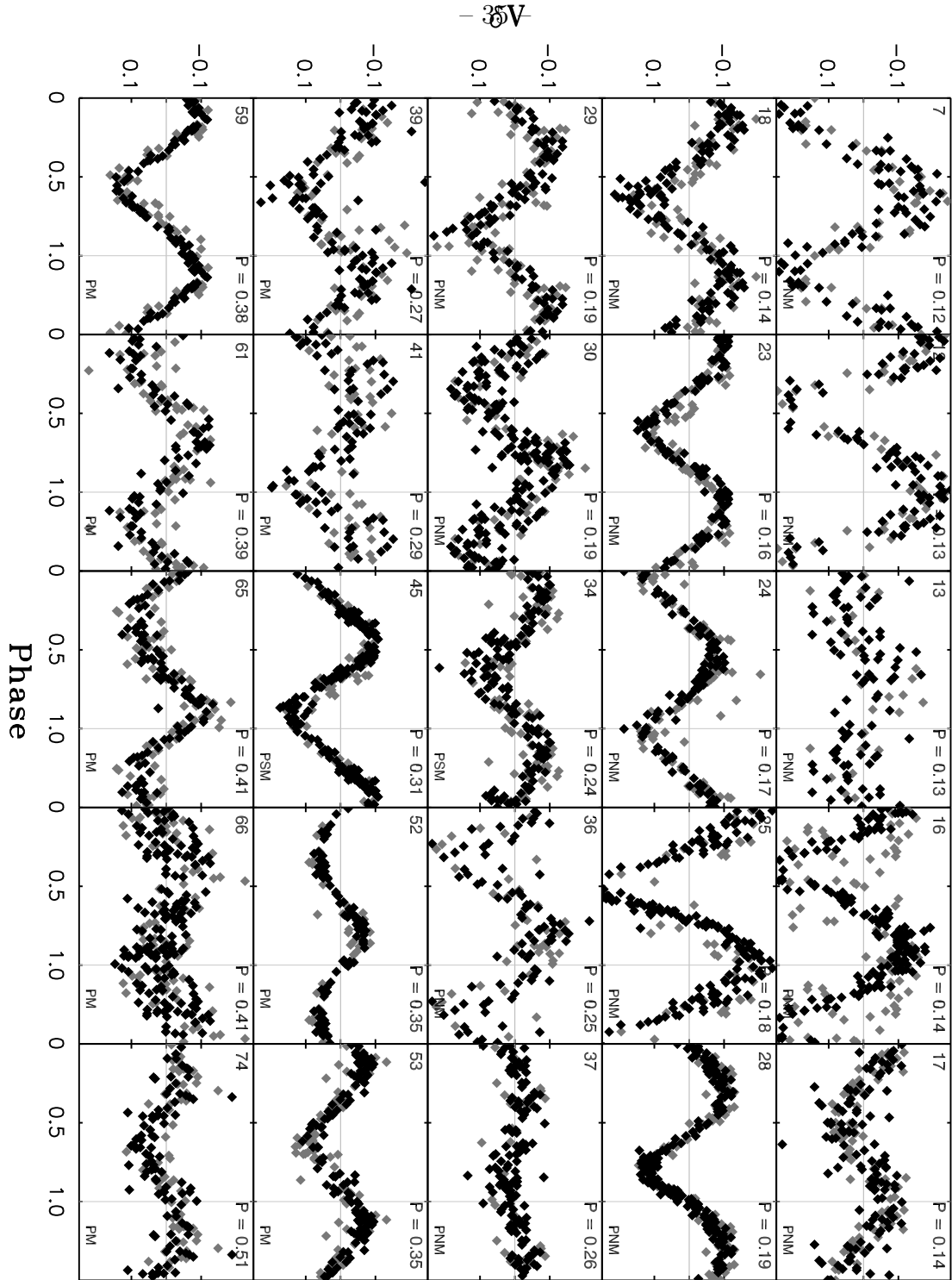


Fig. 13.— Phased light curves for the 441 stars with measured rotation periods.

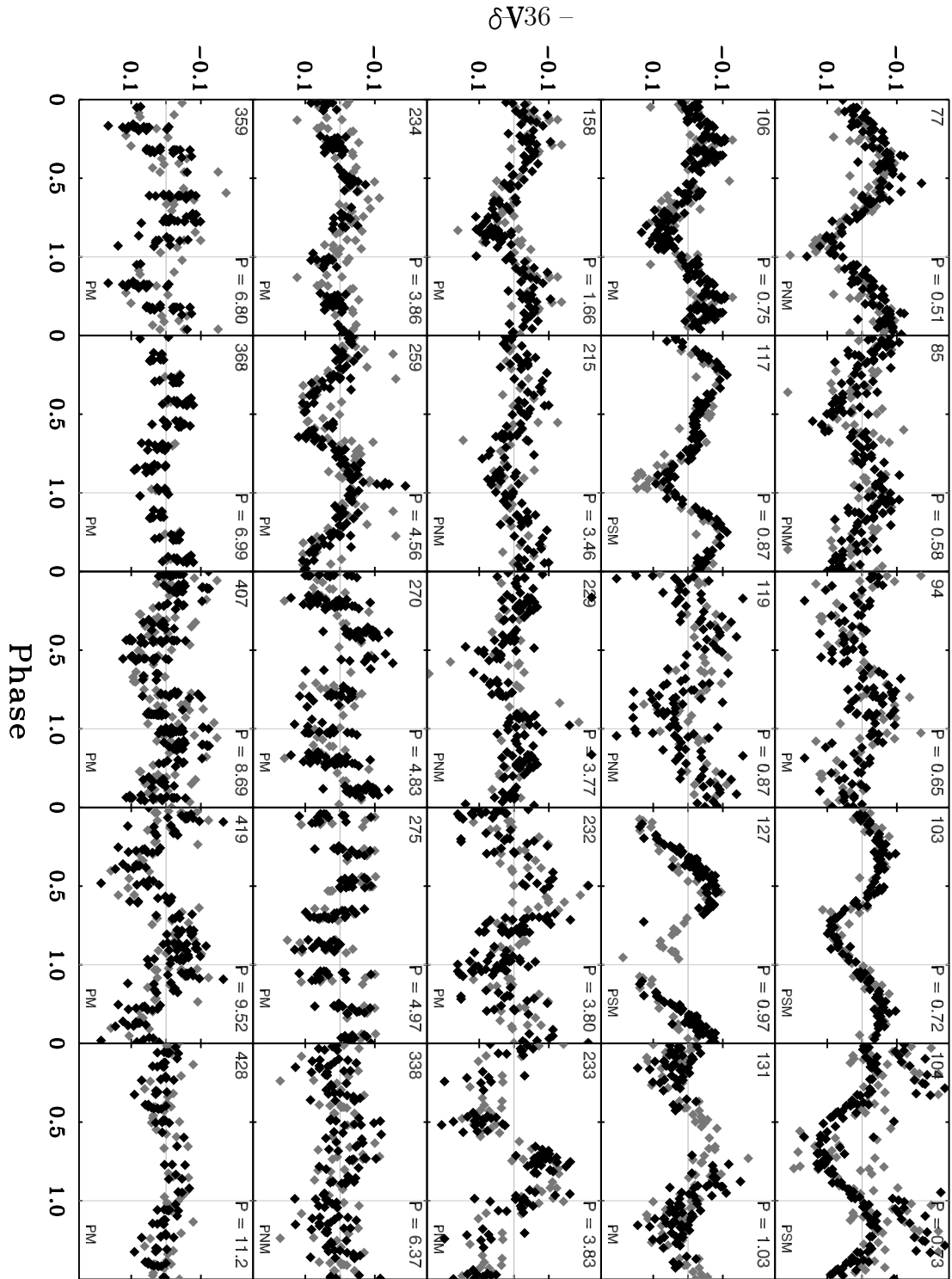


Fig. 13. — Continued.

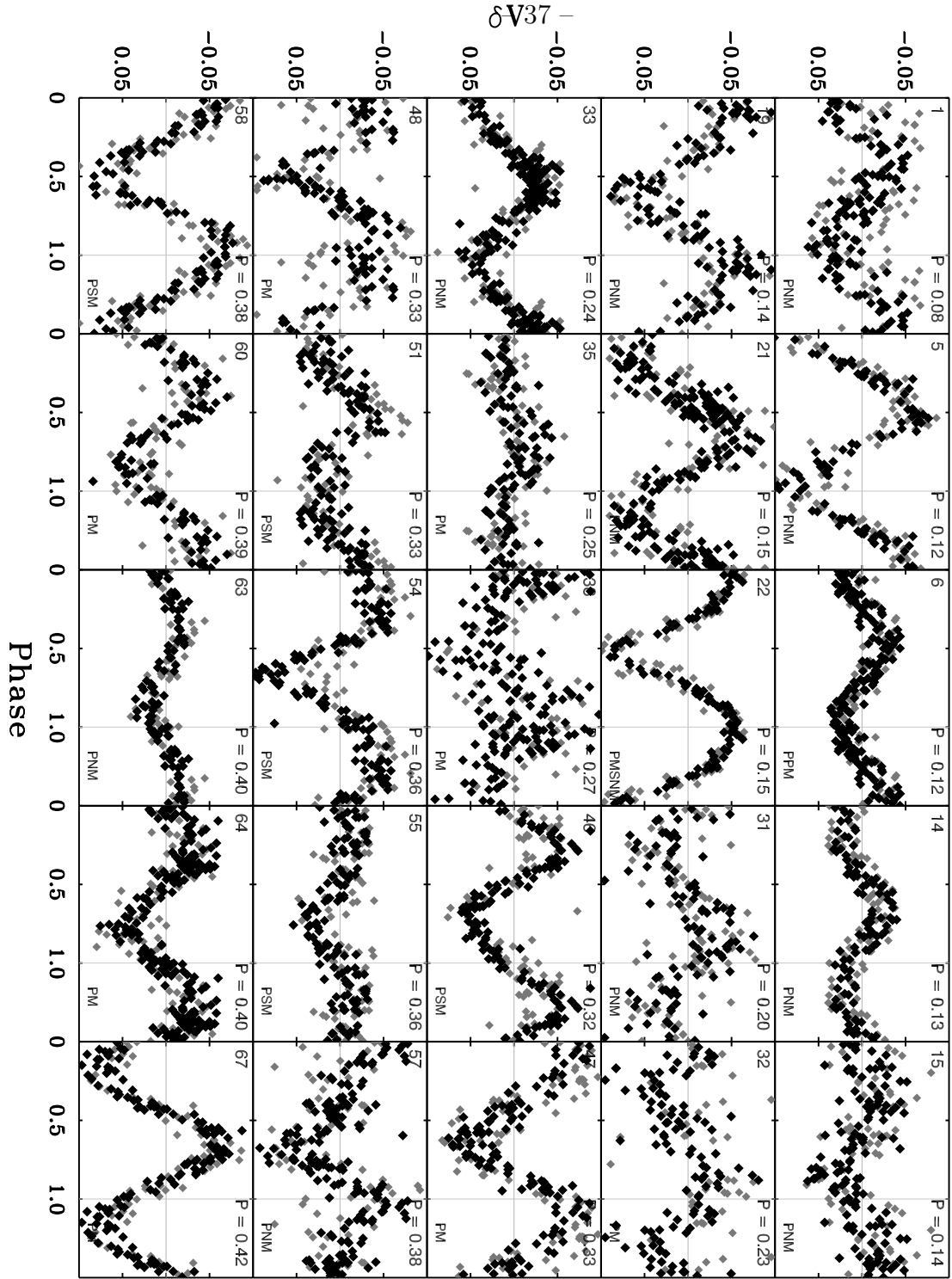


Fig. 13. — Continued.

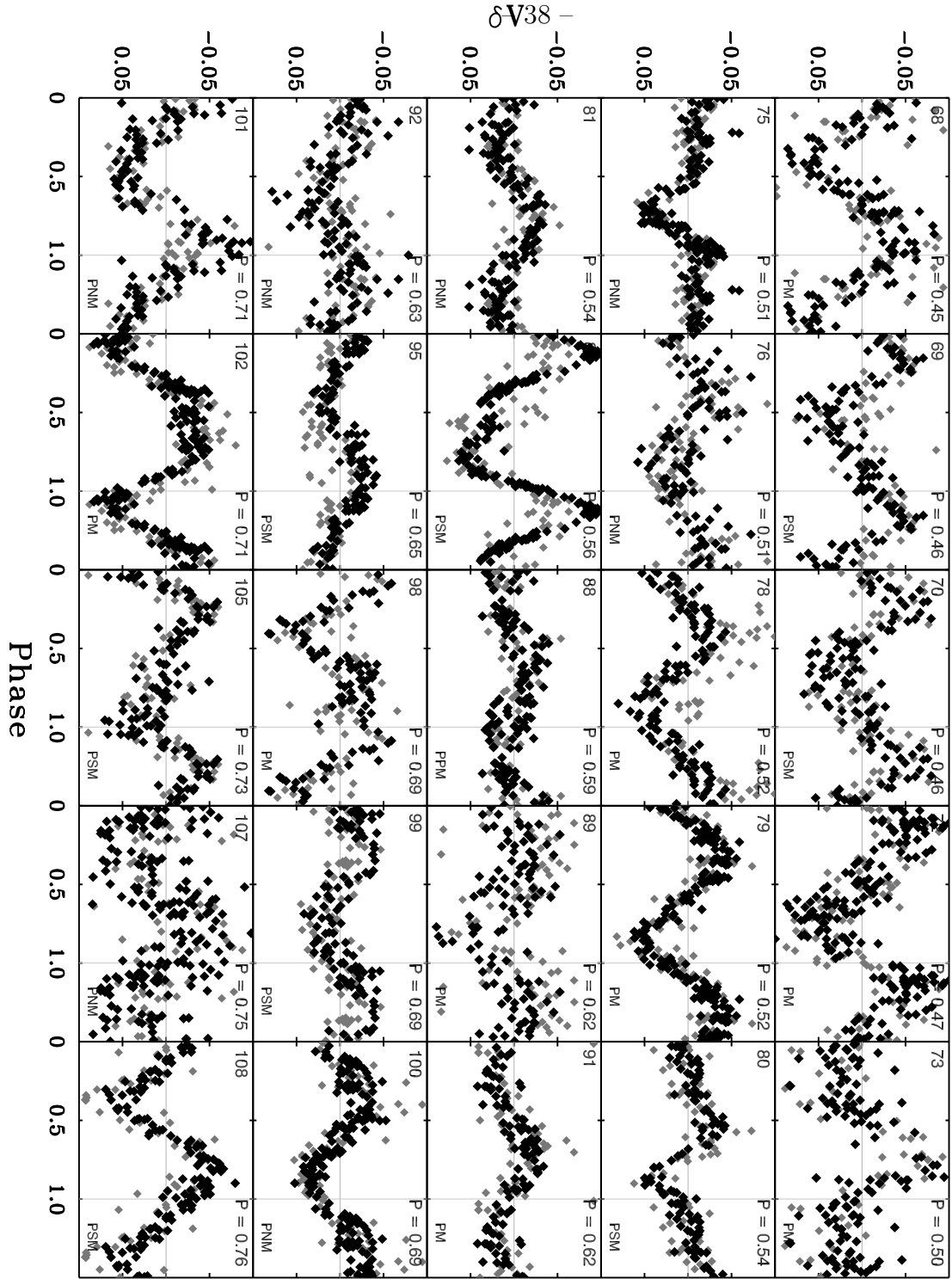


Fig. 13. — Continued.

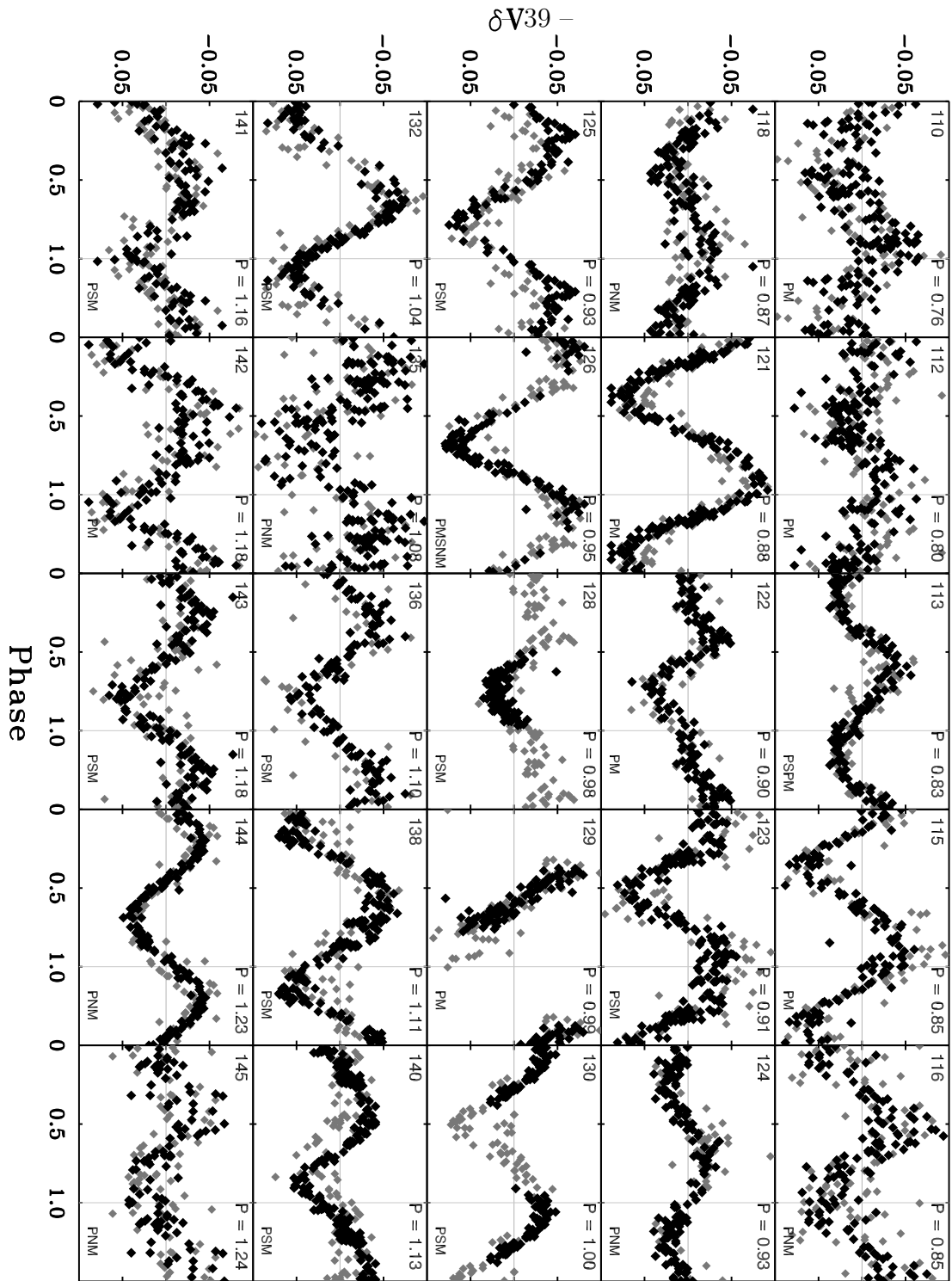


Fig. 13. — Continued.

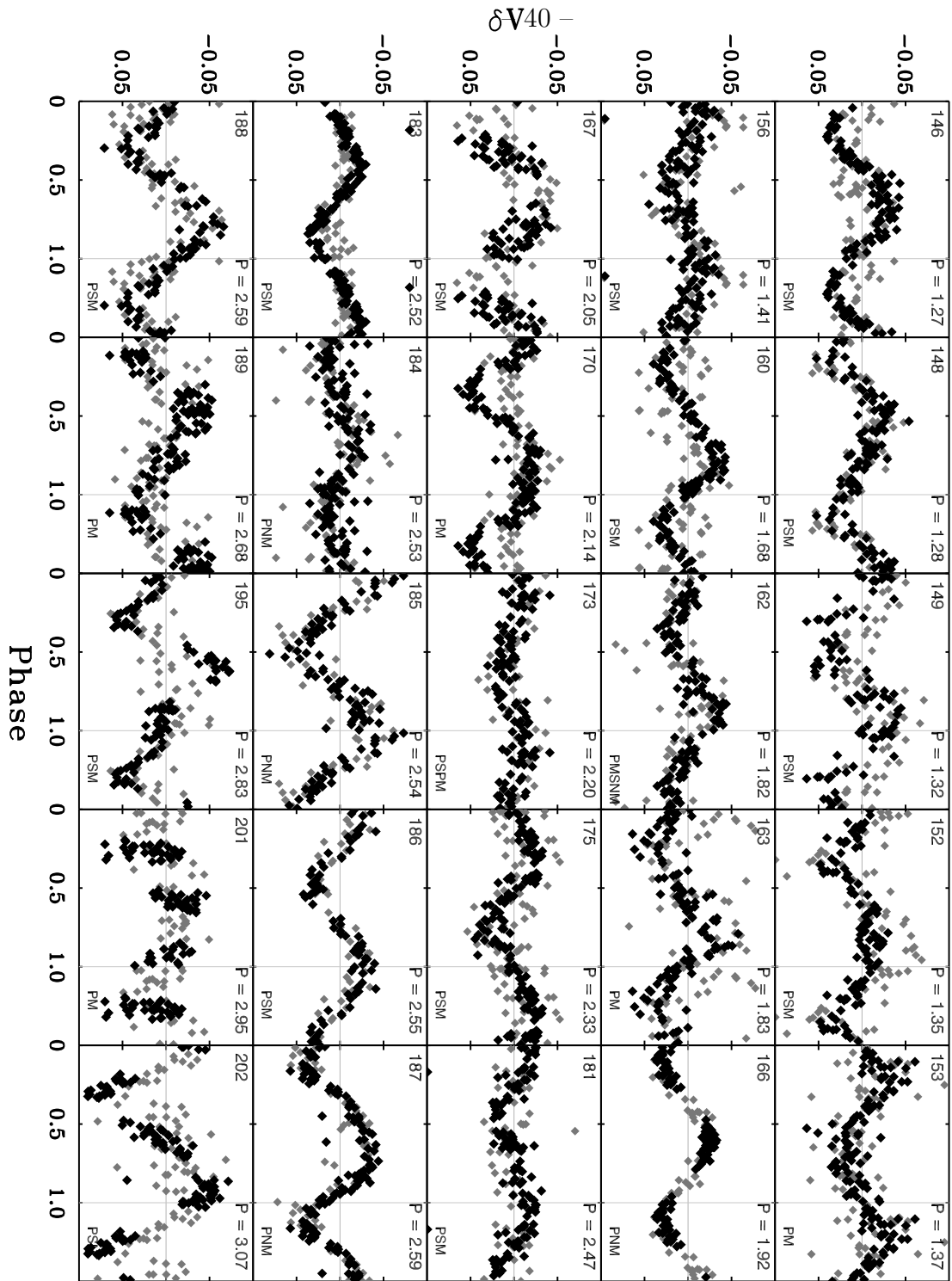


Fig. 13. — Continued.

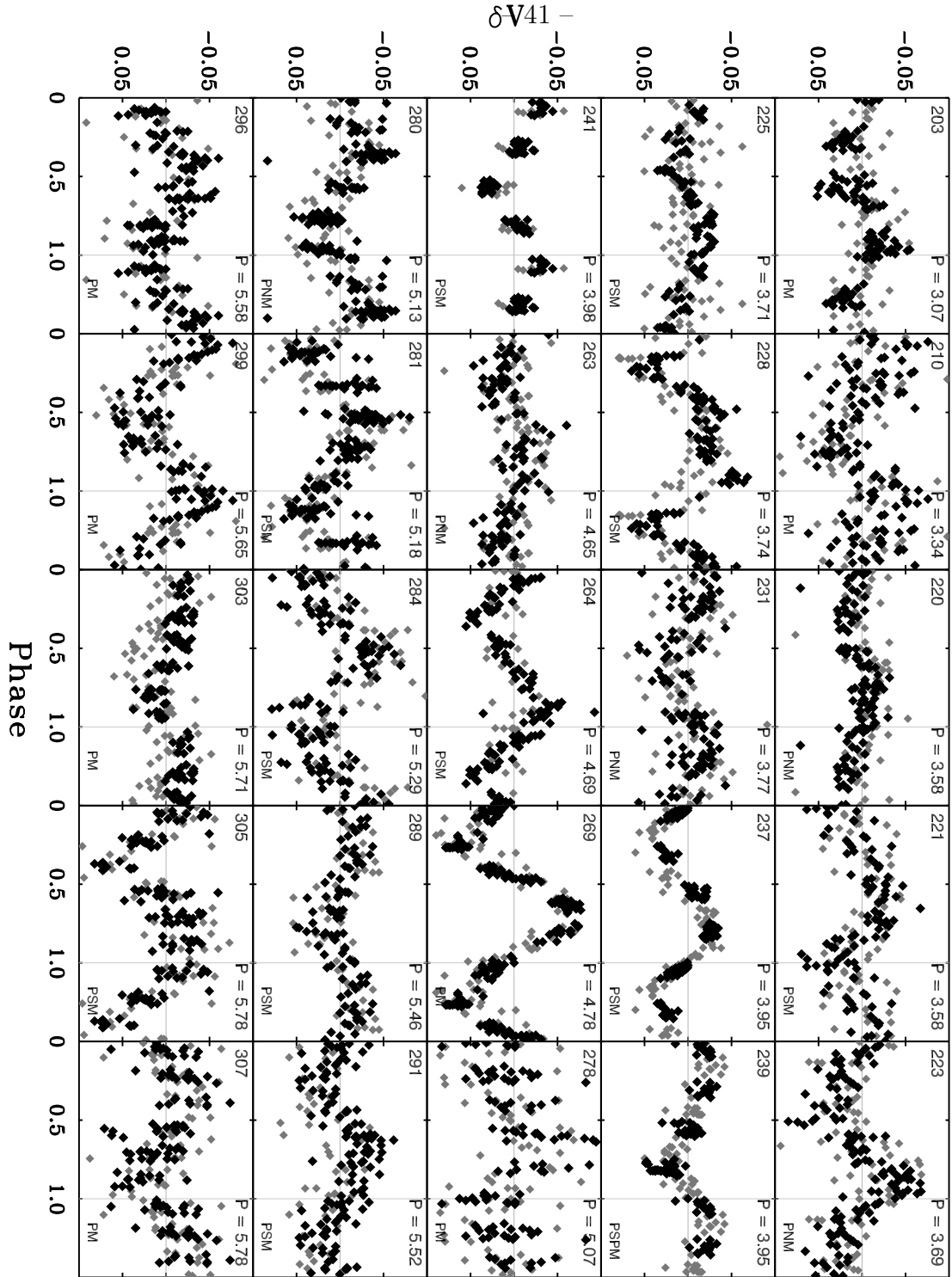


Fig. 13. — Continued.

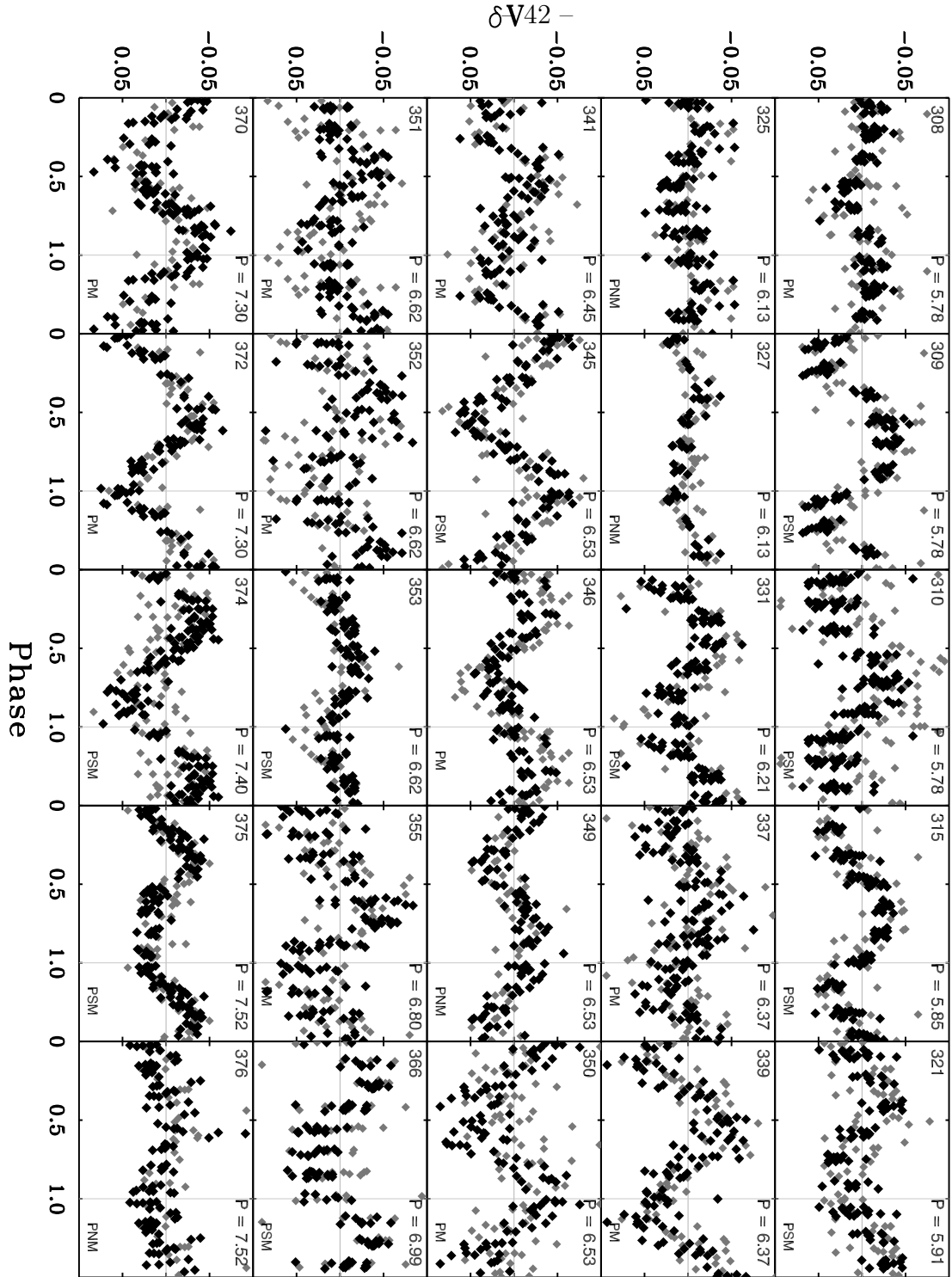


Fig. 13. — Continued.

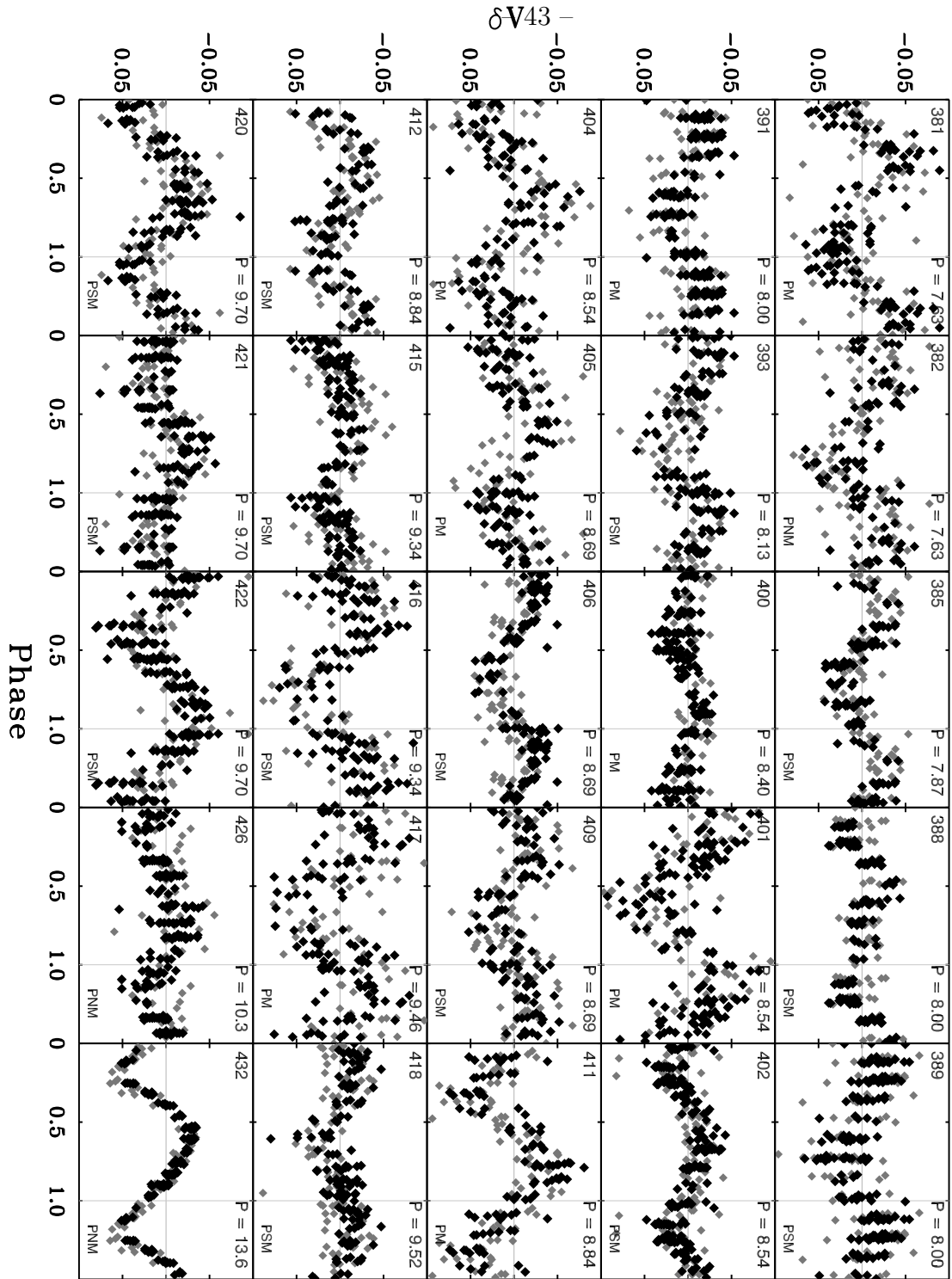


Fig. 13. — Continued.

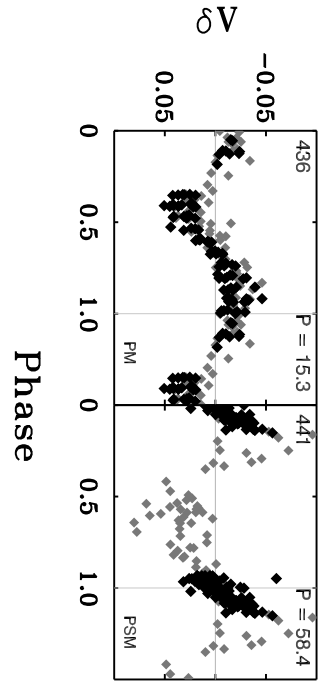


Fig. 13. — Continued.

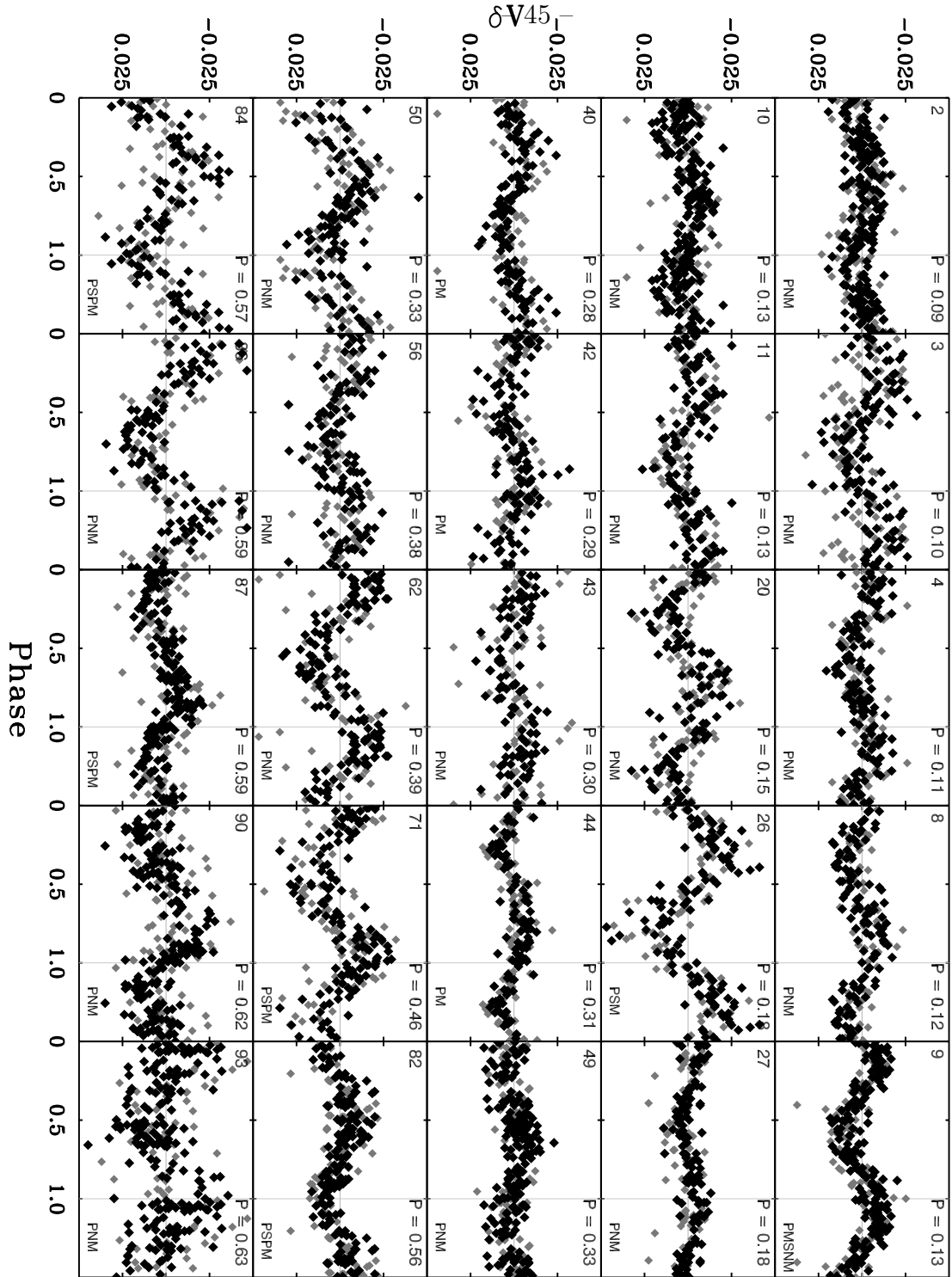


Fig. 13. — Continued.

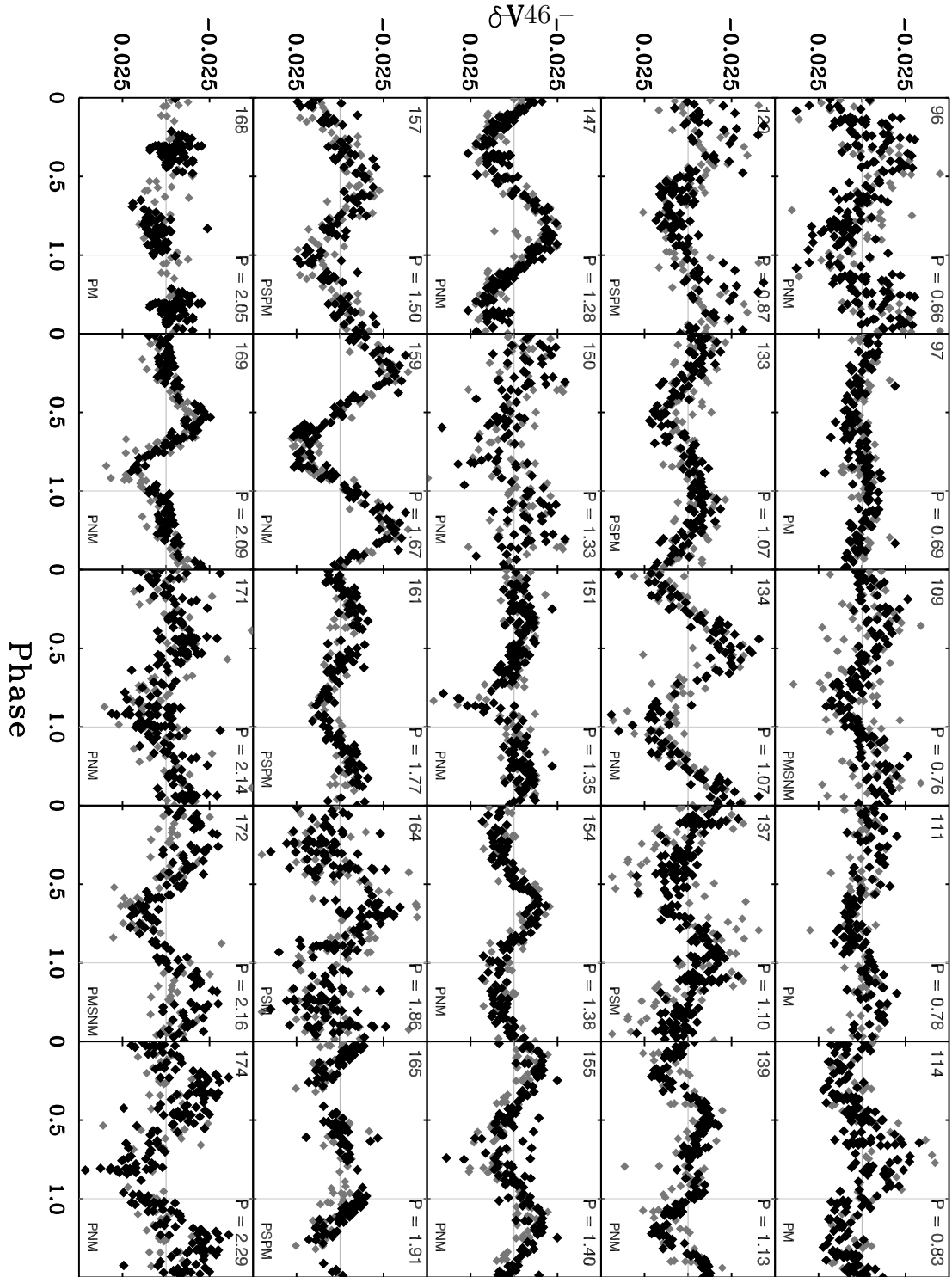


Fig. 13. — Continued.

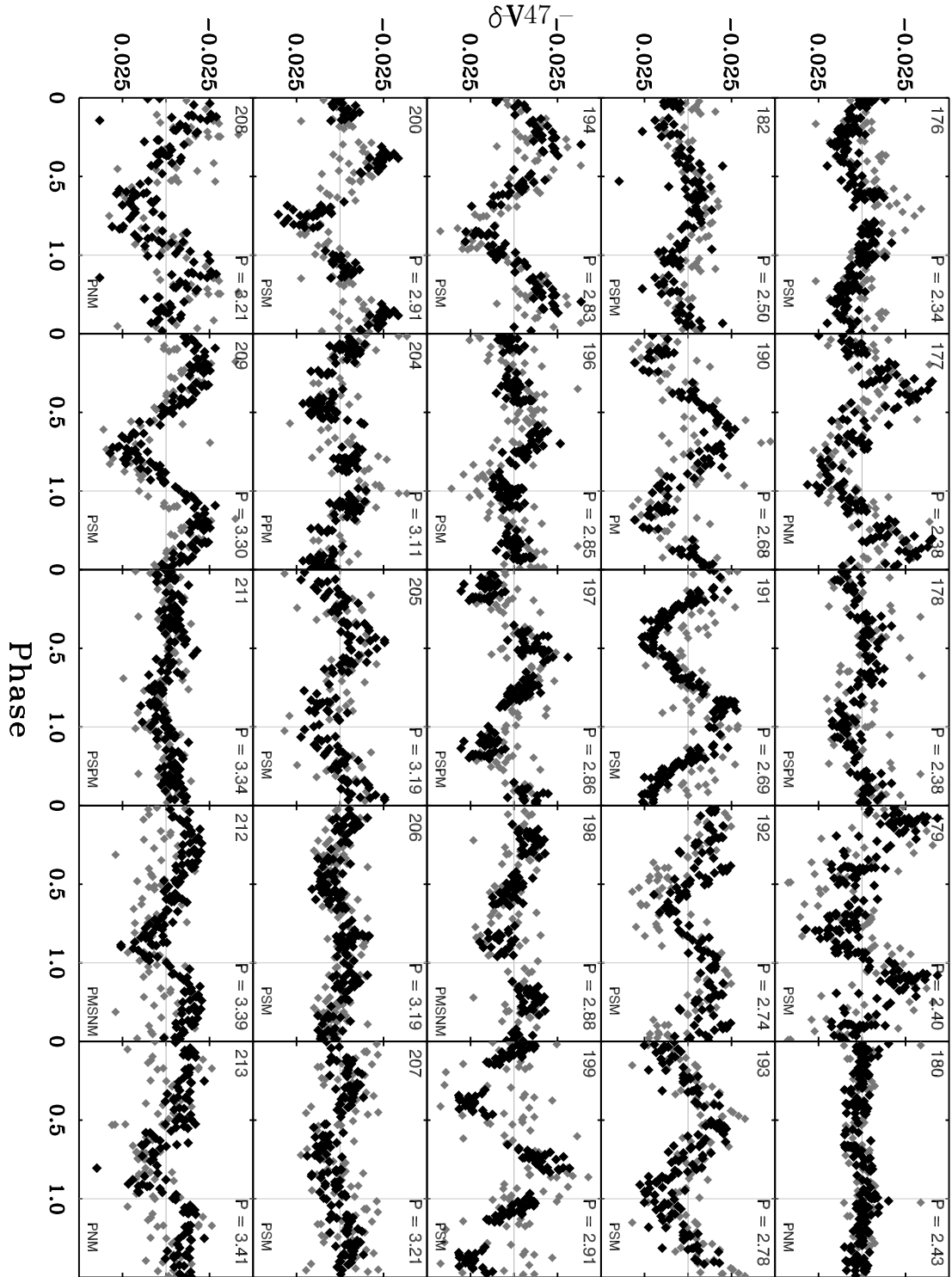


Fig. 13. — Continued.

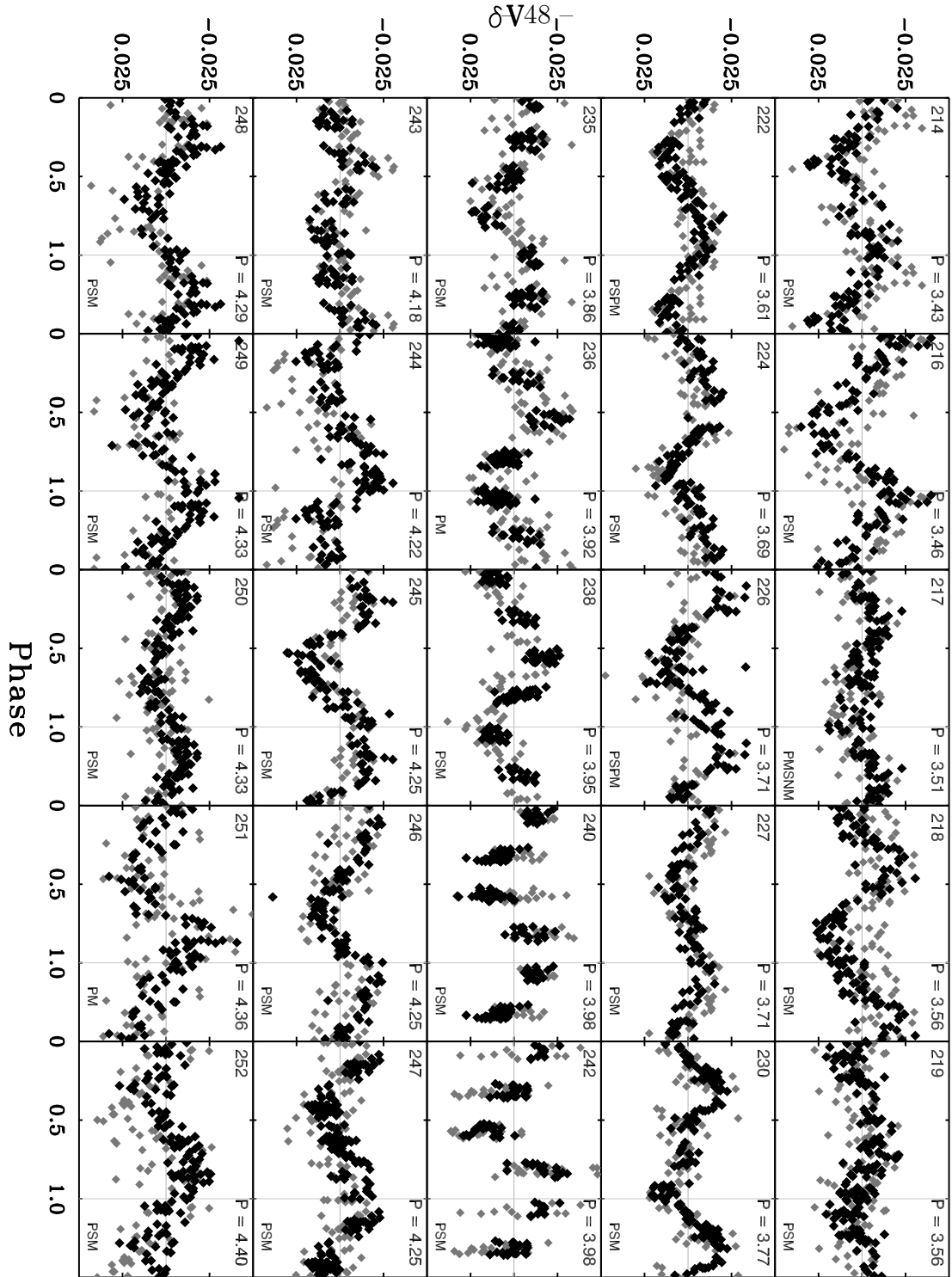


Fig. 13. — Continued.

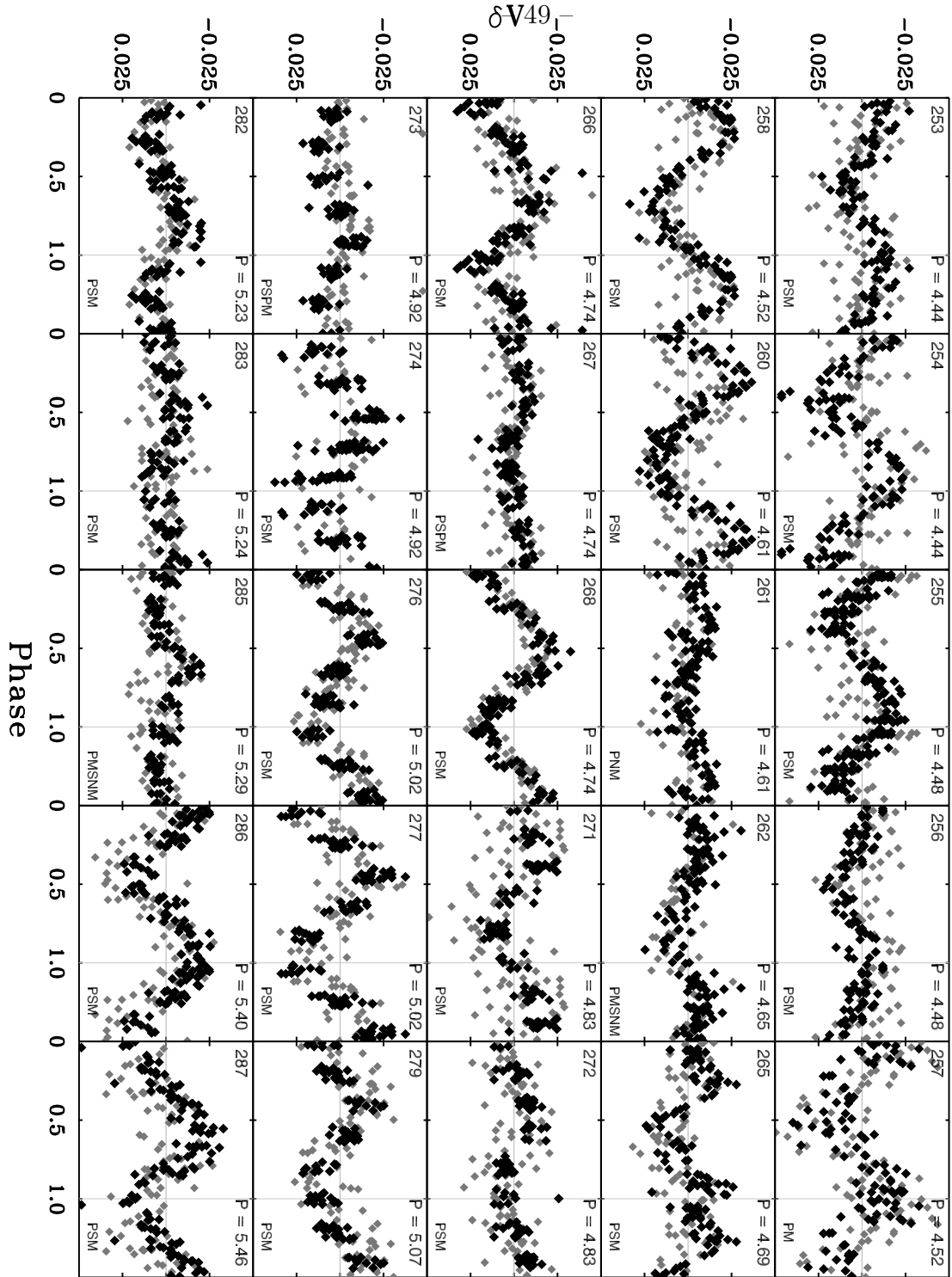


Fig. 13. — Continued.

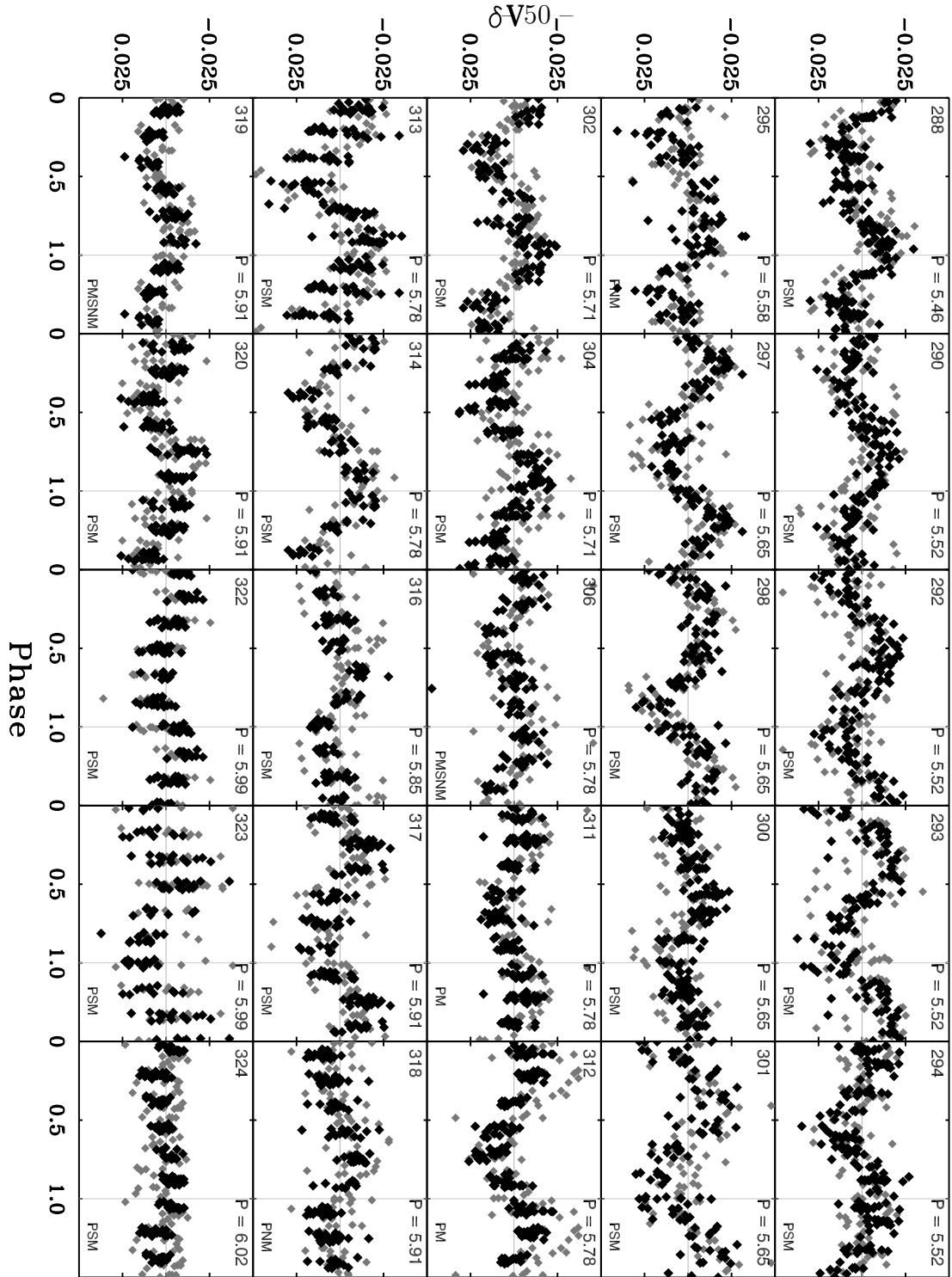


Fig. 13. — Continued.

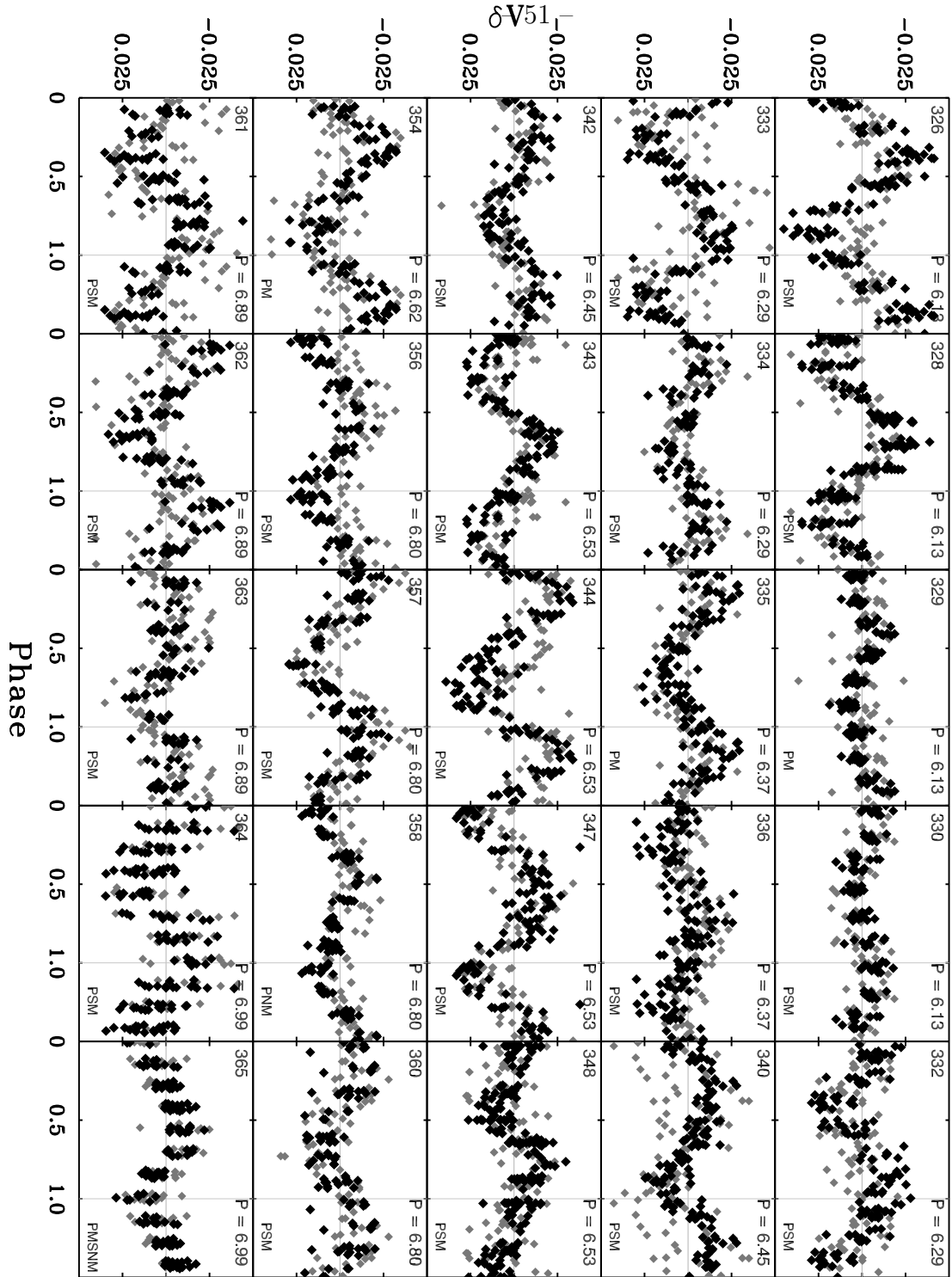


Fig. 13. — Continued.

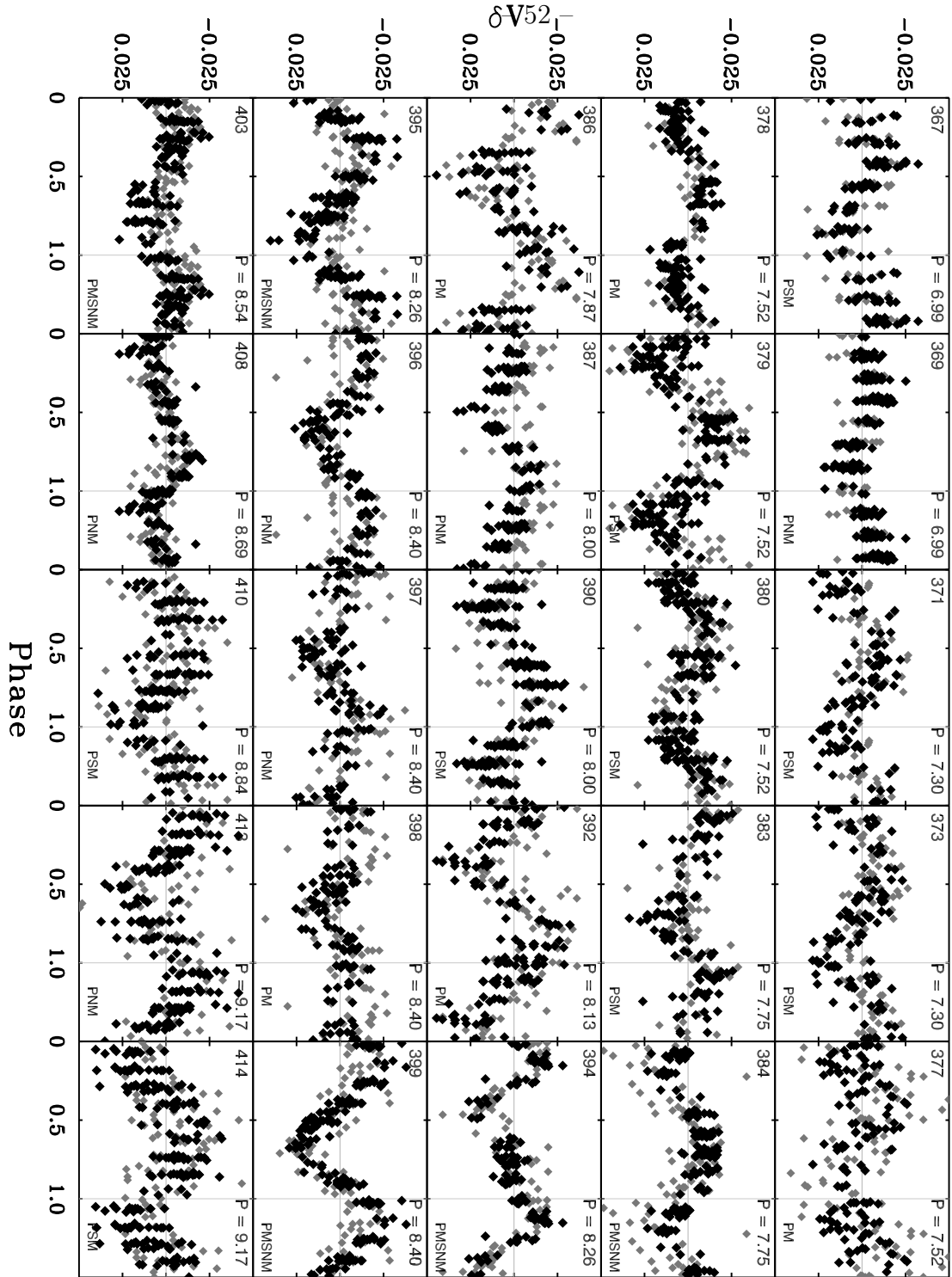


Fig. 13. — Continued.

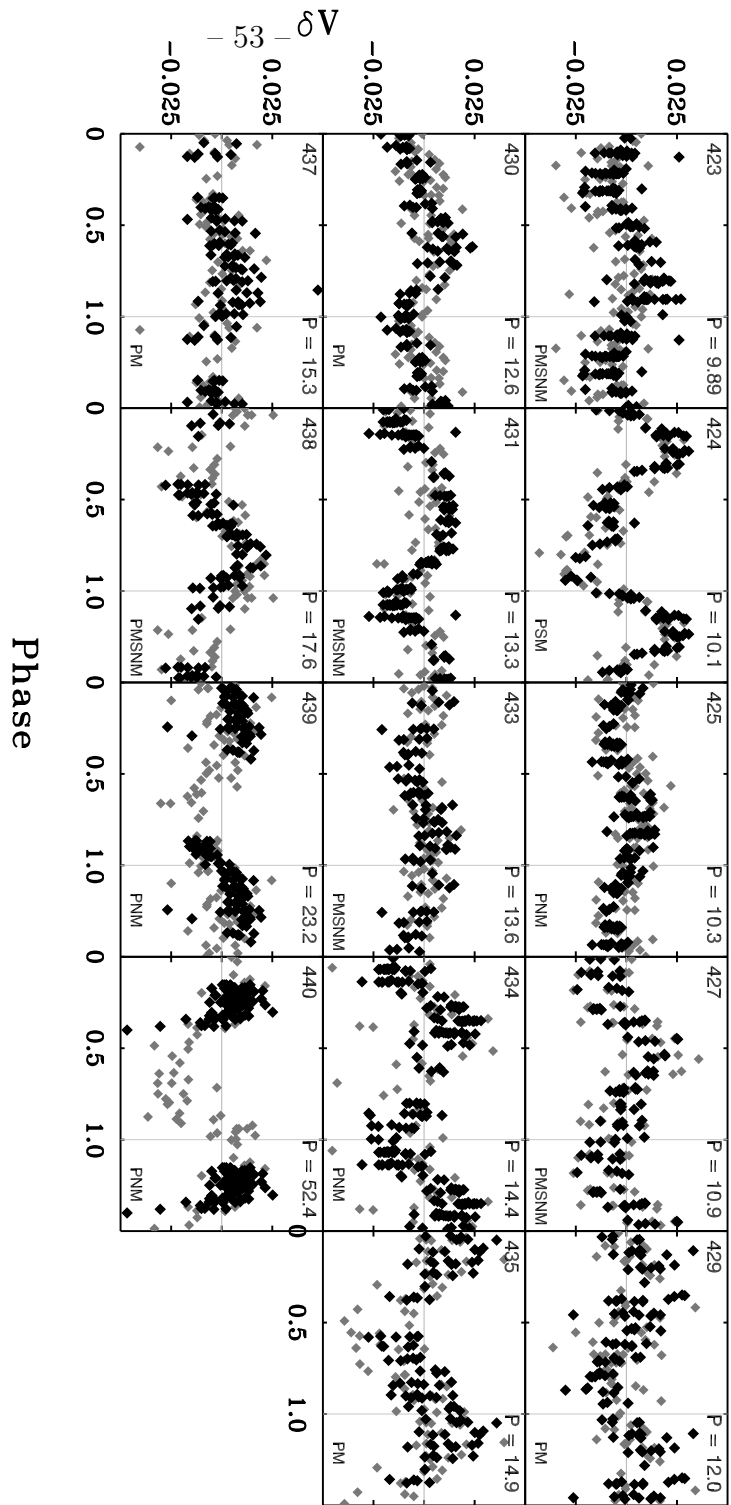


Fig. 13. — Continued.

B. DATA FOR THE 441 STARS WITH MEASURED ROTATION PERIODS IN THE FIELD OF M35

Table ?? presents the results from this study together with information relevant to this paper for 441 stars in the field of M35. The stars appear in order of increasing rotation period, and the running number in the first column corresponds to the number in the upper left hand corner of the stars light curve in Appendix A. Columns 2 and 3 give the stellar equatorial coordinates (equinox 2000). Column 4 lists the measured stellar rotation period in decimal days. Columns 5, 6, and 7 gives the stellar V magnitude and B-V and V-I color indices, respectively, corrected for extinction and reddening. Column 8 presents the number of radial-velocity measurements for the star and columns 9 and 10 give the mean radial-velocity and the velocity standard deviation, respectively. Column 11 list the radial-velocity cluster membership probability calculated using the formalism by Vasilevskis et al. (1958). Column 12 contains a proper-motion cluster membership probability from either Cudworth (1971) or McNamara & Sekiguchi (1986). In column 13 we give the abbreviated membership codes (initialisms) also found in the light curves in Appendix A. The codes denote the type of membership information available for the star and have the following meaning: Photometric Member (PM; described in Section 2.5), Photometric Non-Member (PNM), Photometric and Spectroscopic Member (PSM), Photometric and Proper-motion Member (PPM), and Photometric Member but Spectroscopic Non-Member (PMSNM). In column 14 we give the weights used for each star when fitting the rotational isochrones in Section 5.3 and Section 5.4. Finally, in column 15 the rotational state of the star is indicated by a 1-letter code representing, respectively, the I sequence (“i”), the C sequence (“c”), and the gap (“g”). Stars with a “-” in column 15 have locations in the color-period diagram that do not correspond to either of the sequences or the gap.

Table 2. Data for the 441 stars with measured rotation periods in the field of M35

No. ^a	RA			DEC			P_{rot}	V_0	$(B - V)_0$	$(V - I)_0$	N_{RV}	$\bar{R}V$	σ_{RV}	P_{RV}	P_{PM}	mcode ^b	Weight	Sequence ^c
	<i>h</i>	<i>m</i>	<i>s</i>	$^{\circ}$	$'$	$''$	Days					$km\ s^{-1}$	$km\ s^{-1}$	%	%			
1	92	06	47.016	24	21	16.131	0.088	15.20	0.42	0.50	0	PNM	0.0	-
2	92	08	02.767	24	15	33.227	0.096	15.01	0.47	0.64	0	PNM	0.0	-
3	92	10	47.974	24	30	01.147	0.107	15.90	0.45	0.64	0	PNM	0.0	-
4	92	10	49.237	24	37	24.589	0.112	14.89	0.45	0.61	0	PNM	0.0	-
5	92	34	44.354	24	03	17.857	0.126	16.74	0.73	1.05	0	PNM	0.0	c
6	92	05	55.215	24	05	52.352	0.127	12.29	0.34	0.45	1	7.2	0.0	0	95	PPM	0.75	-
7	92	11	00.718	24	36	34.265	0.128	19.01	...	1.14	0	PNM	0.0	c
8	92	16	52.775	24	23	49.424	0.128	14.82	0.47	0.66	0	PNM	0.0	-
9	92	03	38.271	24	03	08.889	0.130	14.16	0.43	0.59	3	15.3	0.1	0	0	PMSNM	0.0	-
10	92	04	31.280	24	00	46.747	0.132	14.91	0.43	0.62	0	PNM	0.0	-
11	92	28	56.087	24	34	23.644	0.133	15.19	0.48	0.66	0	PNM	0.0	-
12	92	33	45.522	24	33	02.277	0.134	19.09	...	1.20	0	PNM	0.0	c
13	92	35	22.421	24	26	52.779	0.138	19.39	...	1.21	0	PNM	0.0	c
14	92	33	46.758	24	10	24.429	0.139	12.51	0.50	0.64	0	PNM	0.0	-
15	92	03	55.876	24	31	23.826	0.141	16.92	0.54	0.74	0	PNM	0.0	-
16	92	11	56.693	24	16	09.715	0.143	17.96	0.83	1.14	0	PNM	0.0	c
17	92	24	57.079	24	37	21.197	0.148	18.19	...	1.25	0	PNM	0.0	c
18	92	14	02.734	24	36	58.469	0.148	17.91	...	1.05	0	PNM	0.0	c
19	92	19	01.013	24	36	30.742	0.149	17.63	0.60	0.86	0	PNM	0.0	c
20	92	28	53.066	24	32	42.817	0.154	15.07	0.50	0.67	0	PNM	0.0	-
21	92	14	55.001	24	06	27.309	0.158	17.74	...	1.10	0	PNM	0.0	c
22	92	30	27.933	24	05	49.873	0.158	15.33	0.61	0.90	3	0.9	1.4	0	0	PMSNM	0.0	c
23	92	32	42.900	24	25	28.741	0.164	16.38	0.76	0.85	0	PNM	0.0	c
24	92	34	06.423	24	16	03.158	0.179	17.34	0.58	0.95	0	PNM	0.0	-
25	91	55	08.835	24	05	03.676	0.182	17.68	0.60	0.87	0	PNM	0.0	c
26	92	30	43.039	24	25	51.469	0.186	15.96	0.82	1.03	1	1.5	0.0	60	0	PSM	0.75	c
27	92	20	57.715	24	28	07.500	0.187	13.48	0.26	0.43	0	PNM	0.0	-
28	92	06	50.944	24	12	15.287	0.195	17.36	0.66	0.91	0	PNM	0.0	c
29	92	29	21.218	24	04	38.922	0.195	17.40	...	1.14	0	PNM	0.0	c
30	92	03	56.893	24	02	59.160	0.198	18.68	...	1.00	0	PNM	0.0	c
31	92	29	22.564	24	13	29.995	0.203	17.66	0.72	1.16	0	PNM	0.0	c
32	92	15	17.029	24	18	00.567	0.237	17.31	1.14	1.38	1	133.0	0.0	10	0	PM	0.5	c
33	92	03	14.019	24	15	37.264	0.241	16.70	0.38	0.59	0	PNM	0.0	-
34	92	07	57.933	24	27	02.660	0.244	17.32	1.18	1.41	1	-12.9	0.0	60	0	PSM	0.75	c
35	92	30	39.413	24	15	38.466	0.254	16.27	1.11	1.29	0	PM	0.5	c
36	92	17	43.449	24	28	50.759	0.259	19.09	...	1.12	0	PNM	0.0	c
37	92	16	38.602	23	59	45.457	0.263	17.50	...	0.90	0	PNM	0.0	c
38	92	04	37.542	24	04	40.632	0.274	18.45	1.44	1.93	0	PM	0.5	c
39	92	23	40.697	24	29	22.543	0.278	18.30	1.34	1.81	0	PM	0.5	c
40	92	17	41.279	24	31	23.434	0.289	12.64	0.39	0.48	0	PM	0.5	-
41	92	31	27.396	24	03	21.407	0.296	18.91	1.49	2.00	0	PM	0.5	c
42	92	20	20.636	24	35	02.536	0.297	12.61	0.38	0.47	0	PM	0.5	-
43	92	16	23.057	24	13	38.681	0.303	15.47	0.49	0.62	0	PNM	0.0	-
44	92	27	03.642	24	03	38.889	0.319	13.98	0.47	0.63	1	15.0	0.0	0	0	PM	0.5	-
45	91	56	44.745	24	12	08.854	0.320	17.04	1.15	1.33	1	-2.1	0.0	60	0	PSM	0.75	c

Table 2—Continued

No. ^a	RA			DEC			P_{rot}	V_0	$(B - V)_0$	$(V - I)_0$	N_{RV}	$\bar{R}V$	σ_{RV}	P_{RV}	P_{PPM}	mcode ^b	Weight	Sequence ^c
	h	m	s	°	'	"	Days					$km\ s^{-1}$	$km\ s^{-1}$	%	%			
46	92	09	44.143	24	33	18.489	0.325	16.43	1.02	1.16	1	-6.5	0.0	60	0	PSM	0.75	c
47	92	03	47.939	24	23	49.397	0.331	17.49	1.25	1.70	0	PM	0.5	c
48	92	28	24.639	24	25	28.542	0.336	17.31	1.19	1.43	0	PM	0.5	c
49	92	00	58.997	24	05	21.261	0.337	15.29	0.55	0.64	0	PNM	0.0	–
50	92	14	02.679	24	23	37.408	0.337	14.49	0.43	0.57	0	PNM	0.0	–
51	92	20	07.590	24	36	38.625	0.338	17.00	1.16	1.43	1	-6.6	0.0	60	0	PSM	0.75	c
52	92	03	13.689	24	17	47.899	0.353	15.97	0.88	1.00	0	PM	0.5	c
53	92	12	46.434	24	18	57.339	0.359	17.46	1.09	1.49	0	PM	0.5	c
54	92	09	21.154	24	20	43.439	0.360	16.79	1.08	1.32	1	-12.5	0.0	60	0	PSM	0.75	c
55	92	25	45.200	24	27	24.955	0.368	16.68	1.22	1.42	1	-2.5	0.0	60	0	PSM	0.75	c
56	92	21	38.172	24	32	07.620	0.382	15.67	0.56	0.77	0	PNM	0.0	–
57	92	16	24.238	24	01	42.585	0.382	16.39	0.53	0.76	0	PNM	0.0	–
58	92	30	50.867	24	02	06.707	0.384	16.84	1.02	1.37	1	-9.2	0.0	60	0	PSM	0.75	c
59	92	18	34.069	24	06	27.481	0.387	16.68	0.73	1.26	0	PM	0.5	c
60	92	32	35.869	24	01	05.025	0.393	16.71	1.13	1.30	0	PM	0.5	c
61	92	08	09.963	24	38	40.889	0.395	18.16	1.26	1.71	0	PM	0.5	c
62	92	00	15.298	24	20	16.564	0.398	15.63	0.43	0.54	0	PNM	0.0	–
63	92	16	15.723	24	05	22.428	0.404	15.74	0.42	0.66	0	PNM	0.0	–
64	92	10	28.748	24	13	06.889	0.406	16.64	1.03	1.25	0	PM	0.5	c
65	92	35	50.079	24	10	56.529	0.413	17.64	1.16	1.58	0	PM	0.5	c
66	92	16	03.116	24	16	47.165	0.419	18.56	1.38	1.86	0	PM	0.5	c
67	92	04	08.703	24	23	25.508	0.427	16.43	0.97	1.15	0	PM	0.5	c
68	91	57	58.217	24	25	01.982	0.451	17.87	1.17	1.59	0	PM	0.5	c
69	92	17	51.991	24	25	24.078	0.460	16.86	1.05	1.26	1	-10.2	0.0	60	0	PSM	0.75	c
70	92	20	40.823	24	26	30.079	0.464	17.42	1.22	1.44	1	-13.6	0.0	60	0	PSM	0.75	c
71	92	12	35.612	24	32	13.539	0.467	12.80	0.38	0.50	2	-6.4	1.0	82	99	PSPM	1.0	–
72	92	08	26.168	24	07	23.353	0.480	18.07	1.21	1.64	0	PM	0.5	c
73	92	15	02.856	24	33	42.343	0.503	17.70	1.16	1.58	0	PM	0.5	c
74	92	16	15.064	24	11	46.380	0.511	17.95	1.21	1.64	0	PM	0.5	c
75	92	12	03.010	24	11	47.025	0.513	16.50	1.25	1.51	1	-28.8	0.0	10	0	PNM	0.0	c
76	92	31	18.442	24	12	02.907	0.513	16.51	0.60	0.73	0	PNM	0.0	–
77	92	14	56.155	24	23	52.652	0.517	17.58	...	1.33	0	PNM	0.0	c
78	92	22	19.151	24	28	20.182	0.520	16.82	1.06	1.17	1	30.6	0.0	10	0	PM	0.5	c
79	92	05	08.936	24	01	29.339	0.528	16.53	0.85	1.15	0	PM	0.5	c
80	92	16	51.923	24	08	11.103	0.543	15.89	0.84	1.03	1	-9.1	0.0	92	0	PSM	0.75	c
81	92	30	05.356	24	30	32.890	0.548	15.84	0.58	0.76	0	PNM	0.0	–
82	92	15	07.443	24	11	59.907	0.560	13.94	0.66	0.79	3	-7.9	0.2	94	91	PSPM	1.0	c
83	92	06	21.198	24	13	49.811	0.570	15.50	0.81	0.91	5	-9.8	4.7	84	0	PSM	1.0	c
84	92	19	15.954	24	17	12.536	0.580	12.71	0.30	0.42	1	-9.2	0.0	91	99	PSPM	1.0	–
85	92	09	34.475	24	20	30.984	0.582	18.19	...	1.39	0	PNM	0.0	c
86	92	18	57.607	24	23	05.877	0.596	15.35	0.44	0.58	0	PNM	0.0	–
87	92	01	10.477	24	08	26.277	0.596	13.89	0.50	0.63	4	-10.4	0.5	65	91	PSPM	1.0	–
88	91	58	17.552	24	21	12.945	0.597	12.51	0.25	0.31	1	-5.5	0.0	48	94	PPM	0.75	–
89	92	18	26.351	24	15	47.784	0.623	17.40	1.08	1.48	0	PM	0.5	c
90	92	01	25.007	24	09	05.890	0.624	16.04	0.56	0.70	0	PNM	0.0	–

Table 2—Continued

No. ^a	RA			DEC			P_{rot}	V_0	$(B - V)_0$	$(V - I)_0$	N_{RV}	$\bar{R}V$	σ_{RV}	P_{RV}	P_{PM}	mcode ^b	Weight	Sequence ^c
	h	m	s	°	'	"	Days					$km\ s^{-1}$	$km\ s^{-1}$	%	%			
91	92	24	23.928	24	14	58.386	0.629	16.24	0.98	1.17	1	-12.0	0.0	3	0	PM	0.5	c
92	92	26	21.839	24	31	29.690	0.631	16.89	0.48	0.78	0	PNM	0.0	-
93	91	57	14.271	24	05	25.539	0.636	16.75	0.54	0.77	0	PNM	0.0	-
94	92	17	09.721	24	29	47.070	0.651	18.54	1.36	1.84	0	PM	0.5	c
95	92	30	46.143	24	24	38.279	0.654	15.65	0.83	1.03	3	-7.3	0.4	93	0	PSM	1.0	c
96	91	58	33.428	24	08	29.656	0.662	16.45	0.50	0.68	0	PNM	0.0	-
97	92	09	30.053	24	35	44.559	0.691	12.68	0.31	0.40	1	-3.1	0.0	0	40	PM	0.5	-
98	92	16	51.319	24	15	24.390	0.691	16.21	1.04	1.28	0	PM	0.5	c
99	92	21	12.354	24	08	08.239	0.698	16.89	1.19	1.38	1	-5.2	0.0	60	0	PSM	0.75	c
100	92	08	27.349	24	03	45.110	0.699	15.71	0.47	0.62	0	PNM	0.0	-
101	92	25	00.266	24	33	09.974	0.716	16.37	0.54	0.72	0	PNM	0.0	-
102	92	13	33.840	24	09	01.386	0.716	16.36	0.94	1.12	0	PM	0.5	c
103	92	16	25.144	24	11	35.496	0.728	16.67	0.99	1.17	1	-12.8	0.0	60	0	PSM	0.75	c
104	92	03	48.516	24	28	05.344	0.739	16.79	0.96	1.20	1	-6.0	0.0	60	0	PSM	0.75	c
105	92	19	37.762	24	21	34.032	0.739	17.18	1.23	1.34	1	-2.7	0.0	60	0	PSM	0.75	c
106	92	13	26.946	24	10	28.054	0.754	17.70	1.11	1.51	0	PM	0.5	c
107	91	57	56.624	24	13	33.558	0.755	18.35	...	1.13	0	PNM	0.0	c
108	92	03	12.563	24	19	48.810	0.765	16.54	1.00	1.18	1	-7.7	0.0	60	0	PSM	0.75	c
109	92	10	36.026	24	29	19.735	0.766	13.57	0.45	0.57	3	6.0	0.8	0	98	PMSNM	0.0	-
110	92	14	52.749	24	18	00.011	0.766	17.79	1.13	1.55	0	PM	0.5	c
111	92	20	08.029	24	31	50.790	0.781	12.30	0.41	0.49	1	14.2	0.0	0	0	PM	0.5	-
112	92	07	39.750	24	03	08.642	0.809	17.48	0.99	1.43	0	PM	0.5	c
113	92	11	24.586	24	31	56.826	0.831	13.02	0.43	0.56	3	-8.7	0.3	94	98	PSPM	1.0	-
114	91	57	13.200	24	01	50.488	0.832	14.25	0.45	0.58	0	PM	0.5	-
115	92	34	43.392	24	29	10.280	0.852	16.72	1.02	1.33	0	PM	0.5	c
116	92	05	28.601	24	33	50.397	0.859	17.18	0.61	0.84	0	PNM	0.0	c
117	92	28	03.875	24	19	42.767	0.873	16.65	1.00	1.23	1	-7.2	0.0	60	0	PSM	0.75	c
118	92	07	11.873	24	32	32.119	0.874	15.87	0.49	0.73	0	PNM	0.0	-
119	92	17	24.772	24	20	46.825	0.877	18.79	...	1.23	0	PNM	0.0	c
120	92	09	58.041	24	27	11.593	0.879	12.69	0.29	0.39	1	-6.9	0.0	90	98	PSPM	1.0	-
121	92	15	28.784	24	16	34.798	0.882	15.76	0.93	1.09	1	12.1	0.0	0	0	PM	0.5	c
122	92	04	41.662	24	19	49.119	0.901	16.23	0.88	1.04	1	-11.4	0.0	13	0	PM	0.5	c
123	92	01	08.610	24	10	57.642	0.914	16.87	1.08	1.23	1	-9.9	0.0	60	0	PSM	0.75	c
124	92	17	15.077	24	31	18.353	0.933	16.13	1.27	1.43	0	PNM	0.0	c
125	92	28	37.932	24	18	19.663	0.933	15.97	0.92	1.05	3	-8.5	0.9	94	0	PSM	1.0	c
126	92	00	30.679	24	26	47.478	0.952	15.90	0.84	1.01	3	-4.2	2.2	2	0	PMSNM	0.0	c
127	92	17	12.083	24	20	05.537	0.971	16.30	0.92	1.13	1	-9.0	0.0	60	0	PSM	0.75	c
128	92	10	43.030	24	29	38.975	0.984	15.19	0.84	1.02	3	-9.1	0.5	92	0	PSM	1.0	c
129	92	13	24.749	24	27	16.702	0.994	16.38	1.00	1.18	1	-2.4	0.0	0	0	PM	0.5	c
130	92	33	34.645	24	15	23.669	1.006	15.43	0.80	0.92	3	-7.9	0.9	94	0	PSM	1.0	c
131	92	28	52.764	24	08	18.436	1.033	18.31	1.30	1.76	0	PM	0.5	c
132	92	14	51.129	24	34	35.496	1.044	16.28	0.86	1.10	1	-10.0	0.0	79	0	PSM	0.75	c
133	92	07	20.140	24	29	00.221	1.071	13.85	0.53	0.69	15	-8.7	4.4	94	99	PSPM	1.0	-
134	92	22	24.809	24	02	24.759	1.077	15.73	0.43	0.69	0	PNM	0.0	-
135	92	14	30.200	24	15	06.118	1.087	18.09	...	1.42	0	PNM	0.0	c

Table 2—Continued

No. ^a	RA	DEC	P_{rot}	V_0	$(B - V)_0$	$(V - I)_0$	N_{RV}	$\bar{R}V$	σ_{RV}	P_{RV}	P_{PM}	mcode ^b	Weight	Sequence ^c
	<i>h m s</i>	<i>° ' "</i>	Days					<i>km s⁻¹</i>	<i>km s⁻¹</i>	%	%			
136	92 15 37.738	24 19 51.886	1.101	15.68	0.89	1.11	11	-8.4	5.5	94	0	PSM	1.0	c
137	92 06 54.404	24 12 37.267	1.109	15.74	0.88	0.98	3	-5.8	0.5	64	0	PSM	1.0	c
138	92 04 26.144	24 12 25.491	1.111	14.70	0.75	0.88	3	-7.3	1.8	92	0	PSM	1.0	c
139	91 57 44.072	24 07 32.039	1.134	13.35	0.09	0.17	0	PNM	0.0	–
140	92 04 57.482	24 05 02.460	1.139	15.04	0.69	0.77	3	-7.6	0.6	94	0	PSM	1.0	c
141	92 23 09.578	24 17 22.898	1.165	16.70	1.31	1.52	1	-10.7	0.0	60	0	PSM	0.75	c
142	92 03 22.423	24 36 04.114	1.185	17.39	1.03	1.37	0	PM	0.5	c
143	92 08 43.059	24 26 58.897	1.185	16.15	0.93	1.02	1	-8.4	0.0	94	0	PSM	0.75	c
144	92 02 29.551	24 21 00.626	1.231	14.11	0.81	0.92	1	46.6	0.0	0	0	PNM	0.0	c
145	92 33 43.270	24 18 08.642	1.240	16.76	0.53	0.57	0	PNM	0.0	–
146	92 22 11.790	24 25 33.080	1.275	15.07	0.75	0.85	3	-8.9	0.8	93	0	PSM	1.0	c
147	92 09 30.135	24 06 48.300	1.282	13.34	0.21	0.24	0	PNM	0.0	–
148	92 20 53.430	24 31 15.538	1.288	15.32	0.96	1.07	4	-9.0	2.3	92	0	PSM	1.0	c
149	92 20 29.810	24 18 49.889	1.329	15.25	0.92	1.04	4	-5.6	0.7	53	0	PSM	1.0	c
150	92 29 43.795	24 09 02.690	1.336	16.37	0.61	0.88	0	PNM	0.0	c
151	92 13 49.468	24 13 49.591	1.351	14.38	0.31	0.44	0	PNM	0.0	–
152	92 17 17.082	24 06 02.954	1.358	15.62	0.87	0.96	3	-10.0	0.6	78	0	PSM	1.0	c
153	92 11 24.201	24 29 00.331	1.377	16.07	0.93	1.04	1	-11.5	0.0	12	0	PM	0.5	c
154	92 19 10.955	24 31 14.048	1.381	14.21	0.17	0.25	0	PNM	0.0	–
155	92 15 13.019	24 37 30.700	1.404	12.95	0.08	0.13	0	PNM	0.0	–
156	92 13 19.557	24 36 36.380	1.412	17.06	1.00	1.28	1	-11.0	0.0	60	0	PSM	0.75	c
157	92 30 26.312	24 16 52.809	1.510	13.90	0.55	0.62	3	-9.6	0.9	87	79	PSPM	1.0	i
158	92 18 05.092	24 22 51.911	1.665	17.82	1.26	1.70	0	PM	0.5	g
159	92 27 42.149	24 34 58.334	1.671	14.67	0.18	0.34	0	PNM	0.0	–
160	92 23 16.884	24 30 41.171	1.688	15.01	0.78	0.87	8	-9.5	1.5	88	0	PSM	1.0	g
161	92 17 34.056	24 31 44.336	1.778	14.04	0.56	0.65	4	-7.4	0.3	93	95	PSPM	1.0	i
162	92 32 56.852	24 21 41.509	1.830	13.92	0.45	0.57	4	8.9	0.9	0	58	PMSNM	0.0	–
163	92 28 00.414	24 25 07.949	1.837	16.56	0.92	1.14	0	PM	0.5	g
164	92 06 15.101	24 06 06.264	1.864	16.70	1.09	1.18	1	-9.3	0.0	60	0	PSM	0.75	g
165	92 16 54.615	24 27 53.650	1.914	13.94	0.51	0.61	6	-8.6	0.9	94	91	PSPM	1.0	i
166	92 30 31.036	24 07 27.535	1.929	14.35	0.15	0.27	0	PNM	0.0	–
167	92 20 28.848	24 35 58.669	2.055	15.47	0.93	1.09	3	-8.3	1.4	94	0	PSM	1.0	g
168	91 56 04.948	24 08 03.680	2.055	14.53	0.60	0.68	2	25.4	106.5	0	0	PM	0.5	i
169	92 09 11.212	24 25 47.980	2.098	13.47	0.10	0.25	0	PNM	0.0	–
170	92 11 50.760	24 30 24.946	2.143	16.05	0.86	1.05	1	-11.1	0.0	25	0	PM	0.5	g
171	92 13 45.925	24 14 25.475	2.143	15.56	0.57	0.59	0	PNM	0.0	i
172	92 28 07.994	24 20 44.497	2.162	15.15	0.67	0.81	3	21.8	0.5	0	0	PMSNM	0.0	i
173	92 15 38.782	24 20 44.717	2.209	13.02	0.40	0.54	32	-8.3	21.4	94	99	PSPM	1.0	–
174	92 06 30.894	24 00 56.607	2.290	16.06	0.78	0.93	0	PNM	0.0	g
175	92 09 28.295	24 31 45.510	2.333	15.35	0.85	1.03	14	-8.1	34.5	94	0	PSM	1.0	g
176	92 00 49.191	24 13 25.538	2.344	14.11	0.52	0.64	4	-9.3	0.6	91	0	PSM	1.0	i
177	92 11 14.808	24 36 06.634	2.389	13.36	0.39	0.46	1	24.2	0.0	0	5	PNM	0.0	–
178	92 18 42.748	24 31 23.187	2.389	14.33	0.60	0.71	1	-7.9	0.0	94	94	PSPM	1.0	i
179	92 15 52.844	24 17 23.502	2.400	15.35	0.90	1.03	19	-7.1	13.3	91	0	PSM	1.0	g
180	92 06 57.014	24 04 18.563	2.435	12.39	1.49	1.57	0	PNM	0.0	g

Table 2—Continued

No. ^a	RA			DEC			P_{rot}	V_0	$(B - V)_0$	$(V - I)_0$	N_{RV}	$\bar{R}V$	σ_{RV}	P_{RV}	P_{PM}	mcode ^b	Weight	Sequence ^c
	h	m	s	°	'	"	Days					$km\ s^{-1}$	$km\ s^{-1}$	%	%			
181	92	15	46.005	24	20	09.567	2.476	14.37	0.66	0.79	11	-6.9	1.6	90	0	PSM	1.0	i
182	92	17	12.495	24	22	55.516	2.508	14.10	0.55	0.68	4	-9.1	0.2	92	96	PSPM	1.0	i
183	92	05	02.673	24	21	51.514	2.521	14.26	0.54	0.65	15	-8.2	2.1	94	0	PSM	1.0	i
184	92	09	54.662	24	27	51.652	2.534	16.61	0.75	0.89	0	PNM	0.0	g
185	92	32	16.752	24	21	38.351	2.547	16.97	0.97	1.15	0	PNM	0.0	g
186	91	54	49.059	24	24	08.451	2.560	14.14	0.56	0.65	3	-7.8	0.6	94	0	PSM	1.0	i
187	91	57	59.150	24	34	07.920	2.599	12.22	-0.0	0.06	0	PNM	0.0	–
188	92	35	52.661	24	14	57.610	2.599	14.75	0.76	0.80	4	-9.1	0.0	92	0	PSM	1.0	g
189	92	13	08.516	24	22	00.117	2.683	16.61	0.96	1.20	1	11.2	0.0	10	0	PM	0.5	g
190	92	21	01.972	24	12	59.892	2.683	14.60	0.65	0.77	0	PM	0.5	i
191	92	02	37.874	24	15	49.713	2.697	14.19	0.56	0.64	3	-6.8	0.7	89	0	PSM	1.0	i
192	92	33	33.025	24	25	23.529	2.742	14.38	0.58	0.66	14	-9.8	1.3	83	0	PSM	1.0	i
193	92	12	49.016	24	35	31.245	2.788	13.55	0.62	0.71	3	-8.2	0.9	94	0	PSM	1.0	i
194	92	28	54.467	24	17	45.379	2.835	14.42	0.68	0.78	18	-7.5	17.8	94	0	PSM	1.0	i
195	92	23	16.637	24	01	08.905	2.835	15.73	0.89	0.99	3	-8.8	2.0	93	0	PSM	1.0	g
196	92	06	11.063	24	04	41.291	2.851	14.16	0.51	0.62	3	-8.6	0.5	94	0	PSM	1.0	i
197	92	10	27.100	24	17	04.173	2.868	14.28	0.58	0.69	5	-7.4	0.2	93	90	PSPM	1.0	i
198	92	10	20.755	24	23	21.643	2.884	14.16	0.65	0.75	3	5.7	0.4	0	0	PMSNM	0.0	i
199	92	03	51.235	24	25	26.990	2.918	14.52	0.61	0.68	15	-6.0	1.8	70	0	PSM	1.0	i
200	92	29	19.900	24	09	32.092	2.918	14.44	0.69	0.86	1	-9.8	0.0	84	0	PSM	0.75	i
201	92	17	05.381	24	29	48.904	2.952	17.43	1.22	1.65	0	PM	0.5	g
202	92	03	46.208	24	23	16.136	3.079	16.51	0.96	1.14	1	-15.9	0.0	60	0	PSM	0.75	g
203	91	59	19.296	24	31	51.511	3.079	16.59	1.00	1.13	1	73.7	0.0	10	0	PM	0.5	g
204	92	09	11.788	24	02	12.399	3.118	12.39	0.20	0.30	1	-2.6	0.0	0	72	PPM	0.75	–
205	92	24	47.714	24	19	46.922	3.197	14.46	0.68	0.78	3	-7.2	0.4	92	0	PSM	1.0	i
206	92	15	18.979	24	11	45.624	3.197	14.43	0.74	0.86	3	-7.9	0.3	94	0	PSM	1.0	i
207	92	06	49.433	24	29	30.316	3.218	14.62	0.68	0.79	3	-8.5	0.2	94	0	PSM	1.0	i
208	92	27	24.296	24	26	00.896	3.218	16.15	0.78	0.92	0	PNM	0.0	g
209	91	58	42.601	24	23	42.578	3.303	14.43	0.57	0.65	16	-8.8	2.4	93	0	PSM	1.0	i
210	92	13	30.049	24	27	56.816	3.347	17.91	1.16	1.58	0	PM	0.5	g
211	91	59	34.072	24	23	00.672	3.347	13.94	0.48	0.56	4	-7.6	0.1	94	96	PSPM	1.0	–
212	91	57	15.205	24	23	59.497	3.392	14.27	0.59	0.66	3	14.8	0.4	0	0	PMSNM	0.0	i
213	92	27	23.994	24	36	37.080	3.415	14.23	0.94	1.03	2	18.2	0.5	0	0	PNM	0.0	g
214	92	32	47.294	24	14	01.601	3.439	14.68	0.65	0.78	3	-7.7	0.4	94	0	PSM	1.0	i
215	91	55	01.474	24	23	02.375	3.463	17.91	...	1.07	0	PNM	0.0	g
216	92	32	04.722	24	34	31.980	3.463	15.29	0.86	1.03	3	-7.8	0.8	94	0	PSM	1.0	g
217	92	02	59.901	24	33	56.728	3.511	14.67	0.70	0.88	7	34.7	13.9	0	0	PMSNM	0.0	i
218	92	07	34.449	24	26	28.431	3.561	14.49	0.61	0.69	3	-7.9	0.3	94	0	PSM	1.0	i
219	92	07	24.781	24	16	24.093	3.561	14.69	0.63	0.74	4	-8.1	0.9	94	0	PSM	1.0	i
220	92	20	21.652	24	24	09.742	3.587	16.41	0.71	0.84	0	PNM	0.0	i
221	92	17	35.759	24	13	03.339	3.587	17.22	1.36	1.51	1	-4.8	0.0	60	0	PSM	0.75	g
222	92	27	57.914	24	27	00.504	3.612	14.21	0.71	0.80	3	-8.9	0.2	93	67	PSPM	1.0	i
223	92	01	15.531	24	34	41.353	3.692	17.18	0.99	1.18	0	PNM	0.0	g
224	92	26	52.244	24	32	20.014	3.692	14.71	0.66	0.77	3	-8.8	0.2	93	0	PSM	1.0	i
225	92	18	53.569	24	10	42.158	3.710	14.87	0.83	0.92	37	-5.9	8.6	69	0	PSM	1.0	g

Table 2—Continued

No. ^a	RA			DEC			P_{rot}	V_0	$(B - V)_0$	$(V - I)_0$	N_{RV}	$\bar{R}V$	σ_{RV}	P_{RV}	P_{PM}	mcode ^b	Weight	Sequence ^c
	h	m	s	°	'	"	Days					$km\ s^{-1}$	$km\ s^{-1}$	%	%			
226	92	11	16.620	24	19	56.178	3.720	14.34	0.76	0.85	6	-8.0	0.3	94	86	PSPM	1.0	i
227	92	22	17.860	24	00	42.352	3.720	14.38	0.59	0.68	3	-9.8	0.2	83	0	PSM	1.0	i
228	92	21	35.123	24	23	19.569	3.748	15.68	0.88	0.96	3	-7.9	0.5	94	0	PSM	1.0	g
229	92	14	15.835	24	19	50.176	3.776	18.00	...	1.45	0	PNM	0.0	g
230	92	02	57.209	24	27	07.158	3.776	14.57	0.58	0.66	3	-8.1	0.6	94	0	PSM	1.0	i
231	92	25	04.742	24	25	46.278	3.776	17.58	0.77	0.94	0	PNM	0.0	i
232	92	02	23.427	24	17	53.763	3.805	18.84	1.47	1.97	0	PM	0.5	g
233	92	25	41.272	24	33	25.135	3.834	18.51	...	1.36	0	PNM	0.0	g
234	92	10	27.731	24	19	07.220	3.864	17.17	1.25	1.33	0	PM	0.5	g
235	92	30	19.199	24	13	43.061	3.864	14.56	0.58	0.69	3	-7.8	0.1	94	0	PSM	1.0	i
236	92	06	40.479	24	09	39.941	3.924	14.54	0.71	0.84	0	PM	0.5	i
237	92	02	36.693	24	24	23.811	3.955	14.84	0.64	0.73	3	-7.3	0.1	92	0	PSM	1.0	i
238	92	01	58.460	24	32	58.143	3.955	14.58	0.60	0.66	3	-7.7	0.2	94	0	PSM	1.0	i
239	92	01	45.963	24	18	49.916	3.955	14.55	0.62	0.69	1	-6.5	0.0	84	72	PSPM	1.0	i
240	92	13	06.566	24	03	06.294	3.986	14.46	0.56	0.64	3	-8.1	0.5	94	0	PSM	1.0	i
241	92	16	03.940	24	12	41.922	3.986	14.71	0.68	0.77	3	-8.1	0.1	94	0	PSM	1.0	i
242	92	22	58.592	24	10	38.347	3.986	14.41	0.71	0.82	22	-8.1	5.8	94	0	PSM	1.0	i
243	92	25	38.004	24	02	08.190	4.187	14.94	0.76	0.85	3	-7.9	0.5	94	0	PSM	1.0	i
244	91	58	09.066	24	20	02.385	4.222	14.57	0.57	0.65	3	-7.0	0.2	91	0	PSM	1.0	i
245	91	56	05.552	24	30	26.182	4.258	14.63	0.62	0.74	16	-7.0	5.0	91	0	PSM	1.0	i
246	92	32	38.066	24	24	14.398	4.258	14.73	0.64	0.73	5	-8.9	1.2	93	0	PSM	1.0	i
247	92	15	40.182	24	12	51.082	4.258	14.96	0.77	0.85	3	-7.6	0.3	94	0	PSM	1.0	i
248	92	30	26.285	24	20	12.094	4.294	14.75	0.68	0.77	3	-8.7	0.4	94	0	PSM	1.0	i
249	92	08	17.681	24	19	13.228	4.332	14.68	0.63	0.72	3	-8.2	0.4	94	0	PSM	1.0	i
250	92	13	03.517	24	23	28.145	4.332	14.55	0.65	0.76	3	-9.5	0.0	89	0	PSM	1.0	i
251	92	29	18.746	24	10	15.708	4.369	15.23	0.87	1.01	0	PM	0.5	i
252	92	15	32.245	24	29	31.223	4.408	15.26	0.75	0.86	3	-7.5	0.8	93	0	PSM	1.0	i
253	92	22	48.430	24	07	02.850	4.447	14.55	0.64	0.71	3	-8.1	0.7	94	0	PSM	1.0	i
254	92	23	32.073	24	18	09.075	4.447	15.00	0.77	0.90	3	-6.6	0.3	86	0	PSM	1.0	i
255	92	14	21.081	24	15	05.026	4.487	15.02	0.76	0.89	3	-9.0	0.4	92	0	PSM	1.0	i
256	92	20	28.436	24	17	17.006	4.487	14.86	0.69	0.77	4	-8.7	0.4	94	0	PSM	1.0	i
257	92	31	47.254	24	02	55.390	4.527	16.24	1.03	1.08	1	19.2	0.0	0	0	PM	0.5	g
258	92	27	31.080	24	17	02.813	4.527	14.97	0.76	0.82	3	-9.0	0.3	92	0	PSM	1.0	i
259	92	10	37.949	24	23	37.236	4.569	16.37	0.96	1.13	1	2.2	0.0	0	0	PM	0.5	g
260	92	11	39.252	24	31	43.038	4.611	14.96	0.71	0.86	3	-7.9	1.0	94	0	PSM	1.0	i
261	92	04	42.376	24	19	18.900	4.611	13.55	1.57	1.60	0	PNM	0.0	g
262	92	16	35.883	24	26	41.738	4.654	15.23	0.79	0.89	17	-0.7	16.3	0	0	PMSNM	0.0	i
263	92	20	52.167	24	16	56.737	4.654	16.94	0.76	0.95	0	PNM	0.0	i
264	92	15	45.978	24	19	36.210	4.697	15.15	0.80	0.90	14	-9.2	9.1	91	0	PSM	1.0	i
265	92	29	19.213	24	37	49.899	4.697	15.09	0.75	0.87	3	-8.5	0.1	94	0	PSM	1.0	i
266	92	14	06.304	24	27	10.618	4.742	14.91	0.70	0.77	3	-6.2	0.1	79	0	PSM	1.0	i
267	92	29	06.552	24	25	51.846	4.742	14.19	0.67	0.85	3	-7.9	1.0	94	58	PSPM	1.0	i
268	92	22	51.286	24	27	49.682	4.742	14.59	0.64	0.71	3	-8.1	0.3	94	0	PSM	1.0	i
269	92	01	54.368	24	03	16.758	4.787	16.29	0.92	1.05	0	PM	0.5	i
270	92	08	44.405	24	17	08.121	4.833	18.49	1.35	1.82	0	PM	0.5	g

Table 2—Continued

No. ^a	RA			DEC			P_{rot}	V_0	$(B - V)_0$	$(V - I)_0$	N_{RV}	$\bar{R}V$	σ_{RV}	P_{RV}	P_{PM}	mcode ^b	Weight	Sequence ^c
	h	m	s	°	'	"	Days					$km\ s^{-1}$	$km\ s^{-1}$	%	%			
271	92	31	10.615	24	17	34.770	4.833	14.81	0.70	0.71	3	-7.4	0.2	93	0	PSM	1.0	i
272	92	24	45.104	24	16	44.164	4.833	15.01	0.71	0.83	4	-7.4	0.4	93	0	PSM	1.0	i
273	92	17	57.896	24	26	16.188	4.929	14.43	0.59	0.67	4	-6.1	0.2	75	68	PSPM	1.0	i
274	92	05	54.941	23	59	35.130	4.929	15.07	0.69	0.73	1	-7.6	0.0	94	0	PSM	0.75	i
275	92	22	31.099	24	35	49.880	4.978	18.27	1.31	1.78	0	PM	0.5	g
276	92	06	55.640	24	33	11.725	5.028	15.16	0.78	0.82	5	-8.4	1.1	94	0	PSM	1.0	i
277	92	25	20.728	24	36	44.242	5.028	15.05	0.70	0.85	3	-8.3	0.6	94	0	PSM	1.0	i
278	92	22	37.251	24	03	16.223	5.079	18.15	1.29	1.74	0	PM	0.5	g
279	92	29	42.092	24	14	43.266	5.079	14.88	0.73	0.83	3	-9.2	0.3	91	0	PSM	1.0	i
280	92	11	49.360	24	00	33.639	5.131	16.67	0.87	0.94	0	PNM	0.0	i
281	92	14	18.417	24	15	53.318	5.184	17.23	1.24	1.38	1	-11.6	0.0	60	0	PSM	0.75	g
282	92	19	54.708	24	30	52.741	5.238	15.12	0.76	0.84	3	-7.6	0.4	94	0	PSM	1.0	i
283	92	19	48.611	24	17	22.390	5.248	14.93	0.72	0.83	17	-8.9	6.8	93	0	PSM	1.0	i
284	92	33	39.672	24	31	34.537	5.293	17.53	1.25	1.46	1	1.5	0.0	60	0	PSM	0.75	g
285	92	24	45.983	24	04	43.083	5.293	13.16	0.47	0.63	3	25.0	0.3	0	0	PMSNM	0.0	–
286	92	10	44.540	24	26	34.096	5.408	15.06	0.77	0.86	3	-9.5	0.4	88	0	PSM	1.0	i
287	92	25	51.682	24	24	33.747	5.467	14.88	0.70	0.73	3	-8.0	0.5	94	0	PSM	1.0	i
288	92	11	54.056	24	09	42.241	5.467	15.16	0.75	0.81	1	-7.3	0.0	93	0	PSM	0.75	i
289	92	29	05.233	23	59	35.102	5.467	15.85	0.95	1.17	2	-6.5	1.3	84	0	PSM	1.0	i
290	92	08	46.520	24	27	16.983	5.527	15.04	0.80	0.90	3	-9.2	0.5	91	0	PSM	1.0	i
291	92	09	55.734	24	19	24.104	5.527	16.93	1.17	1.25	1	-6.5	0.0	60	0	PSM	0.75	g
292	92	11	13.407	24	22	52.646	5.527	15.30	0.89	1.00	3	-8.9	0.4	93	0	PSM	1.0	i
293	92	12	01.307	24	37	50.002	5.527	15.09	0.73	0.71	3	-8.4	0.5	94	0	PSM	1.0	i
294	92	16	20.777	24	12	18.013	5.527	15.24	0.79	0.84	3	-7.9	0.3	94	0	PSM	1.0	i
295	92	21	38.172	24	25	37.015	5.589	15.96	0.73	0.86	0	PNM	0.0	i
296	92	14	21.795	23	59	36.228	5.589	16.39	0.97	1.10	0	PM	0.5	i
297	92	09	19.341	24	22	17.840	5.652	15.30	0.80	0.85	3	-8.2	0.7	94	0	PSM	1.0	i
298	92	20	43.213	24	34	06.444	5.652	15.44	0.81	0.96	3	-8.8	0.3	93	0	PSM	1.0	i
299	92	23	55.144	24	22	53.174	5.652	17.68	1.12	1.53	0	PM	0.5	g
300	92	04	25.292	24	16	05.170	5.652	15.16	0.72	0.77	3	-9.5	0.5	89	0	PSM	1.0	i
301	92	20	27.640	24	18	21.187	5.652	15.36	0.81	0.87	3	-8.7	0.1	94	0	PSM	1.0	i
302	92	04	15.624	24	27	01.980	5.717	15.14	0.72	0.78	3	-7.7	0.2	94	0	PSM	1.0	i
303	92	24	20.110	24	36	05.584	5.717	16.01	0.89	1.03	0	PM	0.5	i
304	92	10	51.215	24	16	07.264	5.717	15.20	0.78	0.82	3	-9.2	0.4	91	0	PSM	1.0	i
305	92	01	40.223	24	21	50.339	5.783	17.51	1.27	1.41	1	-8.8	0.0	60	0	PSM	0.75	g
306	92	07	42.579	24	22	17.606	5.783	15.71	0.84	0.91	3	18.5	1.5	0	0	PMSNM	0.0	i
307	92	09	21.566	24	32	39.954	5.783	17.59	1.10	1.51	0	PM	0.5	g
308	92	21	37.540	24	20	39.313	5.783	16.52	1.06	1.16	0	PM	0.5	g
309	92	22	30.659	24	32	08.492	5.783	16.52	1.05	1.17	1	-6.7	0.0	60	0	PSM	0.75	g
310	92	11	38.785	24	17	45.379	5.783	16.75	1.08	1.28	1	-13.3	0.0	60	0	PSM	0.75	g
311	91	57	21.467	24	09	13.306	5.783	15.33	0.74	0.77	0	PM	0.5	i
312	91	58	55.208	24	12	03.477	5.783	15.26	0.76	0.83	0	PM	0.5	i
313	92	14	45.745	24	18	25.005	5.783	15.41	0.85	0.92	3	-9.2	0.7	91	0	PSM	1.0	i
314	92	17	55.369	24	11	23.933	5.783	15.30	0.79	0.83	3	-9.0	0.1	93	0	PSM	1.0	i
315	92	08	51.244	24	19	59.268	5.850	16.16	0.96	1.06	1	-8.6	0.0	94	0	PSM	0.75	i

Table 2—Continued

No. ^a	RA			DEC			P_{rot}	V_0	$(B - V)_0$	$(V - I)_0$	N_{RV}	$\bar{R}V$	σ_{RV}	P_{RV}	P_{PM}	mcode ^b	Weight	Sequence ^c
	h	m	s	°	'	"	Days					$km\ s^{-1}$	$km\ s^{-1}$	%	%			
316	92	23	36.934	24	02	52.705	5.850	15.06	0.73	0.81	3	-7.6	1.3	94	0	PSM	1.0	i
317	92	15	28.922	24	32	08.753	5.919	15.38	0.75	0.87	3	-7.4	0.2	93	0	PSM	1.0	i
318	92	02	32.518	24	35	08.167	5.919	15.71	0.64	0.79	0	PNM	0.0	–
319	92	30	56.635	24	32	54.710	5.919	14.46	0.58	0.70	3	21.4	0.3	0	0	PMSNM	0.0	–
320	92	08	19.246	24	05	33.538	5.919	15.26	0.75	0.80	3	-7.7	0.1	94	0	PSM	1.0	i
321	92	19	01.479	24	18	03.293	5.919	16.62	1.04	1.17	1	-9.6	0.0	60	0	PSM	0.75	g
322	92	03	00.698	24	21	26.760	5.990	15.25	0.76	0.81	3	-8.4	0.1	94	0	PSM	1.0	i
323	92	24	42.770	24	28	53.725	5.990	16.07	0.98	1.06	1	-8.3	0.0	94	0	PSM	0.75	i
324	92	13	36.092	24	03	08.024	6.029	14.37	0.56	0.66	19	-7.5	17.5	93	0	PSM	1.0	–
325	91	56	32.880	24	22	48.999	6.137	16.86	0.87	1.12	0	PNM	0.0	i
326	92	07	27.226	24	29	17.806	6.137	15.60	0.87	0.92	3	-8.1	0.5	94	0	PSM	1.0	i
327	92	24	55.651	24	38	44.233	6.137	13.21	0.24	0.38	0	PNM	0.0	–
328	92	10	15.948	24	17	20.666	6.137	15.44	0.81	0.85	3	-8.6	0.8	94	0	PSM	1.0	i
329	91	59	07.650	24	08	59.202	6.137	13.20	0.56	0.61	0	PM	0.5	–
330	92	18	46.730	24	11	03.437	6.137	14.83	0.69	0.76	4	-7.2	0.2	92	0	PSM	1.0	i
331	91	55	53.522	24	24	01.585	6.213	16.49	1.11	1.36	1	-6.2	0.0	60	0	PSM	0.75	g
332	92	09	54.965	24	37	15.320	6.291	15.34	0.73	0.81	3	-8.0	0.6	94	0	PSM	1.0	i
333	92	22	17.805	24	21	51.205	6.291	15.66	0.88	0.92	4	-8.7	0.9	94	0	PSM	1.0	i
334	92	20	43.515	24	15	26.305	6.291	15.54	0.84	0.89	4	-7.3	0.8	93	0	PSM	1.0	i
335	91	57	33.552	24	27	17.643	6.372	15.71	0.85	1.01	0	PM	0.5	i
336	92	11	59.907	24	36	02.185	6.372	15.32	0.74	0.80	3	-8.9	0.2	93	0	PSM	1.0	i
337	92	15	16.013	24	24	53.186	6.372	17.71	1.08	1.48	0	PM	0.5	i
338	92	35	04.047	24	20	22.112	6.372	18.21	...	0.95	0	PNM	0.0	g
339	92	16	41.184	24	12	45.225	6.372	17.30	1.30	1.40	0	PM	0.5	g
340	92	08	02.410	24	20	36.285	6.454	15.46	0.83	0.85	4	-7.2	0.5	92	0	PSM	1.0	i
341	92	16	34.647	24	17	05.162	6.454	17.13	1.37	1.55	0	PM	0.5	g
342	92	18	31.075	24	13	36.737	6.454	15.45	0.82	0.86	3	-8.5	0.9	94	0	PSM	1.0	i
343	92	23	14.989	24	25	17.761	6.538	15.57	0.84	0.91	3	-9.3	0.5	91	0	PSM	1.0	i
344	92	31	57.444	24	28	11.091	6.538	15.87	0.88	1.04	3	-7.6	0.6	94	0	PSM	1.0	i
345	92	34	52.099	24	35	57.598	6.538	16.95	1.13	1.32	1	-10.8	0.0	60	0	PSM	0.75	g
346	92	28	19.942	24	37	59.958	6.538	16.55	1.04	1.16	0	PM	0.5	i
347	92	22	58.455	24	36	14.435	6.538	15.64	0.87	0.94	3	-8.4	0.5	94	0	PSM	1.0	i
348	92	08	36.742	24	08	13.932	6.538	15.52	0.80	0.85	3	-7.0	0.5	91	0	PSM	1.0	i
349	92	15	35.349	24	00	50.935	6.538	16.31	0.82	0.98	0	PNM	0.0	i
350	92	22	40.986	24	16	04.758	6.538	17.66	1.28	1.73	0	PM	0.5	g
351	92	32	06.398	24	23	24.650	6.625	17.20	1.04	1.38	0	PM	0.5	i
352	92	29	26.354	24	29	45.608	6.625	18.17	1.27	1.72	0	PM	0.5	g
353	92	16	37.284	24	21	30.234	6.625	15.77	0.91	0.96	3	-8.2	0.7	94	0	PSM	1.0	i
354	92	27	21.660	24	15	47.159	6.625	15.92	0.95	1.02	0	PM	0.5	i
355	92	12	45.967	24	23	50.186	6.805	17.77	1.14	1.56	0	PM	0.5	g
356	92	18	42.281	24	29	10.417	6.805	15.62	0.82	0.87	3	-8.9	0.5	93	0	PSM	1.0	i
357	92	25	38.882	24	20	51.981	6.805	15.89	0.91	1.02	6	-8.1	1.4	94	0	PSM	1.0	i
358	92	24	17.391	24	21	22.853	6.805	12.62	0.59	0.63	1	-2.1	0.0	0	0	PNM	0.0	–
359	92	16	52.143	24	08	33.686	6.805	18.72	1.44	1.93	0	PM	0.5	g
360	92	25	04.166	24	01	16.712	6.805	15.70	0.87	0.93	3	-8.3	0.4	94	0	PSM	1.0	i

Table 2—Continued

No. ^a	RA			DEC			P_{rot}	V_0	$(B - V)_0$	$(V - I)_0$	N_{RV}	$\bar{R}V$	σ_{RV}	P_{RV}	P_{PM}	mcode ^b	Weight	Sequence ^c
	h	m	s	°	'	"	Days					$km\ s^{-1}$	$km\ s^{-1}$	%	%			
361	92	04	11.697	24	26	26.893	6.898	16.44	0.97	1.09	1	-5.9	0.0	60	0	PSM	0.75	i
362	92	15	46.005	24	34	56.487	6.898	15.46	0.82	0.93	3	-7.7	0.3	94	0	PSM	1.0	i
363	92	26	52.985	24	03	37.303	6.898	15.89	0.97	1.06	1	-8.8	0.0	93	0	PSM	0.75	i
364	92	01	51.923	24	35	35.735	6.995	16.50	1.05	1.14	1	-6.7	0.0	60	0	PSM	0.75	i
365	92	11	04.673	24	22	47.125	6.995	15.16	0.94	1.00	16	-13.6	16.8	0	0	PMSNM	0.0	i
366	92	35	07.233	24	22	10.925	6.995	16.74	1.09	1.26	1	-8.6	0.0	60	0	PSM	0.75	i
367	92	21	41.962	24	27	54.914	6.995	15.88	0.93	0.95	3	-8.7	0.1	94	0	PSM	1.0	i
368	92	16	51.786	24	19	05.517	6.995	17.96	1.19	1.61	0	PM	0.5	g
369	92	08	56.160	24	13	31.471	6.995	15.16	0.61	0.70	0	PNM	0.0	-
370	91	59	31.957	24	20	10.838	7.301	17.29	1.19	1.34	0	PM	0.5	g
371	92	17	39.769	24	28	03.971	7.301	15.93	0.94	0.95	6	-7.7	1.4	94	0	PSM	1.0	i
372	92	16	38.135	24	31	26.037	7.301	17.09	1.12	1.35	0	PM	0.5	i
373	92	34	41.415	24	32	44.719	7.301	16.07	0.98	1.08	1	-9.4	0.0	90	0	PSM	0.75	i
374	92	08	11.968	24	25	11.602	7.409	16.99	1.17	1.28	1	-15.7	0.0	60	0	PSM	0.75	i
375	92	00	47.186	24	28	54.638	7.520	16.08	0.90	0.98	1	-9.1	0.0	92	0	PSM	0.75	i
376	91	55	03.369	24	33	40.509	7.520	16.06	0.51	0.65	0	PNM	0.0	-
377	92	24	51.010	24	27	23.465	7.520	16.12	0.95	1.02	0	PM	0.5	i
378	91	55	18.915	24	13	00.496	7.520	13.65	0.63	0.68	2	14.5	0.2	0	0	PM	0.5	-
379	92	06	27.708	24	12	53.774	7.520	16.27	0.98	1.05	1	-7.5	0.0	93	0	PSM	0.75	i
380	92	05	34.808	24	15	02.506	7.520	15.90	0.88	0.95	1	-7.7	0.0	94	0	PSM	0.75	i
381	92	26	03.657	24	24	54.326	7.635	17.79	1.15	1.56	0	PM	0.5	i
382	92	36	01.450	24	16	45.064	7.635	17.46	...	1.33	0	PNM	0.0	g
383	92	19	42.129	24	27	05.043	7.753	15.97	0.91	0.93	1	-7.2	0.0	92	0	PSM	0.75	i
384	92	15	36.667	24	16	25.405	7.753	13.71	0.64	0.70	6	-3.3	0.5	0	88	PMSNM	0.0	-
385	92	33	32.943	24	32	30.334	7.875	16.40	1.06	1.13	1	-6.9	0.0	60	0	PSM	0.75	i
386	92	31	13.746	24	34	59.089	7.875	16.26	1.00	1.10	0	PM	0.5	i
387	92	14	32.479	24	33	11.595	8.001	13.22	0.66	0.74	1	-1.8	0.0	0	0	PNM	0.0	-
388	92	33	48.241	24	28	58.930	8.001	16.48	1.11	1.19	1	-9.5	0.0	60	0	PSM	0.75	i
389	92	10	11.884	24	11	50.548	8.001	17.04	1.19	1.28	1	-6.1	0.0	60	0	PSM	0.75	i
390	92	12	18.309	24	05	50.388	8.001	15.97	0.88	0.96	3	-6.2	0.7	77	0	PSM	1.0	i
391	92	12	04.164	24	17	59.077	8.001	16.53	1.14	1.16	0	PM	0.5	i
392	92	00	50.565	24	34	09.918	8.131	16.36	0.98	1.07	0	PM	0.5	i
393	92	23	07.628	24	27	23.802	8.131	17.25	1.13	1.37	1	-4.5	0.0	60	0	PSM	0.75	i
394	92	33	02.922	24	30	50.125	8.265	14.86	0.87	0.96	3	-17.8	0.4	0	0	PMSNM	0.0	-
395	92	14	44.399	24	14	41.646	8.265	15.60	1.01	1.09	5	-12.0	7.0	2	0	PMSNM	0.0	i
396	92	02	26.860	24	34	28.478	8.404	12.28	0.65	0.68	0	PNM	0.0	-
397	92	19	23.589	24	28	20.457	8.404	16.07	0.37	0.41	0	PNM	0.0	-
398	92	30	32.465	24	34	37.295	8.404	16.05	0.91	0.98	1	22.2	0.0	0	0	PM	0.5	i
399	92	02	22.932	24	05	50.258	8.404	14.51	0.77	0.82	3	17.7	0.3	0	0	PMSNM	0.0	-
400	91	55	12.076	24	14	23.374	8.404	16.10	0.91	1.05	0	PM	0.5	i
401	92	09	04.592	24	20	53.430	8.547	17.83	1.14	1.56	0	PM	0.5	i
402	92	01	30.253	24	04	42.033	8.547	16.58	0.95	1.12	1	-5.2	0.0	60	0	PSM	0.75	i
403	92	05	24.509	24	07	09.785	8.547	14.91	0.58	0.67	3	11.3	0.1	0	0	PMSNM	0.0	-
404	92	23	00.624	24	01	35.004	8.547	17.72	1.16	1.57	0	PM	0.5	i
405	92	20	38.132	24	27	55.834	8.696	17.06	1.18	1.27	0	PM	0.5	i

C. THE ROTATION PERIOD DISTRIBUTION OF NON-MEMBERS

In this section, we display and briefly comment upon the rotation period distribution of the non-members among the 441 rotators, which presumably are mostly field stars belonging to the Galactic disk. Unlike the cluster members we do not know the ages, distances, or masses of these stars. We will therefore only comment on a comparison between the two distributions and on distinct features in the period distribution of the 131 non-members shown in Figure 14. First, rotation periods are detected over approximately the same range ($\sim 0.1 - 15$ days) as for the 150 Myr cluster members, with only a few stars rotating slower. Second, there appears to be no indication of a bimodal distribution, but rather a distribution with a peak of ultra fast rotators and a long tail of periods up to and beyond 15 days. Third, and most strikingly, as shown by the 0.1 day resolution of the insert in Figure 14, the non-member distribution exhibits a very distinct peak between 0.1 and 0.2 days. The phased light curves for these stars (Appendix A) shows that the majority of these stars have large and well defined photometric variability with with peak-to-peak amplitudes of 0^m1 or higher. It is possible that most of these stars are contact binaries of, e.g., the W UMa-type. Such systems typically have orbital periods of order 0.2-0.5 days and occur with a frequency of $\sim 0.2\%$ (OGLE Variable Star Catalog; Rucinski 1997). The frequency of rapidly varying non-members found in the field of M35 is ~ 20 out of 13700 or $\sim 0.15\%$ and thus in good agreement with that found from the OGLE Catalog. Indeed, if the light curves for these stars represent eclipses rather than spot-modulation, then the measured periods must be doubled bringing them into the expected range for W Uma systems.

REFERENCES

- Alphenaar, P., & van Leeuwen, F. 1981, Informational Bulletin on Variable Stars, 1957, 1
- Barnes, S., & Sofia, S. 1996, ApJ, 462, 746
- Barnes, S. A. 2003, ApJ, 586, 464
- . 2007, ApJ, 669, 1167
- Barrado y Navascués, D., Deliyannis, C. P., & Stauffer, J. R. 2001, ApJ, 549, 452
- Benz, W., Mayor, M., & Mermilliod, J. C. 1984, A&A, 138, 93
- Bouvier, J., Forestini, M., & Allain, S. 1997, A&A, 326, 1023
- Braden, E., Mathieu, R. D., & Meibom, S. 2008, in preparation.

Table 2—Continued

No. ^a	RA			DEC			P_{rot}	V_0	$(B - V)_0$	$(V - I)_0$	N_{RV}	$\bar{R}V$	σ_{RV}	P_{RV}	P_{PM}	mcode ^b	Weight	Sequence ^c
	<i>h</i>	<i>m</i>	<i>s</i>	$^{\circ}$	$'$	$''$	Days					$km\ s^{-1}$	$km\ s^{-1}$	%	%			
406	92	28	33.620	24	29	39.408	8.696	16.55	1.14	1.18	1	-6.9	0.0	60	0	PSM	0.75	i
407	92	05	58.099	24	13	55.435	8.696	17.38	1.21	1.41	0	PM	0.5	i
408	92	08	48.195	24	18	24.009	8.696	13.29	0.85	0.89	0	PNM	0.0	-
409	92	27	49.016	24	10	01.865	8.696	17.13	1.32	1.37	1	-9.4	0.0	60	0	PSM	0.75	i
410	92	05	49.585	24	15	20.277	8.850	16.50	1.08	1.08	1	-7.6	0.0	60	0	PSM	0.75	i
411	92	21	07.520	24	06	12.800	8.850	17.20	0.95	1.32	0	PM	0.5	i
412	92	30	28.867	24	17	07.950	8.850	17.01	1.18	1.29	1	-8.5	0.0	60	0	PSM	0.75	i
413	92	03	55.245	24	01	21.999	9.174	16.37	0.88	1.00	0	PNM	0.0	-
414	92	11	59.687	24	07	47.352	9.174	16.58	1.04	1.31	1	-4.4	0.0	60	0	PSM	0.75	i
415	92	04	54.598	24	20	51.123	9.345	16.88	1.15	1.23	1	-9.5	0.0	60	0	PSM	0.75	i
416	92	32	44.548	24	19	33.896	9.345	17.13	1.13	1.32	1	-9.7	0.0	60	0	PSM	0.75	i
417	92	27	50.197	24	26	52.237	9.468	18.16	1.28	1.74	0	PM	0.5	i
418	92	11	15.302	24	23	18.649	9.523	16.86	1.11	1.25	1	-5.0	0.0	60	0	PSM	0.75	i
419	92	14	39.263	24	22	52.028	9.523	18.42	1.32	1.78	0	PM	0.5	i
420	91	58	38.262	24	35	49.715	9.708	17.04	1.04	1.25	1	-7.4	0.0	60	0	PSM	0.75	i
421	92	12	59.013	24	14	04.759	9.708	17.09	1.21	1.33	1	-9.3	0.0	60	0	PSM	0.75	i
422	91	57	14.793	24	02	02.793	9.708	17.12	1.13	1.31	1	-8.1	0.0	60	0	PSM	0.75	i
423	92	06	07.822	24	15	09.915	9.900	15.51	0.83	0.85	3	-18.5	0.1	0	0	PMSNM	0.0	-
424	92	21	05.350	24	26	20.047	10.132	14.74	0.68	0.76	22	-7.4	28.4	93	0	PSM	1.0	-
425	92	14	15.341	24	12	04.796	10.308	14.65	0.95	1.01	4	7.3	0.2	0	0	PNM	0.0	-
426	92	06	15.760	24	00	03.419	10.308	16.94	0.87	0.92	0	PNM	0.0	-
427	92	32	55.287	24	06	37.032	10.986	14.99	0.75	0.84	3	25.0	0.5	0	0	PMSNM	0.0	-
428	92	16	59.724	24	38	47.886	11.233	17.35	1.00	1.38	0	PM	0.5	-
429	92	29	17.593	24	32	03.370	12.044	15.98	0.97	1.06	0	PM	0.5	-
430	92	15	05.795	24	28	45.341	12.652	13.72	0.69	0.80	2	-16.0	0.4	0	0	PM	0.5	-
431	91	56	54.688	24	05	24.845	13.326	13.33	0.68	0.66	4	13.6	0.2	0	0	PMSNM	0.0	-
432	91	57	29.405	24	04	37.707	13.691	13.80	1.31	1.43	0	PNM	0.0	-
433	92	22	24.534	24	07	32.039	13.691	15.47	0.71	0.83	3	-22.8	1.2	0	0	PMSNM	0.0	-
434	91	57	46.049	24	18	28.891	14.483	12.40	0.65	0.69	1	49.7	0.0	0	0	PNM	0.0	-
435	92	27	19.545	24	06	50.332	14.915	16.37	0.96	1.07	0	PM	0.5	-
436	92	06	41.495	24	29	24.741	15.373	16.08	0.95	1.05	1	27.2	0.0	0	0	PM	0.5	-
437	92	04	16.091	24	32	57.587	15.373	14.94	0.75	0.82	0	PM	0.5	-
438	92	34	30.923	24	33	54.647	17.605	15.20	0.82	0.96	3	30.2	0.4	0	0	PMSNM	0.0	-
439	92	08	57.506	24	27	48.954	23.215	13.56	0.80	0.87	2	21.8	0.0	0	0	PNM	0.0	-
440	92	31	41.376	24	37	15.182	52.465	15.18	1.19	1.46	0	PNM	0.0	-
441	92	07	30.632	24	31	58.076	58.464	16.76	1.42	1.65	1	-16.4	0.0	60	0	PSM	0.75	-

^aRunning number assigned to 310 rotators after sorting by rotation period.

^bbetter code denoting a star's cluster membership status (see introductory text of Appendix for code meaning).

^cletters "i", "c", and "g" mark stars on the I and C sequences or in the gap, respectively.

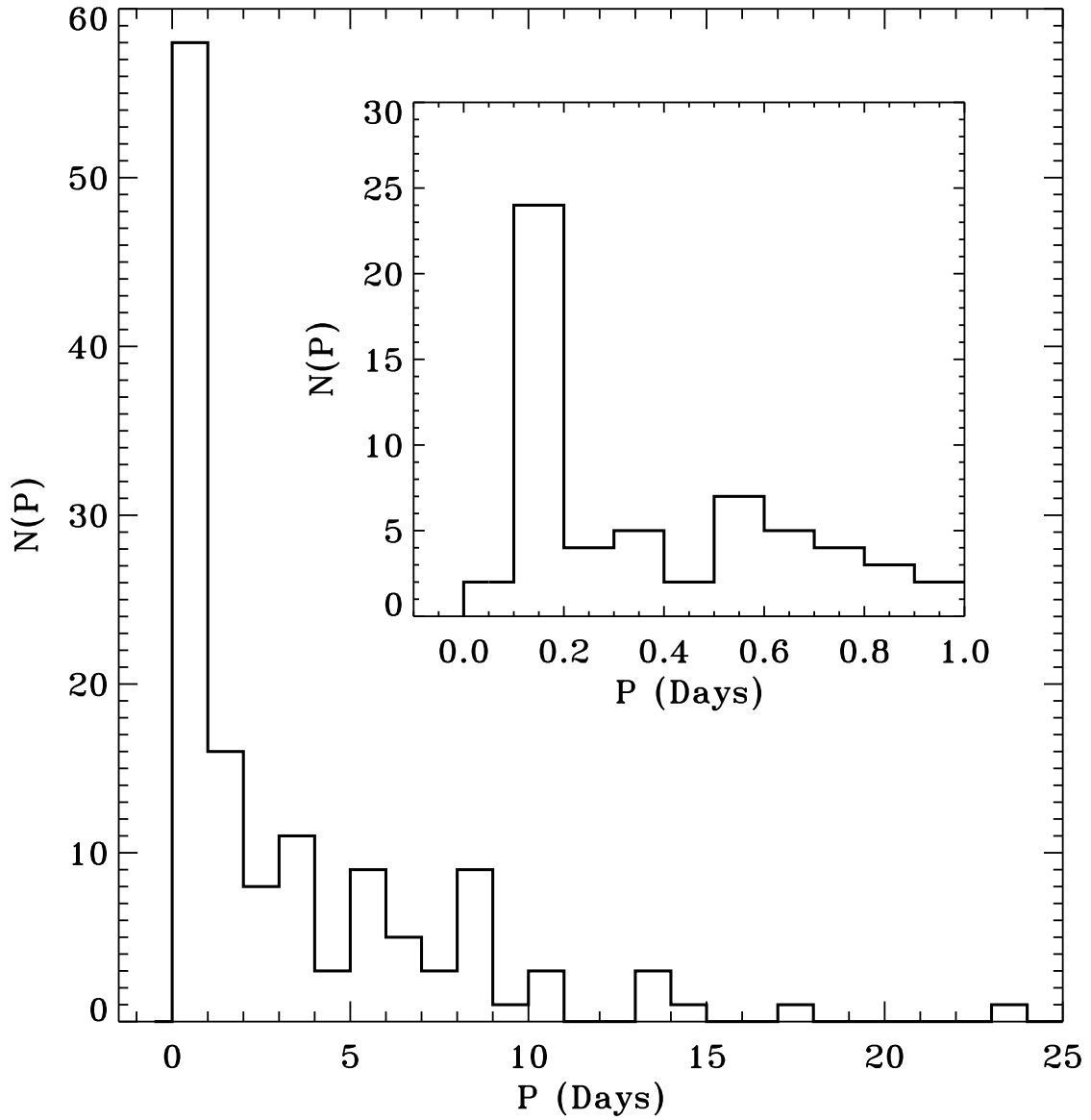


Fig. 14.— The rotation period distribution of the 131 radial-velocity and/or photometric non-members. The insert shows the distribution of periods less than 1 day with increased resolution of 0.1 day.

Cudworth, K. M. 1971, *AJ*, 76, 475

Deliyannis, C. P. 2008, private comm.

- Duvall, T. L., Dziembowski, W. A., Goode, P. R., Gough, D. O., Harvey, J. W., & Leibacher, J. W. 1984, *Nature*, 310, 22
- Edwards, S., Strom, S. E., Hartigan, P., Strom, K. M., Hillenbrand, L. A., Herbst, W., Attridge, J., Merrill, K. M., Probst, R., & Gatley, I. 1993, *AJ*, 106, 372
- Eff-Darwich, A., Korzennik, S. G., & Jiménez-Reyes, S. J. 2002, *ApJ*, 573, 857
- Endal, A. S., & Sofia, S. 1981, *ApJ*, 243, 625
- Geller, A., Mathieu, R. D., Harris, H. C., & McClure, R. 2008, submitted to *AJ*
- Goode, P. R., Dziembowski, W. A., Korzennik, S. G., & Rhodes, E. J. 1991, *ApJ*, 367, 649
- Gough, D. O. 1982, *Nature*, 298, 334
- Herbst, W., Eisloffel, J., Mundt, R., & Scholz, A. 2007, in *Protostars and Planets V*, ed. B. Reipurth, D. Jewitt, & K. Keil, 297–311
- Herbst, W., & Wittenmyer, R. 1996, *Bulletin of the American Astronomical Society*, 28, 1338
- Honeycutt, R. K. 1992, *PASP*, 104, 435
- Horne, J. H., & Baliunas, S. L. 1986, *ApJ*, 302, 757
- Jianke, L., & Collier Cameron, A. 1993, *MNRAS*, 261, 766
- Kalirai, J. S., Fahlman, G. G., Richer, H. B., & Ventura, P. 2003, *AJ*, 126, 1402
- Koenigl, A. 1991, *ApJ*, 370, L39
- Kraft, R. P. 1967, *ApJ*, 150, 551
- Krishnamurthi, A., Pinsonneault, M. H., Barnes, S., & Sofia, S. 1997, *ApJ*, 480, 303
- Lockwood, G. W., Thompson, D. T., Radick, R. R., Osborn, W. H., Baggett, W. E., Duncan, D. K., & Hartmann, L. W. 1984, *PASP*, 96, 714
- MacGregor, K. B., & Brenner, M. 1991, *ApJ*, 376, 204
- Mathieu, R. D. 2000, in *ASP Conf. Ser. 198: Stellar Clusters and Associations: Convection, Rotation, and Dynamos*, 517
- McNamara, B., & Sekiguchi, K. 1986, *AJ*, 91, 557

- Meibom, S., Barnes, S. A., Dolan, C., & Mathieu, R. D. 2001, in ASP Conf. Ser. 243: From Darkness to Light: Origin and Evolution of Young Stellar Clusters, 711
- Meibom, S., & Mathieu, R. D. 2005, *ApJ*, 620, 970
- Meibom, S., Mathieu, R. D., & Stassun, K. G. 2006, *ApJ*, 653, 621
- . 2008, in preparation.
- Meys, J. J. M., Alphenaar, P., & van Leeuwen, F. 1982, *Informational Bulletin on Variable Stars*, 2115, 1
- Najita, J. 1995, in *Revista Mexicana de Astronomia y Astrofisica Conference Series*, 293
- Nordhagen, S., Herbst, W., Rhode, K. L., & Williams, E. C. 2006, *AJ*, 132, 1555
- Perryman, M. A. C., Brown, A. G. A., Lebreton, Y., Gomez, A., Turon, C., de Strobel, G. C., Mermilliod, J. C., Robichon, N., Kovalevsky, J., & Crifo, F. 1998, *A&A*, 331, 81
- Pinsonneault, M. H., Kawaler, S. D., & Demarque, P. 1990, *ApJS*, 74, 501
- Prosser, C. F., Shetrone, M. D., Dasgupta, A., Backman, D. E., Laaksonen, B. D., Baker, S. W., Marschall, L. A., Whitney, B. A., Kuijken, K., & Stauffer, J. R. 1995, *PASP*, 107, 211
- Radick, R. R., Thompson, D. T., Lockwood, G. W., Duncan, D. K., & Baggett, W. E. 1987, *ApJ*, 321, 459
- Rucinski, S. M. 1997, *AJ*, 113, 1112
- Scargle, J. D. 1982, *ApJ*, 263, 835
- Schatzman, E. 1962, *Annales d’Astrophysique*, 25, 18
- Shu, F., Najita, J., Ostriker, E., Wilkin, F., Ruden, S., & Lizano, S. 1994, *ApJ*, 429, 781
- Sills, A., Pinsonneault, M. H., & Terndrup, D. M. 2000, *ApJ*, 534, 335
- Skumanich, A. 1972, *ApJ*, 171, 565
- Soderblom, D. R. 1982, *ApJ*, 263, 239
- Soderblom, D. R., Jones, B. F., & Walker, M. F. 1983, *ApJ*, 274, L37

- Soderblom, D. R., Stauffer, J. R., Hudon, J. D., & Jones, B. F. 1993a, *ApJS*, 85, 315
- Soderblom, D. R., Stauffer, J. R., MacGregor, K. B., & Jones, B. F. 1993b, *ApJ*, 409, 624
- Stassun, K. G., Ardila, D. R., Barsony, M., Basri, G., & Mathieu, R. D. 2004, *AJ*, 127, 3537
- Stassun, K. G., Mathieu, R. D., Mazeh, T., & Vrba, F. J. 1999, *AJ*, 117, 2941
- Stauffer, J. R., Hartmann, L., Soderblom, D. R., & Burnham, N. 1984, *ApJ*, 280, 202
- Stauffer, J. R., & Hartmann, L. W. 1987, *ApJ*, 318, 337
- Stauffer, J. R., Hartmann, L. W., Burnham, J. N., & Jones, B. F. 1985, *ApJ*, 289, 247
- Stauffer, J. R., Hartmann, L. W., & Jones, B. F. 1989, *ApJ*, 346, 160
- Stelzer, B., Fernández, M., Costa, V. M., Gameiro, J. F., Grankin, K., Henden, A., Guenther, E., Mohanty, S., Flaccomio, E., Burwitz, V., Jayawardhana, R., Predehl, P., & Durisen, R. H. 2003, *A&A*, 411, 517
- Terndrup, D. M., Stauffer, J. R., Pinsonneault, M. H., Sills, A., Yuan, Y., Jones, B. F., Fischer, D., & Krishnamurthi, A. 2000, *AJ*, 119, 1303
- van Leeuwen, F., & Alphenaar, P. 1982, *The Messenger*, 28, 15
- Vasilevskis, S., Klemola, A., & Preston, G. 1958, *AJ*, 63, 387
- von Hippel, T., Steinhauer, A., Sarajedini, A., & Deliyannis, C. P. 2002, *AJ*, 124, 1555
- Yi, S. K., Kim, Y., & Demarque, P. 2003, *ApJS*, 144, 259